Copyright is owned by the Author of the thesis. Permission is given for a copy to be downloaded by an individual for the purpose of research and private study only. The thesis may not be reproduced elsewhere without the permission of the Author.

How does the interaction between the Filamin A repeat 10 domain and F-actin lead to severe OPD skeletal disorders?

A thesis presented in partial fulfilment of the requirements for the degree of

Master of Science

in

Biochemistry

at Massey University, Palmerston North,

New Zealand.

Fareeda Maged Barzak

2014

Abstract

The cytoskeleton network allows cells to differentiate, divide, and move in response to the external environment creating a mechanoprotection system against cell stress. The actin cytoskeleton is stabilised and tightly regulated by various actin-binding proteins, one of which are the family of Filamin (*FLN*) proteins that crosslink F-actin into three-dimensional networks. Filamins also link the actin cytoskeleton to the cellular membrane through interactions with transmembrane proteins and function as a molecular scaffold for signalling molecules. In addition to an actin binding domain, each monomer contains a rod region of 24 immunoglobulin-like repeat domains with dimerisation of the monomers occurring at repeat 24. The human filamin family contains three *FLN* isoforms; *FLNA*, *FLNB,* and *FLNC* which are differentially expressed where *FLNA* is identified as the dominant isoform located on the X-chromosome essential for mammalian development.

Mutations in Filamin A (*FLNA*) have been identified to cause distinctly different human diseases affecting the central nervous system, vascular system, or skeletal muscles; however, the molecular mechanisms of FLNA leading to these diseases remain unclear. Mutations cluster in distinct *FLNA* domains, suggesting their functional importance for mediating correct functions. Mutations in the *FLNA* repeat 10 domain are correlated with severe forms of the skeletal disorders Otopalatodigital syndrome spectrum disorders (OPD) thought to be due to an altered or gain-of-function phenotype. The aim of this study was to provide an insight into the biochemical properties of *FLNA* repeat 10 domain by better understanding how mutations in this domain lead to OPD.

Initially, recombinant wildtype (Wt) and mutant (V1249A and A1188T) FLNA repeat 10 domain proteins (FLNAR10) were purified then compared by *in vitro* biochemical studies to investigate secondary structure, stability, and affinity towards F-actin. The FLNAR10 protein was revealed to have relatively weak binding affinity towards F-actin, consistent with being an additional contributor in the filamin protein to bind F-actin. Mutations in the FLNAR10 protein exhibited a slight increase in affinity towards F-actin, accompanied by a slight reduction of thermostability in comparison to the Wt protein, but no significant changes in the secondary structure were observed. This slight increase in the affinity of the mutant FLNA repeat 10 proteins towards F-actin is

consistent with a gain-of function mechanism for the disease phenotype. Overall, these results contribute towards a better understanding of the FLNA function, providing further evidence towards a gain-of function mechanism for OPD.

Acknowledgements

Individually, we are one drop, but together, we are an ocean. There are a number of people who I am greatly indebted to and would like to thank, but I wish to particularly thank the following:

Primarily, I would like thank my supervisor Dr. Andrew Sutherland-Smith, for his continuous support throughout my MSc study and research, and for this amazing opportunity, support, advice, confidence and technical discussions. Thank you for guiding me and believing in my ability.

A special thanks to Dr. Gill Norris, Dr. Mark Patchett, and Prof. Geoff Jameson for all the advice and input throughout the years. Thank you to my fellow labmates, colleagues, friends, and the Structural Biology group for their stimulating discussions, advice, and technical assistances.

I would also like to thank Ann, Cynthia, Colleen, Tara, and Paul for all their help and behind the scenes organisation. Also, thank you to Kathryn Stowell for her constant support and advice throughout my years at Massey University.

Thank you to all my family and parents Maged and Sohair who continue to be a source of encouragement and inspiration throughout my life. I am grateful for all the love, support, and encouragement to always reach for the stars whilst putting up with me through the highs and lows of this journey. I could not have done any of this without everyones belief in me.

Finally thank you to the Institute of Fundamental Sciences (IFS) and the Royal Society of New Zealand Marsden Fund for this opportunity.

Table of Contents

List of Figures

List of Tables

List of Abbreviations

× g	Multiples of gravitational force
Å	Angstrom (10^{-10}m)
A1188T	FLNA repeat 10 mutation Alanine to Threonine leading to FMD
A_{280}	Absorbance at 280 nm
aa	Amino acid
ABC	Ammonium bicarbonate
ABD	Actin binding domain
AEX	Anion Exchange Chromatography
Ala	Alanine
Amp	Ampicillin
ATP	Adenosine-5´-triphosphate
BLAST	Base local alignment search tool
bp	Base pair
CD	Circular Dichroism
cDNA	Complementary DNA
CV	Column Volumes
CH	Calponin homology domain
C-terminal	Carboxyl terminal
DNA	Deoxyribonucleic acid
dNTP	Deoxyribonucleotide Triphosphate
dsDNA	Double-stranded Deoxyribonucleic acid

DTT	Dithiothreitol
E. coli	*Escherichia coli*
EDTA	Ethylenediaminetetraacetic acid
EtBr	Ethidium Bromide
F-actin	Filamentous actin
FLN	Filamin
FLNA	Filamin A
FLNAR10	Filamin A repeat 10 protein
FMD	Frontometaphyseal dysplasia
G-actin	Globular (monomeric) actin
His_6	Hexa-histidine tag
HPLC	High-performance liquid chromatography
Ig	Immunoglobulin
IPTG	Isopropyl-β-D-thio-galactoside
K_d	Dissociation constant
kb	Kilobase pairs (of DNA)
LB	Luria Bertani media
LB-Amp	Luria Bertani media with 100 μg/ml ampicillin
mAU	Milli absorbance units
MeCN	Acetonitrile
Min	Minute
MNS	Melnick–Needles syndrome
MOPS	3-(N-morpholino) propanesulfonic acid

MW	Molecular Weight
N-terminal	Amino terminal
OD	Optical density at 600 nm
OPD	Otopalatodigital spectrum malformation disorders
OPD1	Otopalatodigital syndrome type 1
OPD2	Otopalatodigital syndrome type 2
PBS	Phosphate buffered saline
PCR	Polymerase chain reaction
PDB	Protein data bank
PH	Periventricular nodular heterotopia
pH	Negative decadal logarithm of proton concentration
KOAc	Potassium Acetate
RPM	Revolutions per minute
rTEV	Recombinant tobacco etch virus protease
S1199L	FLNA repeat 10 mutation Serine to Leucine leading to FMD
SEC	Size exclusion chromatography
SDS	Sodium dodecyl sulphate
SDS-PAGE	Sodium dodecyl sulphate polyacrylamide gel electrophoresis
TAE	Tris-acetate-EDTA buffer
TEMED	Tetramethylethylenediamine
TFA	Trifluoroacetic acid
Thr	Threonine
Tm	Melting temperature

TPCK	Tosyl phenylalanyl chloromethyl ketone
Tris	Tris-(hydroxymethyl)-aminomethane
U	Units
UV	Ultraviolet
V1249A	FLNA repeat 10 mutation Valine to Alanine leading to MNS
Val	Valine
v/v	Volume/volume ratio
Wt	Wild-type
w/v	Weight/volume ratio
w/w	Weight/weight ratio

1. Introduction

Foreword

Remodelling of the actin cytoskeleton maintains cell shape, cell migration, differentiation, and division through dynamic regulation by various actin binding proteins. Filamins (*FLN*) are actin binding proteins that crosslink actin filaments (F-actin) into orthogonal three-dimensional networks through their amino-terminal actin binding domain (Hartwig J.H. *et al.*, 1980). Whereas, the other domains bind to a number of other components, linking the cellular membrane through transmembrane receptor complexes, secondary messengers, acting as a molecular scaffold, and recruiting signalling molecules involved in signal transduction (MacPherson M. and Fagerholm S.C., 2010, Hou L. *et al.*, 1990, Stossel T.P. *et al.*, 2001, Feng Y. and Walsh C.A., 2004, Popowicza G.M. *et al.*, 2006). Filamin is at the centre of a complex, fine-tuned mechanism, which allows the organisation of the actin filaments based on signalling transduction.

The human filamin family contains three *FLN* isoforms; *FLNA*, *FLNB,* and *FLNC* which are differentially expressed (Maestrini E. *et al.*, 1993, Xu W. *et al.*, 1998). *FLNA*, the dominant isoform, is located on the X-chromosome and is ubiquitously expressed, (Gorlin J.B. *et al.*, 1990) as well as essential for mammalian development (Feng *et al.*, 2006, Hart A.W. *et al.*, 2006). Each filamin monomer contains an actin binding domain (ABD) at the amino-terminus, followed by a rod region of 24 immunoglobulin-like repeat domains with dimerisation of the filamin monomers occurring at repeat 24 in the carboxy-terminus (Gorlin J.B. *et al.*, 1990, Himmel M. *et al.*, 2003). This allows filamin to sit in a V-shaped structure in order to cross-link F-actin and provide a mechanoprotection system towards external forces (Tyler J.M. *et al.*, 1980, Hartwig J.H. and Stossel T.P., 1981, Alenghat F.J. and Ingber D.E., 2002).

With such important roles, mutations in the filamin A gene have been suggested to cause altered associations with binding partners, which consequently lead to changes in cell function (Gorlin J.B. *et al.*, 1990, Cunningham C.C. *et al.*, 1992). Cells that lack FLNA show impaired motility, and have impaired mechanical resistance resulting in cytoskeletal defects that can be rescued by transfection of FLNA (Cunningham C.C. *et al.*, 1992).

Mutations in FLNA have been identified to lead to distinctly different X-linked human diseases affecting the central nervous system, vascular, bone system, or skeletal

muscles. However, the molecular mechanism leading to these diseases remain unclear (Robertson S.P. *et al.*, 2003, Fox J.W. *et al.*, 1998)**.**

Loss-of-function X-linked mutations in FLNA due to reading frame disruption by deletions, insertions and nonsense mutations have been associated with the neurological disorder Periventricular nodular heterotopia (PH) (Fox J.W. *et al.*, 1998, Guerrini R. *et al.*, 2004, Parrini E. *et al.*, 2006). While the clinically distinct altered or gain-of-function skeletal disorders Otopalatodigital spectrum malformation disorders (OPD) comprises four groups including: OPD1, OPD2, frontometaphyseal dysplasia (FMD) and Melnick-Needles syndrome (MNS) (Robertson S.P. *et al.*, 2003) that are caused by clustered missense mutations that conserve the reading frame (Robertson S.P., 2007). OPD symptoms are diverse and include skeletal malformations, cardiac defects, hernias, and cleft palates. Mutations have been found to cluster in distinct FLNA domains suggesting these regions serve a functional importance for mediating correct function (Kyndt F. *et al.*, 2007). Conserved mutational hotspots in FLNA repeat 10 are correlated with the skeletal disorders Otopalatodigital syndrome spectrum disorders; FMD and MNS which are thought to be due to an altered or gain-of-function phenotype (Robertson S.P. *et al.*, 2003). Interestingly, the FLNA repeat 10 domain functions and binding partners have not been fully characterised, however, Suphamungmee *et al*., revealed that the ABD along with repeat 10 domain of FLNA associate with F-actin allowing the overall binding strength seen for the intact whole FLNA molecule (Suphamungmee W. *et al.*, 2012).

The critical question remains; how do these mutations alter the Filamin structure and or function leading to distinctly different human diseases is yet to be solved. This thesis examines the molecular properties of the Filamin A repeat 10 domain containing mutations associated with the OPD spectrum disorders, MNS and FMD relative to wild type to provide insight and a better understanding of the FLNA mechanisms during the disease and normal state.

1.1 Actin cross-linking proteins

The actin cytoskeleton is a complex structure that is involved in a wide range of cellular functions. Its dynamic reorganisation allows for various roles in maintaining the cells shape, migration, differentiation, and division necessary for the cell to function. The organization of the actin cytoskeleton is tightly regulated by various actin-binding proteins (ABPs) in response to signalling cascades causing the cross-linking of filamentous actin (F-actin) into orthogonal networks or bundles, controlling polymerization or depolymerisation of actin, or acting as molecular motors (Dos Remedios C.G. *et al.*, 2003, Popowicza G.M. *et al.*, 2006). Importantly, crosslinking of F-actin allows maintenance of the viscosity, elasticity and the mechanical resistance properties of the cell (McGough A., 1998).

1.2 Filamins

The Filamins (*FLN*) are a family of actin-binding protein that are large 280 kDa homodimeric proteins, they were first identified in chicken gizzard and rabbit blood allowing actin polymerization (Stossel T.P. and Hartwig J.H., 1975, Shizuta Y. *et al.*, 1976). Filamins are able to organise actin filaments (F-actin) into three-dimensional orthogonal networks, but also function as adapter proteins to link the cellular membrane through transmembrane receptors to the actin cytoskeleton, and recruit signalling molecules involved in signal transduction (MacPherson M. and Fagerholm S.C., 2010, Hou L. *et al.*, 1990). The human filamin family comprises of three isoforms Filamin A, Filamin B, Filamin C (*FLNA*, *FLNB* and *FLNC*). Their sequences are 60-80% conserved with the exception of two hinge regions, which show great variance. The three members are found to be widely expressed during development with highly conserved genomic organization. The human filamin family are widely expressed, *FLNA* and *FLNB* are expressed in similar patterns in many tissues, such as in the heart, kidney, and brain (Xu W. *et al.*, 1998), while *FLNC* is more specific towards cardiac and skeletal muscle (Maestrini E. *et al.*, 1993). The filamin isomers are located on different chromosomes; *FLNA* is located on the X-chromosome (Gorlin J.B. *et al.*, 1990); *FLNB* on chromosome 3 (Xu W. *et al.*, 1998); and *FLNC* on chromosome 7 (Maestrini E. *et al.*, 1993), the *FLN* lead to distinctly different functional roles. Mutations in *FLNA* have been associated with X-linked human genetic diseases leading

to abnormal development of brain, bone and the cardiovascular system, as filamins are essential for human development.

1.2.1 Structural components of Filamin *A*

High-resolution electron micrographs of the human FLNA reveal that this protein is homodimeric, and from its sequence each monomer contains an actin binding domain (ABD) at the N-terminus, which is then followed by a rod region of 24 immunoglobulin (Ig)-like repeat domains that adopts a β-sandwich fold containing, two hinge regions that allow flexibility. Dimerisation of the filamin monomers occurs at repeat 24 in the C-terminus (Gorlin J.B. et al., 1990, Himmel M. et al., 2003). FLNA has been shown in electron micrographs to cross-link actin into a V-shaped position with the monomers held together through the dimerisation domain (Figure 1.1), (Tyler J.M. et al., 1980, Hartwig J.H. and Stossel T.P., 1981), creating a mechanoprotection system when external forces are transmitted through the transmembrane proteins (Alenghat F.J. and Ingber D.E., 2002).

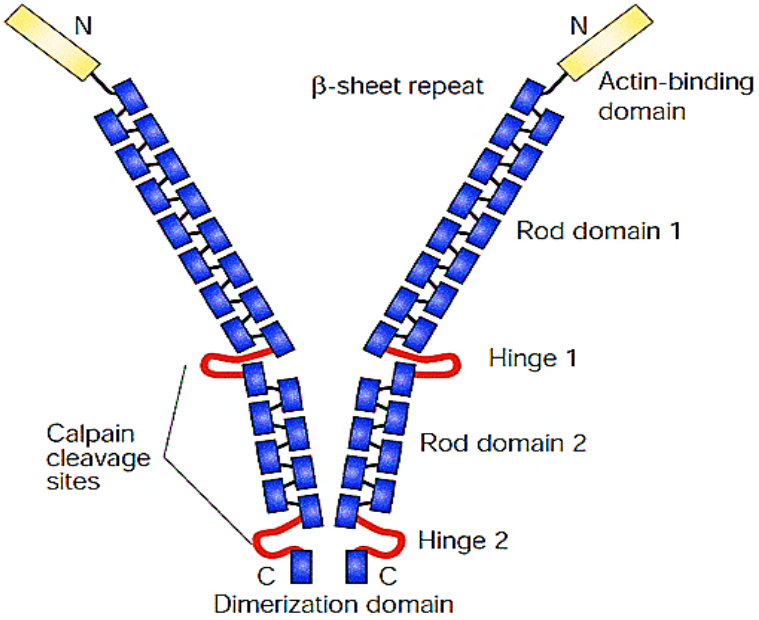

Figure 1.1 Structure of filamin.

The Filamin A structure containing an actin binding domain (ABD) followed by 24-Ig like repeat domains, monomers held together at the dimerisation domain forming a Y-shaped structure. Adapted from (Stossel T.P. *et al.*, 2001).

1.2.2 Dimerisation of filamin

The crystal structure of filamin has revealed that repeat 24 at the C-terminus is required for dimerization of the filamin monomers (Gorlin J.B. *et al.*, 1990, Pudas R. *et al.*, 2005, Seo M.D. *et al.*, 2008, Hartwig J.H. and Stossel T.P., 1981). The molecular organisation of filamins is based on a leaf spring model, where hydrophobic interactions in the dimerisation domain hold the leaves together at one end, while the rod domains containing the two hinge regions allow stiffness and flexibility respectively, to facilitate cross-linking to the actin filaments (Gorlin J.B. *et al.*, 1990). Filamin dimerisation presents a V-shaped structure which is believed to be important for filamin functions in cross-linking F-actin into a branched perpendicular shape and also its interactions with the cell membrane proteins (Gorlin J.B. *et al.*, 1990). Heterodimerisation of filamins at repeat 24 has been suggested to occur between *FLNA* and *FLNB* (Sheen V.L. *et al.*, 2002), but cross-linking assays have suggested that only *FLNB* and *FLNC* repeat 24 formed heterodimers (Himmel M. *et al.*, 2003). While another study showed that *FLNA* and *FLNB* constructs containing repeats 16-23 can heterodimerise (Sheen V.L. *et al.*, 2002) suggesting the importance of the other repeat domains, however whether heterodimerisation occurs *in vivo* remains to be investigated.

1.2.3 Actin binding domain of filamin

The actin binding domain (ABD) of *FLNA* was mapped to the amino-terminus (30 kDa) of the filamin monomer with a conserved structure as for other actin filament binding proteins such as; α-actinin, β-spectrin, fimbrin and utrophin (Gorlin J.B. *et al.*, 1990, Clark A.R. *et al.*, 2009). The ABD is made up of two calponin homology (CH) domains CH1 and CH2 domains, which are the N- and the C-terminal regions of this domain respectively. The crystal structure revealed that each CH domain is made up of four main α-helices that are connected by long loops, and two or three short α- helices, where the CH domains form a triple helical bundle and allows a tight hydrophobic interface for the ABD (Ruskamo S. and Ylanne J., 2009, Clark A.R. *et al.*, 2009). The CH domains within the ABD are responsible for binding F-actin allowing organisation of the filaments into three-dimensional networks. However, a unique calmodulin-binding site within the CH1 of ABD presents binding competition of calcium-activated calmodulin with F-actin for this site (Nakamura F. *et al.*, 2005). Conversely, binding studies have shown that the ABD alone interacts with F-actin with a low affinity (K_d $\sim 1.7\times10^{-5}$ M) as previously seen in the ABD of spectrin superfamily; however, the

intact full-length FLNA dimer is seen to bind F-actin with a significantly higher affinity (K_d ~1.7×10^{-8} M) (Nakamura F. *et al.*, 2007, Nakamura F. *et al.*, 2011). Therefore, suggesting other regions of the molecule are likely to contribute to the overall binding strength of the intact FLNA towards F-actin (Nakamura F. *et al.*, 2007, Nakamura F. *et al.*, 2011), presumably the Ig-repeat domains as observed in other muscle proteins; paladin and kettin (Dixon *et al.*, 2008, Ono *et al.*, 2006).

1.2.4 Structure of filamin repeats

The filamin rod region is made up of 24 immunoglobulin-like repeat domains (11 kDa) with a predominantly β-sheet structure comprising of approximately 96 residues, while one or two flexible hinge regions are also present within the rod region. The rod region regulates the flexibility, orientation, and binding to the F-actin. The crystal structures of the Ig-like repeat domains present an immunoglobulin-like fold adopting a β-sandwich fold comprising of seven β-strands stacked in three-stranded and four-stranded β-sheets in two beta sheets to generate the rod region (Gorlin J.B. *et al.*, 1990, Feng Y. and Walsh C.A., 2004, Popowicza G.M. *et al.*, 2004, Page R.C. *et al.*, 2011). All human filamins contain two hinge regions positioned between repeats 15-16 (hinge 1) and 23-24 (hinge 2) that allow flexibility of filamin, however, hinge 1 maybe lacking in some filamin splice variants (Weihing R.R., 1988). The rod domain is split up into two sections; rod 1 containing domains 1-15, and rod 2 containing domains 16-24.

Based on sequence alignments and functional properties of the repeat domains, they were characterised into four separate classes; A, B, C and D, suggesting that each class binds to similar partners or may function in the same way (Ithychanda S.S. *et al.*, 2009)**.** More than 70 binding partners for the filamins have been identified (Popowicza G.M. *et al.*, 2006). Interactions between FLNA repeat domains and membrane receptors have been identified through structural analysis, revealing that rod 1 generally binds to small proteins such as signalling molecules (Nakamura F. *et al.*, 2006) and contains a secondary F-actin-binding domain of lower affinity (Nakamura F. *et al.*, 2007). Rod 2 on the other hand, does not interact with F-actin leaving it free to interact with multiple larger proteins such as integrins and glycoproteins (Nakamura F. *et al.*, 2006).

The repeat domains that make up the rod region of FLNA are arranged in a specific orientation with respect to one another to allow both mechanical and functional properties. The repeat domains of the rod do not necessarily fold in a linear fashion as

distinct domains (Lad Y. *et al.*, 2007). The repeat domains bind in an alternating fashion between neighbours through intrachain pairing hydrophobic interactions to yield a backbone with an overlapped staggered fashion allowing mechanical elasticity (Gorlin J.B. *et al.*, 1990). Rod 1 repeats 1-15 are consistent and are able to bind in a linear staggered fashion. However, rod 2 containing repeats 16-24 have been shown to diverge from this binding pattern due to slight differences in structure. Sequence and structural analysis has revealed that rod 2 domains are folded presenting a more compact structure, which results from pairing between even-numbered repeats, repeat domains 16, 18 and 20 pair with neighbouring repeats 17, 19 and 21, respectively, to allow the dimer to form within the C-terminal domain and to provide a mechanosensing system (Lad Y. *et al.*, 2007, Heikkinen O.K. *et al.*, 2009). It has been identified that multiple β-integrin interaction sites occur within these pairs (Ithychanda S.S. *et al.*, 2009) suggesting a mechanism of conformational change to uncover binding sites (Lad Y. *et al.*, 2007).

The repeat domains contain clusters of mutations leading to different human disorders, suggesting their importance for the function of FLNA. Interestingly, the FLNA repeat 10 domain has been characterised to be a mutational hotspot leading to different disorders, yet, its functions and binding partners are one of the least characterized. Nonetheless, it has been proposed to be able to bind to F-actin suggesting its significance (Robertson S.P. *et al.*, 2003, Robertson S.P., 2007, Robertson S.P. *et al.*, 2006, Feng Y. and Walsh C.A., 2004).

The FLNA repeat 10 has been characterised as a member of class D filamin repeat domains, which also includes repeats 6, 7, 13 and 14, it is the first structure of class D repeat domains from FLNA to be solved and deposited into the protein data bank (PDB code 3RGH). The structure exhibits the immunoglobulin-like domain fold as previously suggested for the structures of other FLNA repeat domains, with a unique CD-loop (Figure 1.2) (Page R.C. *et al.*, 2011). Class D was found to contain two residues within the CD loop in comparison to the previously determined class A repeat which, contains a conserved serine residue within its binding groove, these residues allow for the structures to adopt different conformations in order to bind to separate ligands (Page R.C. *et al.*, 2011, Nakamura F. *et al.*, 2006, Ithychanda S.S. *et al.*, 2009). All binding partners of FLNA repeat domains have been identified to bind their β-strand between

the C and D strand of the repeat domain to allow an extension of the existing β-sheet (Lad Y. *et al.*, 2007).

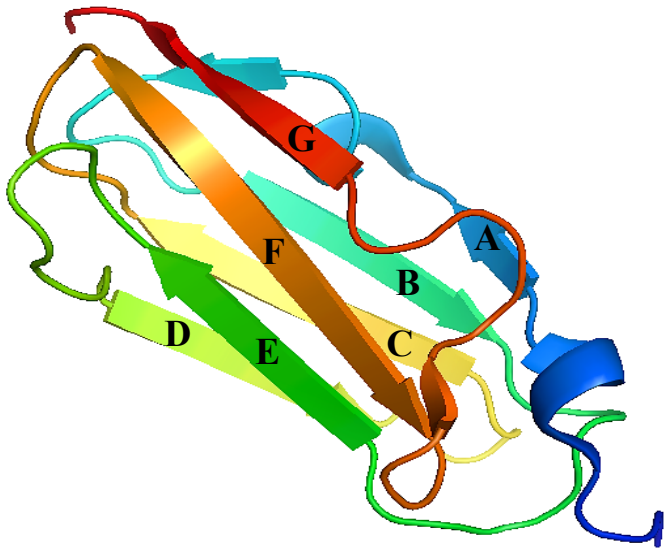

Figure 1.2 The crystal structure of the human FLNA repeat 10 domain.

Ribbon diagram of human Filamin A repeat 10 domain coloured as a rainbow from N-terminus (blue) to C-terminus (red), A-G β-strands labelled. Image prepared using PyMOL software (The PyMOL Molecular Graphics System, Version 1.3 Schrödinger, LLC), from FLNA repeat 10 structure coordinates (PBD-3RGH) (Page R.C. *et al.*, 2011).

1.3 Regulation of Filamin A

The FLNA hinge regions have been shown to be susceptible to proteolysis particularly calpain, a calcium-dependent protease, and the hinges also contain phosphorylation sites (Gorlin J.B. *et al.*, 1990, Weihing R.R., 1988). Phosphorylation near these hinge regions allow regulation of FLNA, causing a decrease in actin binding, causing an increase in resistance to calpain proteolysis and regulating interactions with integrins and glycoproteins (Chen M. and Stracher A., 1989, Ohta Y. and Hartwig J.H., 1995, Goldmann W.H. *et al.*, 1997). Phosphorylation has been suggested to neutralize the clusters of positive charges in specific repeats causing the structure to become more compact as subunits bind together (Gorlin J.B. *et al.*, 1990).

1.4 Roles of Filamin A on cell function

The filamin A homodimer is at the heart of a complex mechanism involved in the organisation of the actin cytoskeleton by not only binding to filamentous actin (F-actin), but also by providing a link to the cellular membrane through transmembrane receptors and acting as a molecular scaffold for signal transduction (Figure 1.3). These functions allow the dynamic remodelling of the actin cytoskeleton in providing cell shape, cell motility, differentiation and division (Feng Y. and Walsh C.A., 2004, Stossel T.P. et al., 2001).

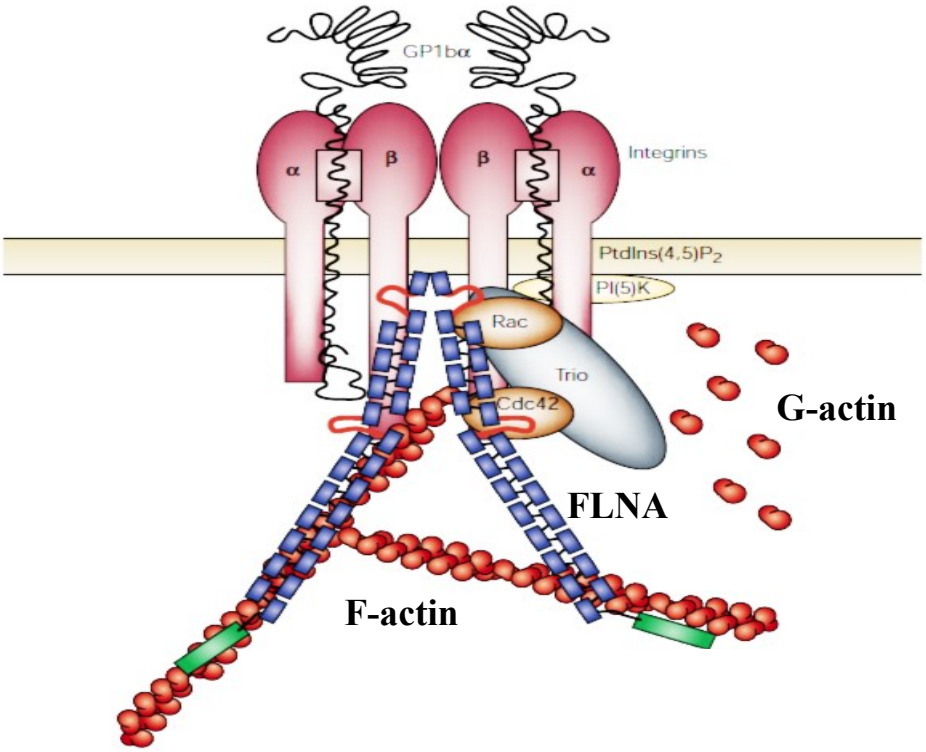

Figure 1.3 Model of FLNA interactions.

FLNA associates with multiple binding partners shown in this model such as; integrins, glycoprotein receptors, kinases, and F-actin, adapted from (Stossel T.P. *et al.*, 2001).

1.4.1 Interactions with transmembrane proteins

Filamins link the cytoskeleton with transmembrane receptors to provide stabilisation of the membrane, regulate adhesion, cell spreading, and transmembrane signalling. Specific regions in filamin allow binding of transmembrane proteins such as the glycoprotein receptor complex (Meyer S.C. *et al.*, 1997), and the β-integrins (Calderwood D.A. *et al.*, 2000).

Integrin adhesion receptors are αβ heterodimers, which provide a structural link between the extracellular matrix and the actin cytoskeleton, by initiating biochemical signals through the plasma membrane (Hynes R.O., 1992). This link is necessary for cell adhesion, cell migration and interactions with the extracellular matrix as they play key roles in physiological processes such as in development, haemostasis and in the immune defence (Huttenlocher A. *et al.*, 1996). The non-covalently bound α and β-subunits each contain a large extracellular ligand-binding domain, followed by a transmembrane domain and a short cytoplasmic domain (Calderwood D.A. *et al.*, 2000). After extracellular ligand is bound, it causes activation of the integrin by conformational changes, allowing intracellular interactions with the cytoskeleton and other proteins to occur which lead to changes in cell adhesion, cell spreading and actin reorganization (MacPherson M. and Fagerholm S.C., 2010).

The actin binding proteins filamin, talin, and α-actinin interact with the cytoplasmic tails of β-integrin providing the link between the integrins and the actin cytoskeleton. However, each actin binding protein binds specifically to different β-integrin cytoplasmic tails allowing for their specific roles (Gorlin J.B. *et al.*, 1990). Filamin A binds tightly to the β7 cytoplasmic tail of β-integrin causing decreased cell migration by inhibiting cell polarization by reducing membrane remodelling (Calderwood D.A. *et al.*, 2001). This suggests that the integrin-filamin interaction is involved in regulating cell motility consistent with previous studies of overexpression of filamin decreasing locomotion (Cunningham C.C. *et al.*, 1992). FLNA also interacts with integrins in response to cell stress through signal transduction, causing resistance of the cell to physical pressure, while *FLNA* knockout increases force-induced apoptosis (Glogauer M. *et al.*, 1998). Regulation of FLNA association with β-integrin tails has been suggested to be caused due to phosphorylation by GTPase RalA enzyme (Ohta Y. *et al.*, 1999).

Another important interaction occurs between filamins and the glycoprotein receptor complex GPIb-V-IX which is located on the platelet surface (Berndt M.C. *et al.*, 1985). The complex contains GPIbα and GPIbβ subunits (Fox J.E. *et al.*, 1988), where GPIbα is the major subunit of the complex shown through immunoblot (Fox J.E., 1985a) and pull-down assays (Meyer S.C. *et al.*, 1997, Xu W. *et al.*, 1998) to associate tightly with filamin (Figure 1.4). This allows a link between the platelet membrane and the actin cytoskeleton (Fox J.E., 1985b) for the maintenance of the shape of the platelets and regulating the receptor adhesive function

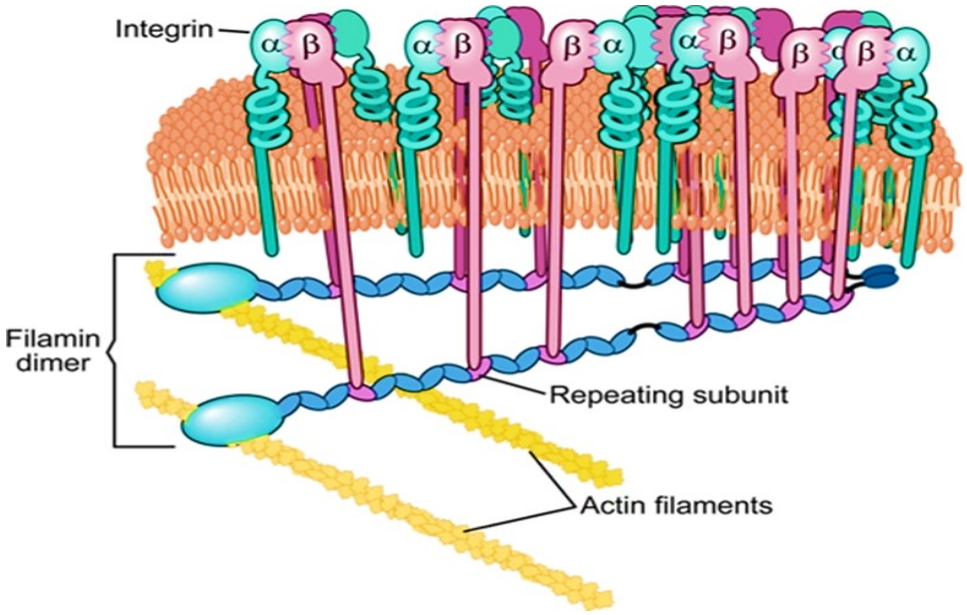

Figure 1.4 Filamins interactions and functions.

FLNA interactions with integrins and actin filaments at specific domains, (Ithychanda S.S. *et al.*, 2009).

Initially, specific domains in the filamin protein were identified to bind to integrins or glycoproteins. The C-terminus of FLNA was thought to bind to integrins (Burridge K. and Chrzanowska-Wodnicka M., 1996), while *in vitro* binding studies identified that the filamin repeat domains 17-19 bind to GPIbα (Cunningham J.G. *et al.*, 1996). However, recent studies revealed that repeat domains of class A were able to bind both the integrin cytoplasmic tails and GPIbα specifically (Ithychanda S.S. *et al.*, 2009). The specificity of binding was compared to the FLNA repeat 10 domain of class D, which showed that no binding to either integrins or GPIb occurs. The repeat 10 domain of FLNA has been proposed to play an important role in the human immunodeficiency virus entry into the immune cells, by its interaction with the T-cell receptor CD4 at the

cytoplasmic domain (Jimenez-Baranda S. *et al.*, 2007). The binding interface between the FLNA repeat 10 domain and CD4 has not yet been defined, but is suggested to differ completely from class A-interacting ligands integrin, GPIb, and migfilin (Nakamura F. *et al.*, 2006, Ithychanda S.S. *et al.*, 2009). These observations point towards the specificity of the filamin repeats for their binding partners.

It has been suggested that spatial clustering of the cell surface receptors GPIb and β-integrins may occur as they might be simultaneously able to be bound by class A repeat domains within FLNA. This binding pattern may be regulated further by ligands in the extracellular domain or by signalling pathways leading to changes in conformation of FLNA (Ithychanda S.S. *et al.*, 2009).

1.4.2 Scaffold for signalling molecules

Filamins also function as molecular scaffolds by tethering membrane receptors to the actin cytoskeleton and recruiting signalling molecules involved in signal transduction to regulate these interactions (MacPherson M. and Fagerholm S.C., 2010). The filamins are able to bind to multiple signalling molecules including the small GTPases; RhoA, Rac1, Cdc42 and their associated signalling kinase pathways (Ohta Y. *et al.*, 1999) leading to distinct effects in the actin cytoskeleton.

Filamin A also allows interactions with the downstream effector of Rac1 and Cdc42; serine/threonine kinase p21-activated kinase 1 (Pak1) which controls actin cytoskeletal rearrangements leading to; ruffle formation, lamellipodia, filopodia and regulating cell motility (MacPherson M. and Fagerholm S.C., 2010, Vadlamudi R.K. *et al.*, 2002, Sells M.A. *et al.*, 1999, Sells M.A. *et al.*, 1997). The C-terminal repeat 23 of FLNA has been shown to contain the binding site of Pak1, while the FLNA-binding site in Pak1 is in the Cdc42/Rac-interacting (CRIB) domain. FLNA is able to interact with Pak1 leading to physiological signals that stimulate Pak1 kinase activity in order to phosphorylate FLNA in the C-terminal region on a serine amino acid. FLNA and Pak1 colocalize in membrane ruffles which, leads to Pak1-induced cytoskeletal reorganization (Vadlamudi R.K. *et al.*, 2002, Ohta Y. *et al.*, 1999, Sells M.A. *et al.*, 1999, Sells M.A. *et al.*, 1997).

Cell membrane ruffle formation is usually regulated as a result of GTPases binding to Pak1 and stimulating their kinase activity to phosphorylate FLNA, however, Pak1 mutants that contain non-functioning GTPase binding sites or kinase activity are still

able to form membrane ruffles suggesting that they are GTPase-independent but dependent on protein-protein interactions. (Vadlamudi R.K. *et al.*, 2002). The FLNA–Pak1 interaction suggests that it acts as a scaffold for activation of Pak1 as it is able to bind signalling molecules.

The interaction between FLNA and RhoGTPase-activating protein; FilGAP regulates the membrane protrusion allowing cell spreading and lamellipodia formation in response to activated Rho kinase (Ohta Y. *et al.*, 2006). FilGAP is involved in controlling the activity of filamin-associated Rac to affect cell polarization. FilGAP consists of a pleckstrin homology domain able to bind membrane lipid, a GTPase activating protein (GAP) domain and a coiled coil domain at the C-terminus. The C-terminus of FilGAP associates with the C-terminus of FLNA specifically at repeat 23.

External signals allow the regulation of the β-integrin tails and FilGAP to associate with FLNA (Figure 1.5), where cell stress leads to increased β-integrin binding to FLNA, and causes FilGAP to dissociate from FLNA causing disruption of cell spreading. While, the overexpression of FilGAP in cells abolishes integrin-mediated cell spreading, (MacPherson M. and Fagerholm S.C., 2010, Ehrlicher A.J *et al.*, 2011, Ohta Y. *et al.*, 2006). These results allow a mechanotransduction system within the actin cytoskeleton. Therefore, FLNA provides a molecular scaffold for multiple signalling proteins in response to the external stimuli that allow regulation of the actin cytoskeleton.

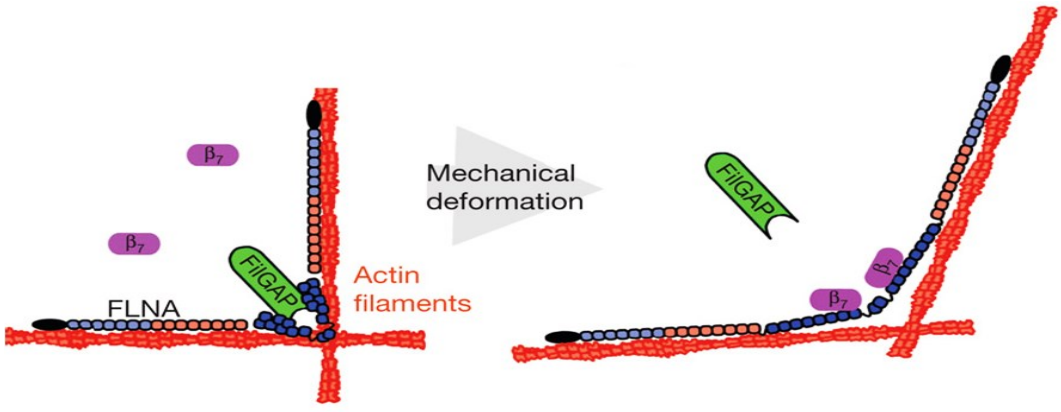

Figure 1.5 Model of β-integrin and FilGAP binding differentially to *FLNA*.

FilGAP binds at repeats 23 causing the β-integrins to become unbound. When mechanically deformed due to stress, uncovers integrin sites on repeat 21 allowing β7-integrin to bind, (Ehrlicher A.J *et al.*, 2011).

1.4.3 Mechanoprotection

The cytoskeleton is regulated through a mechanosensing system that allows the cell to respond to external force and stiffness of the extracellular matrix by balancing the cytoskeletal tension forces (Alenghat F.J. and Ingber D.E., 2002). Filamins bind to extracellular membrane receptors and intracellular signalling proteins providing a link for the cell to sense external forces and substrate stiffness suggestive of a mechanosensing system. Biochemical and structural analysis has revealed that filamins act as molecular springs that are able to resist force in order to prevent cell death, through the stabilisation and regulation of the actin cytoskeleton by means of elastic properties on F-actin networks (Gardel M.L. *et al.*, 2006). FLNA functions by causing tension of the cytoskeleton when external forces are applied. Evidence supports the necessity of FLNA in mechanosensing where; the expression of FLNA is upregulated in response to a force applied to the membrane of human fibroblast and osteoblast cells (D'Addario M. *et al.*, 2001), while in mutant cells lacking FLNA they are unable to cause tension of the cytoskeleton when force is applied and lead to force-induced apoptosis (Kasza K.E. *et al.*, 2010, Kasza K.E. *et al.*, 2009, Stossel T.P. *et al.*, 2001, Gargiulo A. *et al.*, 2007).

This transduction occurs via integrins which sense external force and transmit these forces to the cytoskeletal filaments resulting in a signalling cascade and leading to cytoskeletal rearrangements which is important for the maintenance of cell shape, polarisation, cell division and motility (D'Addario M. *et al.*, 2001). To achieve these mechanical properties, filamin must be able to cross-link F-actin tightly, but also allow flexibility for the filaments to withstand external forces (Gardel M.L. *et al.*, 2006). A mechanism based on molecular dynamics calculations proposes that; filamin bound to the F-actin network undergoes conformational changes induced by a force (Kesner B. *et al.*, 2009, Pentikainen U. and Ylanne J., 2009) leading to the unfolding of FLNA repeat domains and changes in hinge regions uncovering β-integrin binding sites (Lad Y. *et al.*, 2007, DiDonna B.A. and Levine A.J., 2007). FLNA interacts with integrins, causing modifications in the structural length of F-actin filaments due to conformational flexibility and resistance to the cell pressure of FLNA (Kasza K.E. *et al.*, 2010, Kasza K.E. *et al.*, 2009, Gargiulo A. *et al.*, 2007). Whether forced unfolding within FLNA is conserved is yet unclear, however, this mechanism is consistent with plasticity of FLNA under external force.

1.4.4 Interaction with actin cytoskeleton

FLNA is an important building block within the larger complex network of the actin cytoskeleton, which mediates the organisation of the actin filaments in response to cell signals. Cell signals from the external environment allows for the regulation of the actin cytoskeleton in order for the cell to change shape, divide, move (Alenghat F.J. and Ingber D.E., 2002). Filamins have been presented to induce gelation of actin due to the cross-linking of actin filaments into perpendicular orthogonal branched networks through their CH domains within the ABD (Hartwig J.H. and Stossel T.P., 1981). While the filamin covalently cross-linked actin networks have been identified to be irreversibly broken under sheer stress *in vitro* (Janmey P.A *et al.*, 1990).The organisation of actin into networks is dependent on the FLNA:F-actin ratio, which was observed to form tighter and more branched networks with increased concentrations of FLNA (Gorlin J.B. *et al.*, 1990, Xu W. *et al.*, 1998). Examining the F-actin branching and cross-linking revealed as previously suggested, that dimerization of the FLNA monomers at the C-terminus and an intact ABD are needed to mediate rigid perpendicular branching of F-actin to withstand cell stress whilst allowing flexibility through the hinge regions (Figure 1.3) (Nakamura F. *et al.*, 2007, Stossel T.P. *et al.*, 2001).

Mutations within the ABD have led to distinct human disorders possibly due to alterations in cross-linking F-actin within the actin cytoskeleton. *In vitro* studies have presented mutations in the CH2 domain of ABD (E254K) that lead to an increase in F-actin binding (K_d ~1.3×10^{-5} M) compared with wild type (K_d ~4.8×10^{-5} M) due to the removal of a conserved salt bridge, suggesting importance of this domain in mediating correct cell function (Clark A.R. *et al.*, 2009). Binding studies revealed that the intact full-length FLNA dimer binds to F-actin with a moderately high affinity (K_d ~1.7×10^{-8} M), though the ABD alone interacts with F-actin with a lower affinity (K_d ~1.7×10^{-5} M), suggesting an additional region within the molecule contributes to binding affinity (Nakamura F. *et al.*, 2007, Nakamura F. *et al.*, 2011). Actin co-sedimentation assays conducted for full length FLNA produced a 1:1 hyperbolic binding model however, deletion constructs did not fit this model suggesting that an alternative binding model or mechanism may apply for other regions of the FLNA (Figure 1.6).

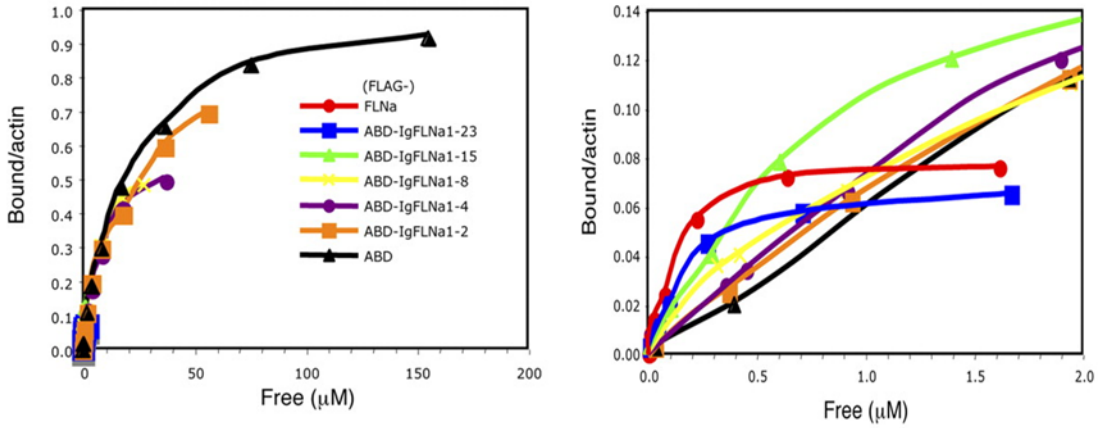

Figure 1.6 Actin co-sedimentation assay of different recombinant FLNA constructs.

FLNA constructs to determine FLNA:F-actin binding affinity (Nakamura F. *et al.*, 2007).

Deletion constructs containing different fragments of FLNA were examined using electron microscope showing that a region within rod 1 of which was further defined to be repeat 10 domain, was involved in F-actin binding (Nakamura F. et al., 2007, Suphamungmee W. et al., 2012), but its affinity towards F-actin was not measured. The FLNA Repeat 10 domain was identified to contain multiple mutations leading to severe diseases suggesting importance of function in binding to F-actin on the cell (Robertson S.P. et al., 2003).

1.5 Filamin A associated with Diseases

Mutations in filamin family members have been linked to human genetic diseases affecting the; nervous, skeletal and vascular systems, as they are expressed differentially and play an important role during development (Fox J.W. *et al.*, 1998, Robertson S.P. *et al.*, 2003). Mutations in *FLNA*, *FLNB,* and *FLNC* isoforms lead to a wide range of genetic syndromes, based on differences in expression location. More importantly, mutations in the ubiquitously expressed *FLNA* lead to phenotypic diversity during development, two distinctive diseases are; periventricular nodular heterotopia (PH) and, otopalatodigital spectrum malformation disorders (OPD), that affect the neurological or skeletal tissues, respectively (Figure 1.7).

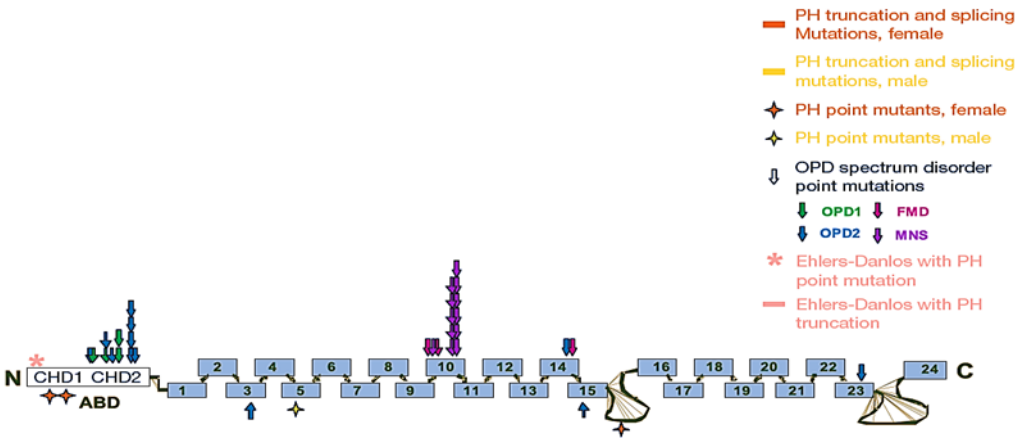

Figure 1.7 Filamin A mutations associated with different diseases.

Mutations in *FLNA* lead to various human diseases that cluster in specific domains of the FLNA protein, (Feng Y. and Walsh C.A., 2004), where each symbol representing a patient-case

1.5.1 Periventricular nodular heterotopia

Periventricular nodular heterotopia (PH) is an X-linked dominant brain abnormality that occurs as a result of loss-of-function mutations in *FLNA*. (Fox J.W. *et al.*, 1998, Guerrini R. *et al.*, 2004). PH occurs as a result of unmigrated neurons from the ventricular zone to the cortex during embryonic brain development, which appear as nodules conveying *FLNA*'s involvement in the neuronal migration signalling events (Fox J.W. *et al.*, 1998). Most mutations identified for PH are due to reading frame disruptions that completely abolish FLNA expression, while a few missense mutations have been identified (Parrini E. *et al.*, 2006). Heterozygous females with PH have shown a wide range of clinical symptoms such as seizures, cardiovascular malformation, a propensity to premature stroke and small joint hyper-extensibility due to random X-inactivation, while males with PH are generally embryonic lethal resulting from *FLNA*'s location on the X-chromosome (Robertson S.P. *et al.*, 2003, Fox J.W. *et al.*, 1998, Moro F. *et al.*, 2002).

Survival of males with PH was identified to be due to hypomorphic or mosaic mutations resulting in some *FLNA* function to be present (Pudas R., 2006, Van Kogelenberg M., 2010). However, a few rare cases of males with mild PH have been identified with similar clinical symptoms as females with PH distinct from males with hypomorphic or mosaic mutations (Sheen V.L. *et al.*, 2001, Feng Y. and Walsh C.A., 2004, Guerrini R. *et al.*, 2004, Parrini E. *et al.*, 2004, Gargiulo A. *et al.*, 2007, Van Kogelenberg M., 2010)

resulting in a loss of dimerisation of the FLNA monomers, but partial function of FLNA (Van Kogelenberg M., 2010). Studies had previously suggested that dimerisation of FLNA is crucial to effectively cross-link F-actin through its ABD by mediating the V-shaped orientation (Gorlin J.B. *et al.*, 1990, Weihing R.R., 1988). However, a few rare cases of males with mild PH have been identified with similar clinical symptoms as females with PH distinct from males with hypomorphic or mosaic mutations (Sheen V.L. *et al.*, 2001, Parrini E. *et al.*, 2004, Van Kogelenberg M., 2010) resulting in a loss of dimerisation of the FLNA monomers, but partial function of FLNA (Van Kogelenberg M., 2010). The partial loss-of-function observed proposes that FLNA dimerisation may not be that important as originally thought for F-actin cross-linking suggesting either an alternative dimerisation mechanism or an alternate actin binding mechanism unaffected by dimerisation to compensate for this effect.

1.5.2 Otopalatodigital spectrum malformation disorders

This group of disorders are clinically and phenotypically distinct from the previously described loss-of-function PH disorder, allowing the conservation of the reading frame hence resulting in full-length mutant FLNA protein. The missense mutations cluster in discrete regions within the FLNA domains resulting in otopalatodigital spectrum malformation disorders (OPD). These include four phenotypically related X-linked human disorders; otopalatodigital syndrome types 1 (OPD1) and 2 (OPD2), frontometaphyseal dysplasia (FMD) and Melnick–Needles syndrome (MNS), which all lead to skeletal disorders (Robertson S.P. *et al.*, 2003). The group of OPD disorders have a diverse range of clinical symptoms including; skeletal malformations, cardiac defects, hernias and cleft palates (Robertson S.P., 2007, Robertson S.P., 2005).

The OPD spectrum disorders present with varying degrees of severity ranging from mild skeletal dysplasia to prenatal lethality in males depending on the location and recurrence of the mutation. Mutations leading to the different OPD disorders have been identified to cluster in four regions within *FLNA*; the ABD, repeats 3, 10, 14, and 15, while skewed X-inactivation in females correlates with the severity of the OPD disorders making it less predictable (Figure 1.7) (Robertson S.P. *et al.*, 2003, Robertson S.P. *et al.*, 2001, Sheen V.L. *et al.*, 2002).

Studies indicate that the OPD spectrum disorders lean towards an altered or gain-of-function mechanism based on the observations of the clinical distinctions of OPD from

the loss-of-function PH disorder, the clustering of point mutations, the skewed X-activation in females, and mutations in ABD increased affinity to F-actin, implicating FLNA in multiple functions during embryonic development (Sheen V.L. *et al.*, 2002, Robertson S.P. *et al.*, 2003, Robertson S.P. *et al.*, 2001, Robertson S.P., 2007, Robertson S.P., 2005, Clark A.R. *et al.*, 2009). However, the underlying biochemical mechanism of OPD and the cellular functions of FLNA remain unclear. Further understanding of mutations within FLNA will provide new insights into the complex molecular mechanism of FLNA and its human disorders.

1.5.2.1 *OPD1 and OPD2*

Males with OPD 1 are characterised with having the mildest phenotype of the OPD spectrum disorders. Clinical symptoms include mild skeletal anomalies, cleft palate, conductive deafness, supraorbital hyperostosis, characteristic dysmorphism, reduced stature and abnormal digits (Dudding B.A. *et al.*, 1967). While, males with OPD2 have more severe skeletal dysplasias in comparison to OPD1, typically characterised by bowed bones, absent or small digits, mental retardation, as well as craniofacial disorders (Fitch N. *et al.*, 1983).

In females these conditions are usually mild, however can occasionally manifest with a more severe phenotype (Gorlin R.J. *et al.*, 1973, Robertson S.P. *et al.*, 2001). All mutations associated with OPD1 to date have been identified in the CH2 of the ABD, while mutations in the CH2 of ABD and repeat domains 14-15 lead to OPD2 (Robertson S.P. *et al.*, 2003). Mutations of the CH2 region of ABD have shown an increased binding affinity of the FLNA to F-actin, supporting the gain-of–function mechanism (Robertson S.P. *et al.*, 2003, Clark A.R. *et al.*, 2009).

1.5.2.2 *FMD*

FMD in males presents with distinctive symptoms from OPD1 and 2 including; severe skeletal dysplasia, facial manifestations, deafness, septal heart defects and urogenital defects (Gorlin R.J. and Cohen M.M., 1969), while in females lead to substantial skeletal dysplasia (Robertson S.P. *et al.*, 2006).

FMD mutations are the most widely located in different regions of FLNA; CH2 of ABD, in repeats 3, 10, 14, and 22–23 (Robertson S.P. *et al.*, 2003). However, some mutations result in different severities depending on their location, the two associated

mutations of FMD in repeat 10 domain; P1223L and V1249A were identified to lead to prenatal lethality in males (Robertson S.P. *et al.*, 2006, Robertson S.P. *et al.*, 2003) suggesting importance of this region on FLNA function.

1.5.2.3 *MNS*

MNS is the most severe disease of the OPD spectrum disorder that is mostly characterised in heterozygous females, and leads to severe skeletal dysplasia, as it causes prenatal or early post-natal death in males (Robertson S.P. *et al.*, 2003). Females with MNS have distinctive features such as irregular ribs, bowed long bones, short stature, thoracic restriction and unimpaired intelligence that may lead to death depending on severity (Melnick J.C. and Needles C.F., 1966, Robertson S.P. *et al.*, 2003, Robertson S.P., 2007).

All cases of MNS were found to associate with missense mutations within repeat domain 10 of FLNA resulting in substitution of residues, suggesting the importance of this region of FLNA for its associated binding partners and function. Two highly recurrent mutations A1188T and S1199L were identified to correlate with MNS that are physically situated near the N-terminal or C-terminal region of FLNA repeat 10, respectively (Robertson S.P. *et al.*, 2003, Page R.C. *et al.*, 2011), suggesting a specific single mechanism for causing this disorder. This suggests that specific regions of FLNA mediate very specific functions linking this strong genotype–phenotype correlation.

1.6 FLNA repeat 10 and diseases

Curiously, the majority of missense mutations correlated with severe forms of the otopalatodigital syndrome spectrum disorders; MNS and FMD were identified to be clustered within the FLNA repeat 10 domain. All cases of lethal MNS and two of the three known mutations correlated with lethal FMD are located in FLNA repeat 10 (Feng Y. and Walsh C.A., 2004, Robertson S.P., 2007, Robertson S.P. *et al.*, 2003, Robertson S.P. *et al.*, 2006). Significantly, mutational hotspots in FLNA repeat 10 are conserved in vertebrates and distantly related phyla, where sequence alignment and comparison to the structure of *Dictyostelium* rod-domain repeat 5 suggests that the mutations do not greatly alter the structure (McCoy A.J. *et al.*, 1999). As the FLNA repeat 10 domain is a mutational hotspot leading to different OPD spectrum disorders it is signifies its importance. However, binding partners of the FLNA repeat 10 domain is one of the least characterized. Initial studies suggested that these mutations might disrupt

interactions of FLNA repeat 10 domain with binding partners or lead to significant changes in its structure or stability. One binding partner of FLNA repeat 10 domain that has been characterised is the T-cell receptor CD4 at the cytoplasmic domain, which, plays an important role in the human immunodeficiency virus entry into immune cells. (Jimenez-Baranda S. *et al.*, 2007).

An early model suggests that F-actin binding occurs initially through the ABD, then further binding of the FLNA strand to F-actin stabilizes the branched configuration (Gorlin J.B. *et al.*, 1990). Preliminary binding studies revealed that not only the ABD alone binds actin, but it suggested that other regions of the FLNA molecule, presumably the Ig repeat domains, are likely to contribute to the overall binding strength of the intact FLNA towards F-actin (Nakamura F. *et al.*, 2007, Nakamura F. *et al.*, 2011) as observed for other muscle proteins; paladin and kettin (Dixon *et al.*, 2008, Ono *et al.*, 2006). Studies used constructs containing fragments of FLNA to characterise whether different actin binding sites in FLNA were present. F-actin co-sedimentation assays in fact revealed that a construct including repeats 9–15 domains displayed F-actin binding capacity, suggesting a role for repeat domains in actin interaction (Nakamura F. *et al.*, 2007, Nakamura F. *et al.*, 2011). To define the repeat domain involved in binding to F-actin, further actin co-sedimentation assays were conducted then were analysed using electron microscopy (EM) with three-dimensional reconstruction (3DEM). 3DEM revealed that not only the CH domain of the ABD was able to bind to F-actin, but repeat 10 domain of FLNA also showed a statistically significant increase in density of structure in comparison to the other constructs reflecting the association to F-actin. Moreover, binding of repeat 10 domain to F-actin showed discrete differences in density when compared to the intact FLNA molecule, which is consistent with idea of being an additional contributor to the binding of F-actin (Figure 1.8). However, the idea that other domains *in vivo* may favour or contribute to the F-actin interactions of FLNA repeat 10, that was not observed under conditions *in vitro* (Suphamungmee W. *et al.*, 2012), cannot be dismissed.

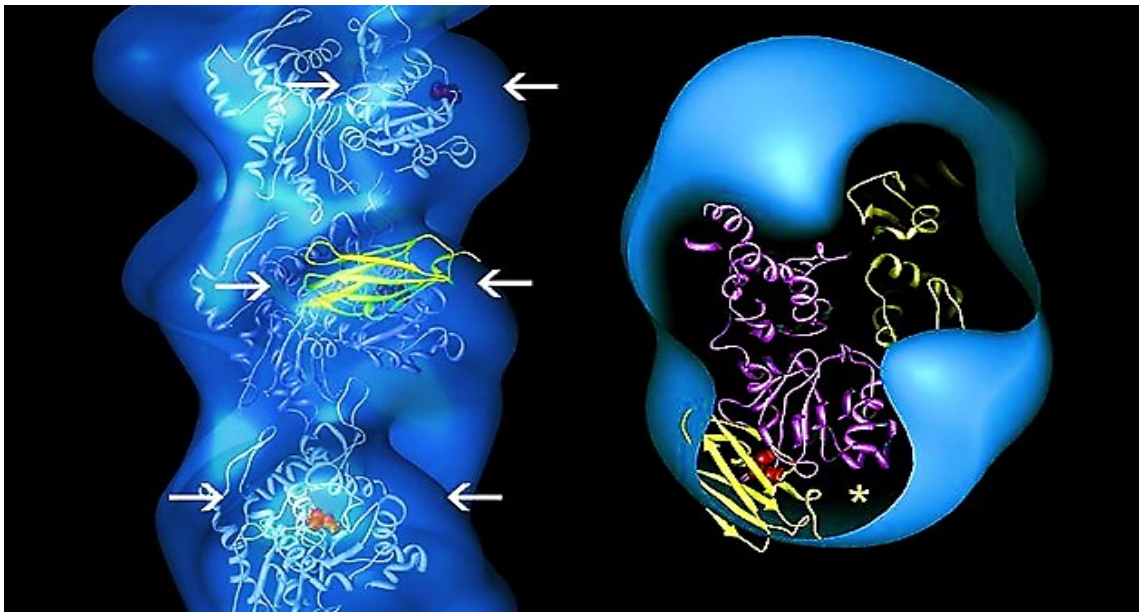

Figure 1.8 Fitting the Filamin A repeat 10 domain crystal structure within the N-terminal F-actin.

A. The FLNA repeat 10 crystal structure bound to F-actin reconstructed using electron microscopy, **B.** Cross-section of the FLNA repeat 10 - F-actin interaction. FLNA repeat 10 crystal structure in yellow, F-actin in blue, aspartate residue representing N-terminus of F-actin in red, volume occupied by actin in magenta and olive, unoccupied volume indicated by an asterisk. Adapted from (Suphamungmee W. *et al.*, 2012).

Modelling the binding of F-actin to FLNA repeat 10 domain suggests that the crystal structure of FLNA repeat 10 docks near the N-terminus of the F-actin, however, the orientation and polarity of the repeat 10 domain during binding remains theoretical (Suphamungmee W. *et al.*, 2012). A model where electrostatic interactions between a region of negatively charged amino acids on the N-terminus of F-actin and complementary region of basic residues (Lys1162, Lys1164, Arg1172, Lys1234, and Lys1246) on repeat 10 domain of FLNA may be the driving force for this interaction (Figure 1.8) (Page R.C. *et al.*, 2011). The conserved basic amino acids have been proposed to form a groove allowing an interface for the interaction to the acidic residues of F-actin. However, as other FLNA repeat domains contain these conserved residues and were unable to interact with F-actin (Nakamura F. *et al.*, 2007) another factor must play a role in facilitating this interaction. The overall Ig-fold of repeat domains between classes is very similar however; homology models and sequence alignments have revealed that slight differences within the structure occur due to the sequence, therefore

allowing for the different preferences of binding partners and functions (Ithychanda S.S. *et al.*, 2009). It has been proposed that neighbouring residues to the basic amino acid groove may allow this interaction to occur, however, is not fully understood.

A model for the FLNA cytoskeletal interaction has been proposed, where weakly interacting ABD and repeat 10 domain of FLNA cooperatively promote FLNA binding to F-actin resulting in a stronger interaction, while allowing flexibility and binding to other ligands. Then nearby filaments cross-link to form a mechanically organised network, which can be disrupted due to the weak interactions between FLNA and F-actin during cytoskeletal remodelling (Suphamungmee W. *et al.*, 2012). The binding mechanism of weakly interacting domains during FLNA to F-actin binding may suggest a common mechanism for organising the actin cytoskeleton. This was established for tropomyosin binding to F-actin through multiple weakly interacting pseudo-repeats (Li X. E. *et al.*, 2011) and has been suggested for; myosin-binding protein C (Shaffer J.F. *et al.*, 2009), elongated dystrophin and utrophin (Sutherland-Smith A.J. *et al.*, 2003).

Recurrent mutations in FLNA repeat 10 that had originally arisen *de novo* were observed to lead to either MNS or FMD, residues associated with these severe diseases are buried, with predicted minimal side-chain solvent exposure. The recurrent mutations A1188T and S1199L correlated with MNS (Robertson S.P. *et al.*, 2003) are located near the N-terminal or C-terminal region of FLNA repeat 10, respectively. A1188 in FLNA has been proposed to act as an end cap for the hydrophobic core of FLNA repeat 10 domain (Page R.C. *et al.*, 2011). The mutation of alanine to threonine at this position has been proposed to lead to disruptions of the BC loop due to clashes with side chains of Val1163, Cys1185 and Tyr1235, promoting disorder of the hydrophobic packing. While, the S1199L mutation would result in significant disruption of the CD-loop region due to extensive clashes with the side chains of Tyr1229, Leu1203, Ala1201 and the backbone of Glu1200 and Pro1204 (Page R.C. *et al.*, 2011).

The P1223L and V1249A mutations have been identified to correlate with lethal FMD in males (Robertson S.P. *et al.*, 2006, Robertson S.P. *et al.*, 2003). These residues are situated near the carboxy-terminal end of the FLNA repeat 10 hydrophobic core. Mutation P1223L would lead to large steric clashes with nearby residues and would alter loops AB and EF resulting in a distortion of the FLNA repeat 10 structure. Peculiarly, mutation V1249A does not lead to steric clashes with other residues, but it is

correlated with severe FMD; alternatively, it has been suggested to alter the hydrophobic packing however its mechanism of how this mutation affects the structure of FLNA remains unclear (Page R.C. *et al.*, 2011). These mutations imply the importance of hydrophobic packing in FLNA repeat 10 domain, which possibly reduce the stability and impairs folding as the structure is disrupted.

As previously shown in the ABD of FLNA (Clark A.R. *et al.*, 2009) and FLNB (Sawyer G.M. *et al.*, 2009), mutations in these domains resulted in a reduced stability, and an increased affinity for F-actin which suggests that the OPD causing mutations in FLNA repeat 10 domain may also increase its binding to F-actin and cause a distortion of structure, consistent with a gain-of-function mechanism for OPD.

Nonetheless, high-resolution structures are needed in order to resolve the binding interface and specificity of the interaction between FLNA repeat 10 domain to F-actin. Additional studies are also required to define how these disease-causing mutations affect the stability, structure, and binding of FLNA repeat 10 to F-actin

1.7 Aim

OPD male lethal diseases associated mutations have been demonstrated to cluster within repeat 10 domain of FLNA, which has been established to be involved in binding to F-actin (Suphamungmee W. *et al.*, 2012, Robertson S.P. *et al.*, 2003), however, FLNAR10 affinity towards F-actin was not determined. The precise effects and mechanisms leading to these diseases are yet to be revealed. Studies have suggested that distortion of structure may lead to an increase in binding to F-actin causing these diseases, consistent with a gain-of-function mechanism for OPD (Page R.C. *et al.*, 2011, Clark A.R. *et al.*, 2009).

The main objectives of this study were to initially express and purify the FLNA repeat 10 domain protein to determine its binding affinity towards F-actin. Furthermore, to determine whether FLNAR10 containing mutations associated with the OPD disorders lead to any changes in the proteins stability and affinity towards F-actin. This will permit for a better understanding of the FLNA mechanisms and its associated diseases.

2. Materials and Methods

2.1 Chemicals and media

2.1.1 Chemicals

Unless specified otherwise, all water used for this work was milliQ, which was purified over two ion-exchange filters and two organic filters in a Barnstead NANOpure II system (Thermo scientific). MilliQ will be referred to as either water or H_2O throughout this thesis. Chemicals that used were of the highest grade available.

2.1.2 Sterilisation

Media and buffers were sterilised by autoclaving at 121℃ for 20 minutes. Solutions that have undergone autoclaving will be referred to as sterile in this thesis.

2.1.3 Luria-Bertani (LB) medium

Luria broth (LB) media (Invitrogen) was made up at a concentration of 25 g/L with H_2O then was sterilised. LB agar plates were made up with 25 g/L of LB and 15 g/L of Agar bacteriological (Oxoid) dissolved in H_2O before being sterilised then poured into plates. Ampicillin was added to LB growth media or LB agar at a concentration of 100 µg/ml from a 100 mg/ml stock after autoclaving to maintain plasmids in *E. coli*. LB media or LB agar containing ampicillin will be referred to as LB-amp or LB amp plates, respectively throughout this thesis.

2.1.4 Ampicillin

Ampicillin (Sigma) stock solutions were prepared at a concentration of 100 µg/ml in H_2O, filter sterilised through 0.22 µm minisart filters (Sartorius Stedim), and then stored as 1 ml aliquots in sterile Eppendorf tubes at -20℃ for later use.

2.2 Electrophoresis methods

2.2.1 Agarose Gel Electrophoresis

Agarose gels were made up by dissolving agarose (AppliChem) in TAE buffer (40 mM Tris, 20 mM acetic acid, 1 mM EDTA pH 8.6) based on w/v and heated in a microwave until the boiling stage was achieved. The solution was slightly cooled then poured into a gel casting apparatus (Owl™ EasyCast™ Mini Gel Electrophoresis System, Thermo Scientific) and left to set. DNA samples were mixed at a 1:1 (v/v) ratio with 6× sample loading buffer (30% glycerol, 0.25% bromophenol blue) before being loaded onto the gel and run at 100 V until the dye front migrated to the end of the gel. Gels were then

stained in ethidium bromide solution (0.5 µg/ml in H_2O) for 30 minutes before being transferred to H_2O for 15 minutes to remove residual stain. Gels were visualized using a BioRad GelDoc XR gel documentation system and Image Lab™ software.

2.2.2 SDS-PAGE Gel Electrophoresis

Proteins were separated based on size using SDS-PAGE gel electrophoresis according to Laemmli (Laemmli U.K., 1970). Gels were prepared as outlined in Tables 2.1 and 2.2 before being cast and run using Mighty Small™ II Mini Vertical Electrophoresis System (Hoefer™). A 1:1 ratio of 6× sample treatment buffer (Table 2.3) to sample were boiled for 5 minutes before being loaded onto the gel. Electrophoresis was performed using running buffer (Table 2.4) at room temperature at 200 V until the dye front reached the bottom of the gel (approximately 40 – 50 minutes). Gels were then stained using either Coomassie blue or silver staining (Section 2.2.2.1 & 2.2.2.2) before being destained, then visualized using a BioRad GelDoc XR gel documentation system and Image Lab™ software.

Table 2.1 Preparation of Separating Gel for SDS-PAGE.

Component	**12.5%**	**15%**
H_2O	3.1 ml	2.3 ml
1.5 M Tris-HCl, pH 8.8	2.5 ml	2.5 ml
10% SDS	100 µl	100 µl
30% Acrylamide:Bis 29.1	4.2 ml	5 ml
10% ammonium persulfate	100 µl	100 µl
TEMED	5 µl	5 µl
Total Volume	**10 ml**	**10 ml**

Table 2.2 Preparation of Stacking Gel for SDS-PAGE.

Component	4%
H_2O	3.05 ml
1.5 M Tris-HCl, pH 6.8	1.25 ml
10% SDS	50 µl
30% Acrylamide:Bis 29.1	0.65 ml
10% ammonium persulfate	50 µl
TEMED	5 µl
Total Volume	**10 ml**

Table 2.3 Preparation of 6× Sample treatment buffer.

Component	Concentration
0.5 M Tris-HCl, pH 6.8	0.35 M
SDS	0.35 M
Glycerol	30% v/v
DTT	0.6 M
Bromophenol Blue	0.175 mM

Table 2.4 Preparation of 5X running buffer.

Component	Amount
Tris base	30.3 g
Glycine	72 g
SDS	2.5 g
	Made up to 500 ml with H_2O

2.2.2.1 *Coomassie Blue Staining of SDS-PAGE Gels*

Gels were stained with Coomassie stain (0.025% (w/v) Coomassie Brilliant Blue R-250 in 40% methanol, 7% acetic acid) for 30 minutes (or overnight) with gentle agitation. Destaining was performed by replacing stain solution with destain solution (40% methanol, 7% acetic acid) and incubating until background staining was removed (overnight). The gel was placed into H_2O and then visualized using BioRad GelDoc XR gel documentation system and Image Lab™ software.

2.2.2.2 *Silver Staining of SDS-PAGE Gels*

Silver staining detects proteins with increased sensitivity of less than 1 ng of protein in comparison to Coomassie staining of 100 ng (Weiss W. *et al.*, 2009). All steps were performed with gentle agitation. Gels were initially fixed in fixing agent (50% methanol, 12% acetic acid, 0.05% of formaldehyde (35%)) overnight then rinsed with H_2O three times for 5 minutes. Gels were then washed in sensitizing buffer (0.02% $Na_2S_2O_3$) for 2 minutes then rinsed with H_2O three times for 5 minutes. The gels were then stained in silver nitrate stain (0.2% $AgNO_3$, 0.05% of formaldehyde (35%)) for 20 minutes then washed twice with H_2O for 1 minute before the addition of developer solution (6% Na_2CO_3, 0.05% of formaldehyde (35%) and 0.0004% $Na_2S_2O_3$). The reaction was stopped by washing the gel with stop solution (50% methanol, 12% acetic acid) for 5 minutes, after which it was washed in H_2O. Gels were visualized using BioRad GelDoc XR gel documentation system and Image Lab™ software and stored in 1% acetic acid at 4℃.

2.3 Measurement of Nucleic Acid Concentration

The nucleic acid concentration was measured on a Nanodrop ND-1000 spectrophotometer (Thermo Scientific) at both 260 and 280 nm using ND-1000 software V3.1.0 to convert absorbances into concentrations.

2.4 Measurement of Optical Density of cultures

The optical density (OD) of a cell culture was measured on a Smart Spec^{TM} Plus Spectrophotometer (BioRad) at 600 nm. Sterile LB media was used as blank.

2.5 Measurement of Protein Concentration

Protein concentrations were measured using a Nanodrop ND-1000 spectrophotometer (Thermo Scientific) at an absorbance of 280 nm (A_{280}) with appropriate buffers used to zero instrument. Protein concentrations were calculated using Beers Law with the appropriate extinction coefficient calculated by ExPASy-ProtParam (http://web.expasy.org/protparam/).

2.6 Plasmids and Bacterial Strains used

FLNA repeat 10 cDNA was derived from two previously cloned plasmids containing FLNA cDNA. A pGEX 4T3 plasmid containing FLNA repeat 10 cDNA (from amino acid 1158 - 1252) was donated by Ben Waite and a pFastBac plasmid containing full

length FLNA cDNA was donated by Manohar Mulinti. These will be referred to as pGEX-FLNAR10 and pFastBac-FLNA in this thesis.

The pPROEX HTb (Invitrogen^{TM}) plasmid encodes an N-terminal His-tag that was used as a cloning vector for the FLNA repeat 10 cDNA to enable the production of recombinant protein expression with a Ni^{2+} affinity tag. The plasmid also contains a tobacco etch virus (TEV) protease site to allow the removal of the His-tag by the rTEV protease (refer to 9.1.1).

Cloning of the recombinant plasmid was carried out using the *E. coli* cell strain Top10 (Invitrogen^{TM}), and protein expression was obtained using the BL21 *E. coli* cells (Invitrogen^{TM}).

2.7 Transformation of *E. coli* Cells

2.7.1 Preparation of Chemically Competent cells

Initially, chemically competent cells were made capable of transformation by growing the desired *E. coli* strain onto an LB plate at 37℃ overnight. A single colony from the LB plates was inoculated into 5 ml of LB and grown overnight at 37℃ as a starter culture. Then 2 ml from the initial starter culture was inoculated into 200 ml of LB and grown further to an OD of approximately 0.5-0.7 before being centrifuged at 4,000 × g for 10 minutes at 4℃. The supernatant was discarded, while the cell pellet was resuspended in 80 ml of transformation buffer 1 (30 mM KOAc, 100 mM $RbCl_2$, 10 mM $CaCl_2$, 50 mM $MnCl_2$, 15% glycerol, pH 5.8) and incubated on ice for 5 minutes. The resuspended cells were centrifuged and the supernatant discarded as described previously, after which the pellet was resuspended in 4 ml of transformation buffer 2 (10 mM MOPS/KOH pH 6.5, 75 mM $CaCl_2$, 10 mM $RbCl_2$, 15% glycerol) and stored in 100 µl aliquots at -80℃.

2.7.2 Transformation of chemically competent cells

Plasmids were transformed into the chemically competent Top10 *E. coli* strain by firstly adding 2 ng of plasmid DNA to 100 µl of thawed competent Top10 cells then incubating on ice for 10 minutes. The cells were heat shocked at 42℃ for 90 seconds in a TS1 Thermoshaker heating block (Biometra) and then placed on ice for 2 minutes. The cells were incubated for 30 - 40 minutes at 37℃ then plated onto sterile LB-amp plates and incubated at 37℃ overnight.

2.7.3 Plasmid Isolation

A single colony from an overnight LB-amp agar plate was inoculated into 5 ml of LB-amp and grown overnight at 37℃ with shaking. The culture was harvested by centrifugation and the plasmid was purified using a High Pure Plasmid Isolation Kit (Roche) according to the manufacturer's instructions.

2.8 Cloning

2.8.1 Bioinformatics and sequence analysis

Based on the previous literature (Page R.C. *et al.*, 2011, Robertson S.P. *et al.*, 2003) there were slight disagreements with the domain boundaries for FLNA, therefore protein domain boundary predictions were performed and aligned by running the FLNA FASTA sequence (NCBI) through pFAM (http://pfam.xfam.org/), SMART (http://smart.embl-heidelberg.de/) and UniProt (http://www.uniprot.org/) databases. The N-terminus of FLNA repeat 10 was selected to start at amino acid 1155 or 1158 and the C-terminus to end at amino acid 1252, to include the site for the 1249 mutation.

2.8.2 PCR primer design

Forward and reverse primers (Sigma) were designed using primer-BLAST software (http://www.ncbi.nlm.nih.gov/tools/primer-blast/, NCBI) to contain *Bam*HI and *Sal*I restriction sites respectively (refer to 9.1.1), in order to clone FLNAR10 1155, and FLNAR10 1158 into matching sites within the pPROEX HTb expression vector.

2.8.3 PCR

PCR was carried out with solutions (Table 2.5) mixed in thin walled PCR tubes and put on ice before being subjected to temperature cycling in Mastercycler ep gradient S (Eppendorf) as outlined in Table 2.6. PCR products were confirmed on a 1% agarose gel (refer to 2.2.1) and purified using a High Pure PCR Product Purification Kit (Roche) according to manufacturer's instructions.

Table 2.5 PCR reaction components.

Solution	Volume	Final concentration
DNA sample (10 ng/ul)	1 µl	0.2 ng
10 µM dNTPs mix	1 µl	0.2 µM
10 × Pwo SuperYield PCR buffer with Mg^{2+}	5 µl	1 ×
25 mM $MgSO_4$	1.5 µl	0.75 mM
Forward primer (10 pmol)	2 µl	0.4 pmol
Reverse primer (10 pmol)	2 µl	0.4 pmol
H_2O	36.5 µl	-
Pwo SuperYield DNA polymerase (5 U/µl)	1 µl	0.1 U/µl
Total volume	**50 µl**	

Table 2.6 Thermal cycling PCR protocol.

Process	Temperature	Time	Repeat
Denaturation	95℃	3 minutes	-
Denaturation	95℃	30 seconds	30 cycles
Annealing	57℃	30 seconds	
Extension	68℃	1 minute	
Extension	68℃	1 minute	-

2.8.4 Restriction digest

Restriction digests were carried out on PCR products FLNAR10 1155, FLNAR10 1158, and the pPROEX HTb vector using *Bam*HI and *Sal*I (Roche) enzymes as outlined in Table 2.7. Reactions were then incubated for 3 hours at 37℃ and stored at -20℃ for later use.

Digestion products were confirmed on a 1% agarose gel (refer to 2.2.1) and purified using a High Pure PCR Product Purification Kit (Roche) according to the manufacturer's instructions. DNA concentrations were then determined using a Nanodrop spectrophotometer (Thermo Scientific) (refer to 2.3).

Table 2.7 Restriction digest protocol.

Solution	**Uncut**	***Bam*HI (single digest)**	***Sal*I (single digest)**	***Bam*HI/*Sal*I (double digest)**
DNA (PCR product or vector)	3 µl	10 µl	10 µl	10 µl
10 × buffer H	3 µl	3 µl	3 µl	3 µl
H_2O	24 µl	16 µl	16 µl	15 µl
*Bam*HI	-	1 µl	-	1 µl
*Sal*I	-	-	1 µl	1 µl
Total volume	**30 µl**	**30 µl**	**30 µl**	**30 µl**

2.8.5 Ligation

Ligation reactions were setup in a total volume of 30 µl containing 1x T4 ligation buffer, 1 U of T4 DNA ligase (Roche) and a 3:1 molar ratio of insert to vector per ligation reaction. The ligation reaction was then incubated for 2 hours at room temperature to allow the enzyme to covalently link the two ends of the DNA together. A ligation reaction without the insert was also performed as a negative control.

2.8.6 Transformation

Initially, 15 µl of ligation reaction was added to 100 µl of thawed competent Top10 cells transformed following protocol 2.7.2 and plated onto sterile LB-amp plates then incubated at 37℃ overnight. The plasmid was isolated following protocol 2.7.3, then it was digested with restriction enzymes (refer to 2.8.4) and ran on a 1.5% agarose gel (refer to 2.2.1) to ensure the insert of the appropriate size was present.

2.8.7 Colony PCR Screening

Using pPROEX HTb forward and M13 reverse sequencing primers (refer to 9.1.1) colony PCR was carried out to determine the colonies that contained the recombinant plasmid. A single colony was picked from the LB-amp plates (refer to 2.8.6) and swirled into the PCR mix (Table 2.8) in PCR tubes before being subjected to temperature cycling in a Mastercycler ep gradient S (Eppendorf) thermocycler as outlined in Table 2.6. PCR products were then run on a 1% agarose gel to check for the presence of product (insert).

Table 2.8 Colony PCR protocol.

Solution	Volume	Final concentration
DNA sample	Colony	-
5 µM dNTPs mix	1 µl	0.125 µM
10 × Taq buffer with Mg^{2+}	5 µl	1.25 ×
50 mM $MgCl_2$	1.5 µl	1.875 mM
Forward primer (5 pmol)	1 µl	0.125 pmol
Reverse primer (5 pmol)	1 µl	0.125 pmol
H_2O	29.5 µl	-
Taq DNA polymerase (1 U/µl) (Roche)	1 µl	0.025 U/µl
Total volume	**40 µl**	

2.8.8 Sequencing

Sequencing was performed by the Massey Genome Service (Massey University, Palmerston North), using a capillary ABI3730 Genetic Analyzer (Applied Biosystems Inc.). Reactions were performed in a total volume of 15 µl, containing approximately 200 ng/µl plasmid and 3.2 pmol of pPROEX HTb and M13 reverse primers (refer to 9.1.1 - 9.1.4). Sequences were viewed using FinchTV software (version 1.4, Geospiza®) and confirmed through sequence alignment using BLAST® (http://blast.ncbi.nlm.nih.gov/Blast.cgi, NCBI).

2.8.9 Whole plasmid PCR mutagenesis

2.8.9.1 *Mutagenesis Primer Design*

Forward and reverse primers (Sigma) were designed using QuikChange® Primer Design software (Genomics, Agilent Technologies) containing missense mutations; V1249A, A1188T, and S1199L, in order to carry out whole plasmid PCR mutagenesis (refer to 9.1.1).

2.8.9.2 *Whole plasmid PCR mutagenesis*

Mutagenesis was carried out based on the Quikchange Site-directed mutagenesis protocol (Agilent Technologies) to generate mutant constructs. PCR reactions were setup in a total volume of 50 µl as outlined in Table 2.9, and then subjected to

temperature cycling (as outlined in Table 2.10) in a Mastercycler ep gradient S (Eppendorf) where extension time was based on 1 minute per Kb**.**

Table 2.9 Whole plasmid PCR mutagenesis components.

Solution	Volume	Final Concentration
DNA sample (10 ng/µl)	1 µl	0.2 ng
10 µM dNTPs mix	1 µl	0.2 µM
10 × KOD buffer with Mg^{2+}	5 µl	1 ×
25 mM $MgSO_4$	3 µl	1.5 mM
Forward primer (100 ng/µl)	1.25 µl	125 ng
Reverse primer (100 ng/µl)	1.25 µl	125 ng
H_2O	36.5 µl	-
KOD Hot Start DNA polymerase (1 U/µl) (Novagen)	1 µl	0.02 U/µl
Total Volume	**50 µl**	

Table 2.10 Whole plasmid PCR mutagenesis Thermal cycling protocol.

Process	Temperature	Time	Repeat
Denaturation	95℃	30 seconds	-
Denaturation	95℃	30 seconds	12 cycles
Annealing	55℃	1 minute	
Extension	68℃	5 minutes	

The PCR samples were put on ice for 2 minutes followed by the addition of 0.5 µl of 20 U/µl *Dpn*I restriction enzyme (Roche) in order to digest the wild-type parental DNA template and incubation for an hour at 37℃. The samples were heat inactivated for 20 minutes at 80℃ before a ligation reaction was carried out to ensure circular DNA was reformed as outlined in Table 2.11. Transformation using 10 µl of *Dpn*I digested sample was added to 50 µl of thawed Top10 competent *E. coli* cells then incubated on ice for 30 minutes. The cells were heat shocked at 42℃ for 45 seconds in a TS1 Thermoshaker heating block (Biometra) and placed on ice for 2 minutes. The cells were added to 500 µl of preheated LB media following incubation for an hour at 37℃, while shaking. Then 150 µl of the sample was plated onto sterile LB-amp plates and incubated at 37℃

overnight (16 hours). Plasmid isolation was then carried out as previously described in 2.7.3, and sequenced (refer to 2.8.8) to check that the correct mutation had been obtained.

Table 2.11 Whole plasmid PCR mutagenesis ligation reaction.

Components	Volume
DNA	15 µl
T4 10 × buffer	6 µl
H_2O	8 µl
DNA ligase	1 µl
Total	**30 µl**

2.9 Protein Expression and Solubility Trials

To assess the expression and solubility of the recombinant FLNA repeat 10 protein, *E. coli* BL21 (DE3) cells were transformed with approximately 50 ng of plasmid DNA following protocol 2.7.2. A single colony from the LB-amp plates was inoculated in 3 ml of LB-amp and grown to an OD between 0.5-0.7 at 37℃. Protein expression was then induced by the addition of IPTG (Isopropyl-β-D-thio-galactoside) to a final concentration of 0.5 mM. The cultures were then left to grow for either 2, 4 or 18 (overnight) hours to determine optimum expression time, before being pelleted via centrifugation at 14,000 × g for 1 minute at 4℃ and the pellets were then frozen at -20℃. The frozen cell pellets were thawed at room temperature and resuspended in 750 µl PBS buffer and subjected to sonication to achieve lysis. The whole cell extract was centrifuged at 3,000 × g for 15 minutes to pellet unlysed cells, cellular debris and insoluble protein, then the supernatant was removed into a separate tube, while the pellet was resuspended in 700 µl 1 × PBS (Table 2.12). The supernatant, resuspended pellet and an uninduced sample were then analysed by SDS-PAGE gel (refer to 2.2.2).

Table 2.12 1 × PBS buffer components.

Components	Concentration (mM)
NaCl	137
KCl	2.7
Na_2HPO_4	10
KH_2PO_4	1.8

2.10 Scaled-up Protein Expression and Purification

2.10.1 Induction and Expression

E. coli BL21 (DE3) cells were transformed with approximately 50 ng of plasmid DNA following protocol 2.7.2. A single colony from the LB-amp plates was inoculated in 50 ml of LB-amp and grown overnight at 37℃ with shaking as a starter culture. The starter culture was added to 2 L of LB-amp and grown to an OD between 0.5-0.7 at 37℃. Protein expression was then induced by the addition of IPTG to a final concentration of 0.5 mM followed by the incubation of the cultures for a further 4 hours (optimum expression time determined in 2.9). The cultures were then harvested via centrifugation (Thermo Scientific) at 4,000 × g for 15 minutes at 4℃ and the pellet was resuspended in 10 ml of 1 × PBS buffer (Table 2.12) to remove any remaining LB media. The resuspended pellet was centrifuged as previously and the resulting cell pellet was frozen at -20℃ for later use.

2.10.2 Cell Lysis

The frozen cell pellet was thawed at room temperature and resuspended in a final volume of 10 ml of buffer A (2 × PBS, 26 mM NaCl, 25 mM imidazole pH 7.4) containing cOmplete EDTA-free Protease Inhibitor Cocktail Tablet (Roche) at 1x concentration. Cells were then lysed in liquid homogenization using two passages through a French Press at 5 kPa, then sonicated and put on ice for 10 minutes. The whole cell extract was later spun at 14,000 × g for 20 minutes in a Mikro 22 R (Hettich Zentrifugen) to pellet any unlysed cells, cellular debris, and insoluble protein.

2.10.3 Ni^{2+}-NTA Affinity Chromatography

The clarified cell lysate (10 ml) was syringe-filtered through a 0.45 μm minisart filter (Sartorius Stedim) to remove any particulates before being loaded on to a pre-

equilibrated (with buffer A, 2 × PBS, 26 mM NaCl, 25 mM imidazole pH 7.4) 5 ml HisTrap™FF Ni^{2+}-NTA column (GE Healthcare). Using the ÄKTA protein purification system (GE Healthcare), protein was eluted over an increasing linear gradient between 25 - 400 mM imidazole buffer concentration using buffer A and buffer B to 80% (2 × PBS, 26 mM NaCl, 500 mM imidazole pH 7.4). A flow rate of 1.5 ml/min was used and fractions were collected in 2 ml which were analysed by SDS-PAGE gels (refer to 2.2.2). The fractions determined to contain the purest form of the protein of interest, were pooled together, and concentrated down to 0.5 ml in a 3 kDa cut-off vivaspin 20 concentrator (GE Healthcare).

2.10.4 Size Exclusion Chromatography

The pooled sample from Ni^{2+}-NTA Affinity Chromatography (refer to 2.10.3) was spun at 14,000 × g for 30 minutes and then 0.5 ml was loaded onto a pre-equilibrated (with SEC buffer, 1 × PBS, 1 mM DTT, 2 mM EDTA) Superdex 75 10/300 GL column (GE Healthcare). Using the ÄKTA protein purification system (GE Healthcare) the protein sample was eluted with the SEC buffer at a flow rate of 0.5 ml/min and fractions of 2 ml were collected then analysed by SDS-PAGE gels (refer to 2.2.2). The purest protein of interest fractions were pooled together, concentrated in a Nanosep 3K Omega concentrator (Pall Corporation) with a 3 kDa cut-off range then stored at 4℃ for later use.

2.11 Mass Spectrometry

2.11.1 Colloidal Coomassie Staining

Initially, SDS-PAGE gels were run then fixed in a solution containing; 40 % ethanol, and 10 % acetic acid with gentle agitation for 1 hour. Gels were then washed twice with H_2O for 10 minutes, before being stained with working Colloidal Coomassie stain (4:1, dye stock: methanol) overnight (Table 2.13). Gels were then washed in 1% acetic acid to remove any residual stain.

Table 2.13 Colloidal coomassie stock solution buffer.

Components	Concentration (w/v)
Coomassie Brilliant Blue G250	0.1%
Phosphoric acid	2%
Ammonium sulphate	10%
	Made up to 500 ml with H_2O

2.11.2 In-Gel Tryptic Digest

To characterize the protein bands, in-gel tryptic digestion followed by mass spectroscopy was carried out. After the gel was washed from the colloidal stain (refer to 2.11.1), the protein bands of interest were excised and sliced then placed in sterile 1.5 ml Eppendorf tubes. The gel pieces were destained by the repeated addition of 300 µl of fresh 50 mM ABC (ammonium bicarbonate - $(NH_4)HCO_3$) solution at 45℃ until the gel pieces became colourless, then the destain solution was discarded.

Dehydration of the gel pieces was achieved by the addition of 300 µl of 80% acetonitrile (MeCN-C_2H_3N) solution for 1 minute at room temperature. The MeCN solution was discarded and then the gel pieces were dried for 15 minutes under a vacuum using a SpeedVac centrifugational evaporator (Thermo Scientific).

The gel pieces were then reduced by the addition of 50 µl of fresh reducing agent (10 mM DTT in 50 mM ABC), followed by incubation for 1 hour at 37℃, while shaking to reduce any potential disulfide bonds. The reducing agent was discarded, followed by washing of the gel pieces with 50 mM ABC solution for 5 minutes and was then replaced with 80% MeCN solution for 1 minute before this solution was removed. The gel pieces were then dried using the SpeedVac for 10 minutes.

To rehydrate the gel pieces, 50 µl of fresh alkylation solution (20 mM iodoacetamide in 50 mM ABC) was added to them followed by incubation for 20 minutes in the dark at room temperature. The alkylation solution was discarded, then the gel pieces were washed in 50 mM ABC solution for 5 minutes and replaced twice with 80% MeCN for 1 minute. The remaining wash solution was discarded and the gel pieces were dried using a SpeedVac for 10 minutes.

Bands were digested with protease inhibitor (TPCK) treated trypsin (Proteomics Grade T6567, Sigma) (20 ng/µl Trypsin in 50 mM ABC) and incubated for 10 minutes on ice. The trypsin solution was discarded before the addition of 30 µl of 50 mM ABC solution to keep the gel pieces moist and incubated at 37℃ overnight.

After incubation, the samples were centrifuged briefly for 1 minute then sonicated for 2 minutes and the supernatant was collected in a new 1.5 ml Eppendorf tubes. 60 µl of extraction buffer 1 (5% formic acid in 80% MeCN) was added to the original tubes containing the gel pieces then sonicated for 2 minutes before the supernatant was pooled with the previous collection. 60 µl of extraction buffer 2 (0.1% formic acid in 80% MeCN) was further added to the original tubes containing the gel pieces then treated as previously described, the supernatant was combined with the previous collection. The collected supernatant samples were then concentrated down to 20 µl using the speedvac and transferred to HPLC sample vials.

Trevor Loo then processed samples, on an Agilent 6520 Q-TOF mass spectrometer (Agilent Technologies). Sample analysis was performed using Agilent MassHunter Workstation Qualitative Analysis software version B.03.01 (Agilent Technologies, Santa Clara, CA, USA) and by searches on Mascot servers (version 2.4.1) housed in Walter and Eliza Hall Institute (Melbourne, Australia).

2.12 High-performance liquid chromatography (HPLC)

A 0.20 mg/ml Wt FLNAR10 protein sample was loaded onto a Jupiter C18 column (4.6 × 250 mm 5 um 300A, Phenomenex) and run using an Ultimate 3000 analytical HPLC system (Dionex). The sample was run along a gradient from 0.1% TFA/water into 0.08% TFA/70% MeCN/water over 16 min at flow rate of 1 ml/min. Peak fractions were then collected manually into protein Lobind microcentrifuge tubes (Eppendorf) and analysed on an SDS-PAGE gel (refer to 2.2.2).

2.13 Protein temperature instability analysis

To analyse whether temperature affects the stability of Wt FLNAR10 protein, protein samples of 0.30 mg/ml were incubated overnight at a range of temperatures; -20, 4, 20, and 37℃. Then the samples were run on an SDS-PAGE gel and stained with Coomassie stain (refer to 2.2.2.1).

2.14 His-tag removal

The His-tag of the Wt FLNAR10 protein was removed using the rTEV protease. Wt FLNAR10 protein samples were incubated overnight with a 1:1 or 1:2 (w/w) ratio of rTEV to protein then the samples were run on SDS-PAGE gels (refer to 2.2.2).

2.15 Protease resistance analysis

FLNA repeat 10 protein samples were tested for protease resistance, using a ratio of 300:1 (w/w) of FLNA repeat 10 protein sample to either chymotrypsin or subtilisin (from JBS Floppy-choppy Jena Bioscience). Samples were treated at room temperature with either; chymotrypsin for 0, 60, 300 minutes and overnight or subtilisin for 0, 15, 180 minutes and overnight. Samples were then immediately denatured to end the reaction and analysed on SDS-PAGE gels (refer to 2.2.2).

2.16 Circular dichroism spectroscopy

CD spectra in the far-UV region (190-260 nm) were obtained using the Chirascan CD spectrometer (AppliedPhotophysics). A cell cuvette with 1 mm pathlength was used with a 0.07 mg/ml protein concentration at 20℃. For all protein samples 10 runs were performed with 1 nm readings taken every second followed by the data being averaged, smoothed and the baseline representing a buffer blank being subtracted.

CD thermal denaturation was then performed with the same parameters as previously mentioned. The temperature controller (Quantum Northwest TC 125™) was used to take readings every 5℃ between 5-90℃, with a 60 seconds equilibration time at each temperature. Smoothing and baseline subtraction on the CD thermal denaturation spectra were also carried out as before.

The CD units of millidegrees were converted into mean residual ellipticity units to take into account the concentration, and the size of the protein. Deconvolution of the CD spectra was also performed using CDNN software (version 2.0.3.188, AppliedPhotophysics) and further analysed using GraphPad Prism software (version 6.00 for Windows, GraphPad Software), CAPITO (http://capito.nmr.fli-leibniz.de/, Pubmed), and K2d3 (http://k2d3.ogic.ca/) online servers.

2.17 F-actin co-sedimentation assay

The FLNAR10 F-actin binding affinity was analysed by co-sedimentation assays based on the method from (Sawyer G.M. *et al.*, 2009). A vial of 1 mg of actin (cytoskeleton.com) was diluted with 100 µl of sterile water to a final concentration of 10 mg/ml and buffers were made up as outlined in Table 2.14 then stored at 4℃. In a sterile eppendorf tube, G-actin was prepared by initially diluting the 10 mg/ml actin to a final concentration of 5.6 mg/ml (133 µM) with buffer A (Table 2.14) and incubating on ice for 1 hour, before being spun at 14,000 × g for 15 minutes. G-actin was then polymerised in a 1:9 volume ratio of buffer C (Table 2.14) to G-actin (133 µM) and incubated for 1 hour at room temperature producing polymerised F-actin.

In polycarbonate centrifuge tubes (Beckman) various concentrations of FLNA repeat 10 protein samples were made up to 42 µl with 1 × PBS buffer (Table 2.12) and spun at 214,000 × g for 30 minutes at 25℃ to remove any precipitated protein. In new ultracentrifuge tubes 40 µl of the spun FLNA repeat 10 protein was added to 5 µl of buffer B (Table 2.14) and 5 µl of F-actin (or buffer E for controls) was also added. This mixture was incubated at room temperature for 45 minutes, followed by centrifugation at 214,000 × g for 45 minutes at 25℃.

The supernatant was removed without disrupting the pellet and placed in an Eppendorf tube with 10.4 µl of 6× sample treatment buffer (Table 2.3). The pellet was dislodged and resuspended in 50 µl of buffer D and 10.4 µl 6× sample treatment buffer (Table 2.3) then transferred to sterile Eppendorf tubes. Samples were run on SDS-PAGE gels, and the gels were analysed by densitometry using GelAnalyzer, GelQuant and further analysed using GraphPad Prism software (version 6.00 for Windows, GraphPad Software).

Table 2.14 Actin co-sedimentation assay buffers.

Components	Buffer A	Buffer B	Buffer C	Buffer D	Buffer E
10 × PBS	0.03 ×	1.3 ×	-	.13 ×	.13 ×
$MgCl_2$	-	20 mM	20 mM	2 mM	2 mM
Na_2ATP	0.2 mM	10 mM	10 mM	-	1 mM
DTT	0.5 mM	10 mM	-	-	1 mM
KCl	-	-	500 mM	-	-

3. Cloning of Filamin A repeat 10 domains

3.1 Introduction

To carry out biochemical studies on the repeat 10 domain of FLNA, the cDNA of human FLNA repeat 10 was cloned into the *E. coli* expression vector pPROEX HTb. Furthermore, constructs containing point mutations with the amino acid substitutions V1249A, A1188T, and S1199L associated with severe forms of OPD spectrum disorders were constructed by whole plasmid PCR mutagenesis. These disease-associated mutations, were selected as they are physically situated in different regions of the FLNA repeat 10 domain suggesting that a specific single mechanism may cause these disorders. Possible changes in the structure or packing of the FLNA repeat 10 domain that might cause disruptions in the interactions between FLNA repeat 10 domain its binding partners maybe caused by these mutations, suggesting a possible mechanism for these disorders by allowing a genotype–phenotype correlation.

3.2 FLNA Repeat 10 boundary

Based on the previous literature (Page R.C. *et al.*, 2011, Robertson S.P. *et al.*, 2003) and database analysis (Uniprot), the exact boundaries of the FLNA repeat domains vary in definition. The FLNA FASTA protein sequence was obtained from NCBI and analysed by; pFAM, SMART and UniProt database servers then were aligned (refer to 2.8.1). Two different N-termini starting either at amino acid 1155 or 1158 were selected to determine whether slight sequence differences lead to any differences in protein expression and solubility. The C-terminus end of FLNA repeat 10 sequence was selected to be at amino acid 1252 based on database analysis and in order to include the V1249A amino acid mutation within the protein (Figure 3.1).

Figure 3.1 FLNA repeat 10 domain boundary alignments.

Alignments of the FLNA repeat 10 domain sequence based on data from UniProt, pFAM, SMART servers and the X-ray structure of FLNA repeat 10 domain (Page R.C. *et al.*, 2011) (refer to 2.8.1) (grey shading). Highlighted areas represent the selected mutation sites for A1188T; green, S1199L; blue, and V1249A; yellow.

3.3 Cloning of human FLNA repeat 10 domain

Initially, FLNA cDNA was derived from pGEX-FLNAR10 or pFastBac-FLNA plasmids containing FLNA repeat 10 or full length FLNA, respectively (refer to 2.6). A trial using a double digest of *Bam*HI/*Sal*I restriction enzymes (based on 2.8.4) was carried out on the pGEX-FLNAR10 plasmid in order to clone out the FLNA repeat 10 cDNA. However, it revealed that no product (FLNA repeat 10 cDNA) had been produced as a result of inefficient digestion and supercoiled plasmid (not shown).

Therefore, PCR was instead carried out to amplify the FLNA repeat 10 cDNA from either the pGEX-FLNAR10 or pFastBac-FLNA plasmids (refer to 2.8.2 and 2.8.3). Different primer combinations were used in order to produce two constructs starting at the N-terminal amino acids 1155 or 1158, which were estimated by BLAST to produce fragments of approximately 294 bp or 285 bp in size, respectively. Primers that were used contained 5´-*Bam*HI and 3´-*Sal*I sites in order to allow cloning into the pPROEX HTb expression vector. Analysis of the PCR reactions on an agarose gel resulted in a fragment of approximately 300 bp to be produced, which is consistent with the previously estimated size of FLNA repeat 10 cDNA. However, the pGEX-FLNAR10 plasmid that was subjected to PCR using the FLNAR10 1155 primer had no observed product, as seen in lane 3 of Figure 3.2. This was concluded to occur as a result of the

FLNA repeat 10 cDNA sequence that was originally cloned into pGEX-4T3 plasmid only extended until amino acid 1158. Therefore, this construct was not used further in this study.

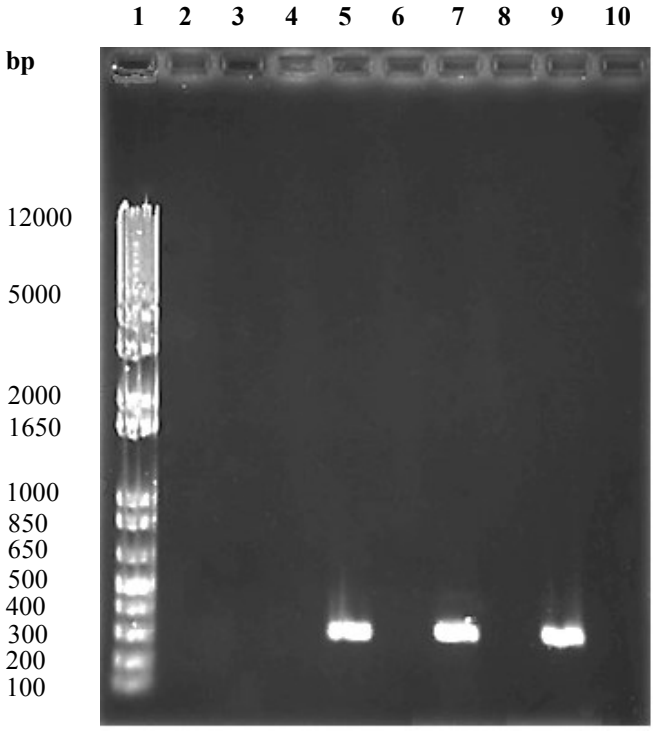

Figure 3.2 Agarose gel of PCR reaction products.

PCR reactions to amplify the FLNA repeat 10 cDNA were loaded onto a 0.5% agarose gel and run at 100 V for 70 minutes (refer to 2.8.3 and 2.2.1). PCR reactions were carried out using different primer combinations and plasmids containing FLNA repeat 10 (refer to 2.8.2). Lane 1; 1kb Plus™ ladder, Lane 3; pGEX-FLNAR10 plasmid with FLNAR10 1155 Forward and 1252 Reverse primers, Lane 5; pGEX-FLNAR10 plasmid with FLNAR10 1158 Forward and 1252 Reverse primers, Lane 7; pFastBac-FLNA plasmid with FLNAR10 1155 Forward and 1252 Reverse primers, Lane 9; pFastBac-FLNA plasmid with FLNAR10 1158 Forward and 1252 Reverse primers. All other lanes that were not mentioned were empty.

The pPROEX-HTb plasmid was cut with restriction enzymes *Bam*HI and *Sal*I to assess the efficiency of the restriction enzymes (refer to 2.8.4). The pPROEX-HTb expression vector was cut with either *Bam*HI, *Sal*I or double digested with both *Bam*HI/*Sal*I, while also including an uncut control sample. It appeared that the restriction digests produced a single band at approximately 5000 bp corresponding to the linearized form of the plasmid. This suggested that the digests were successfully producing the correct sized product, in comparison to the control uncut sample.

The PCR product (FLNA repeat 10 cDNA) was also cut using *Bam*HI and *Sal*I in order to clone into the linearized pPROEX HTb expression vector (refer to 2.8.4). However, as only small fragments were digested no obvious difference in size was observed on an agarose gel, but assumed that the fragment was cut as treated with the same conditions as the pPROEX-HTb expression vector.

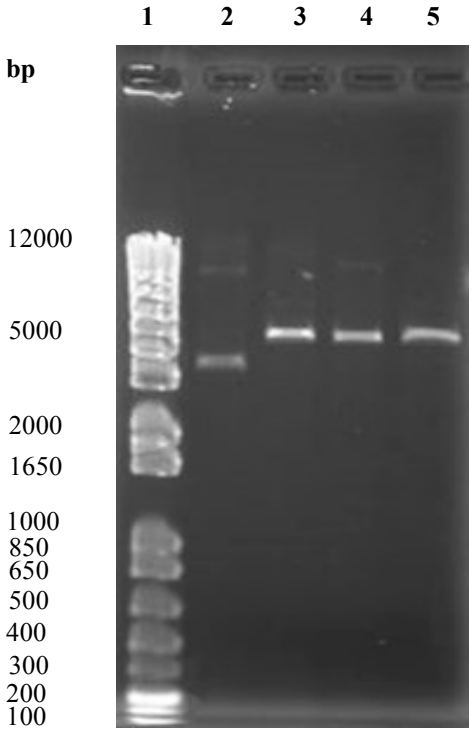

Figure 3.3 Agarose gel of the digested pPROEX-HTb expression vector.

pPROEX-HTb expression vector digested using *Bam*HI and *Sal*I restriction enzymes (refer to 2.8.4) and analysed on a 1.5% agarose gel then run at 100 V for 70 minutes (refer to 2.2.1). Lane 1; 1kb Plus™ ladder, Lane 2; Uncut vector, Lane 3; Vector cut with *Bam*HI, Lane 4; Vector cut with *Sal*I, Lane 5; Vector cut with both *Bam*HI and *Sal*I.

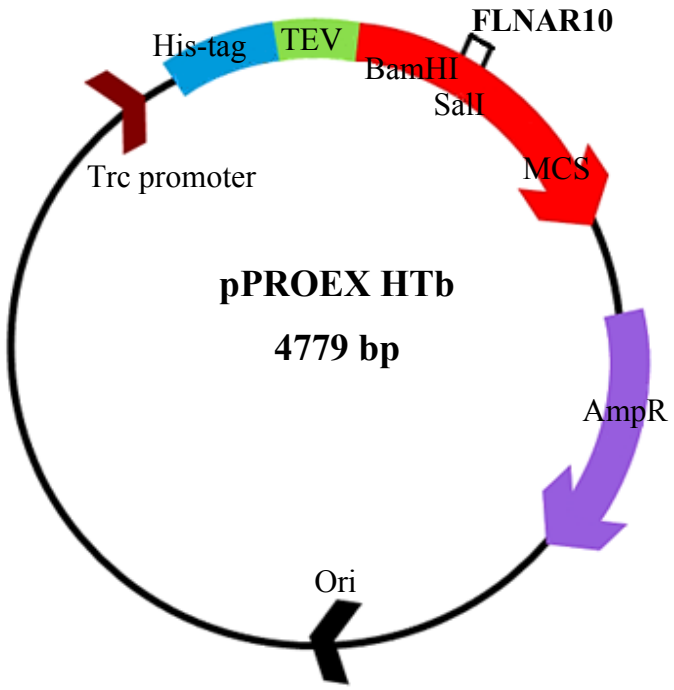

Figure 3.4 Vector Map of pPROEX HTb with FLNAR10 cDNA cloned between *Bam*HI and *Sal*I restriction sites.

pPROEX HTb plasmid map showing key elements required for *E. coli* expression. FLNAR10 nucleotide sequence cloned into pPROEX HTb within *Bam*HI and *Sal*I restriction sites. His-tag; Histidine-tag, TEV; Tobacco Etch Virus protease site, MCS; multiple cloning site, AmpR; Ampicillin resistance, Ori; origin of replication, Trc promoter; Tac promoter.

The purified double digested PCR products were then ligated into compatible sites in the linearized expression vector pPROEX HTb (Figure 3.4) at a molar ratio of 3:1 (insert to vector) then transformed into the chemically competent *E. coli* Top10 cells (refer to 2.8.5 and 2.8.6). Colonies were then selected for colony PCR and analysed using on an agarose gel (refer to 2.8.7), however, this did not produce a clear result (data not shown). Therefore, colonies were instead selected for plasmid isolation and double digested using *Bam*HI/*Sal*I then run on an agarose gel to confirm whether the correct sized insert had been inserted into the expression vector (refer to 2.7.3, 2.8.4, and 2.2.1).

Examining the agarose gel resulted in a fragment of approximately 300 base pairs corresponding to the correct size of the FLNA repeat 10 insert (294 or 285 bp for 1155 or 1158 primers used, respectively). While, the empty linearized pPROEX HTb vector

used as a control resulted in a fragment of approximately 5000 bp corresponding to the pPROEX HTb vector (4779 bp) as seen in the cut vector (Figure 3.5). This provided evidence that the insert has been successfully cloned into the pPROEX-HTb vector.

Sequencing using pPROEX HTb Rus and M13-48 Rev F primers confirmed the correct sequence of FLNA repeat 10 insert had been obtained in both constructs (refer to 9.1.1 - 9.1.3). Constructs will be referred to as Wt FLNAR10 1155 or 1158 in this thesis.

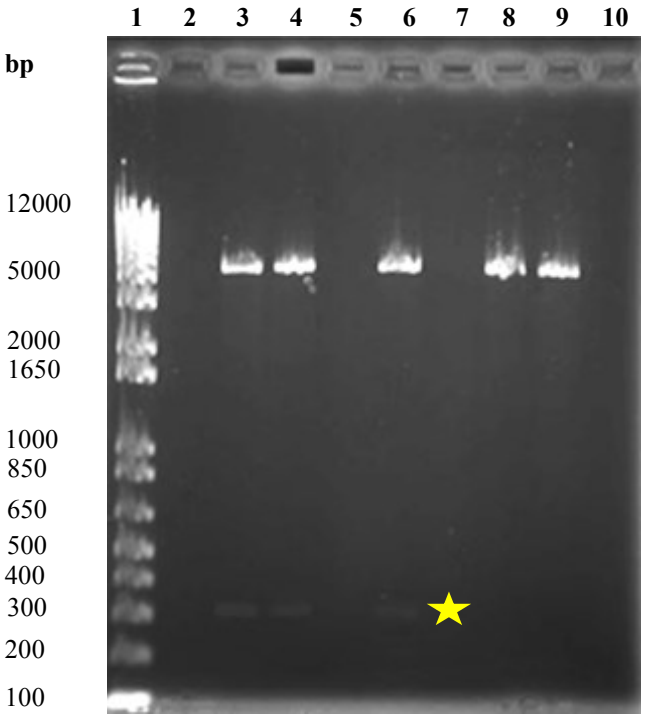

Figure 3.5 Plasmid digests of FLNA repeat 10 constructs.

Restriction digest reactions ran on a 1.5% agarose gel electrophoresis at 100 V for 70 minutes (refer to 2.8.4 and 2.2.1). Lane 1; 1kb Plus™ ladder, Lanes contain *Bam*HI/*Sal*I double digests of recombinant plasmid, Lane 3; contains construct Wt FLNAR10 1155 (originally derived from pFastBac-FLNA), Lane 4; contains construct Wt FLNAR10 1158 (originally derived from pFastBac-FLNA), Lane 6; contains construct Wt FLNAR10 1158 (originally derived from pGEX-FLNAR10), Lane 8 and 9; contain an empty pPROEX HTb vector used as a control. The star represents the FLNA repeat 10 insert, all other lanes that were not mentioned were empty.

3.4 Constructing mutant FLNA repeat 10 domain

Mutant constructs containing A1188T, S1199L, or V1249A mutations were generated from the Wt recombinant FLNAR10 1155 or 1158 plasmid using a whole plasmid PCR mutagenesis protocol (refer to 2.8.9). These specific repeat 10 mutations were chosen as

they are physically situated in different regions of the FLNA repeat 10 domain and lead to severe forms of the OPD spectrum skeletal disorders (MNS and FMD) (Feng Y. and Walsh C.A., 2004, Robertson S.P. *et al.*, 2003, Robertson S.P. *et al.*, 2006, Page R.C. *et al.*, 2011). Furthermore, these mutations suggest that a specific single mechanism may cause the disorders that may affect the FLNA repeat 10 functions (Figure 3.6).

Briefly, PCR reactions were setup and subjected to a cycling temperature program, the PCR product was purified before being digested using the *Dpn*I restriction enzyme in order to digest the wild-type parental DNA template (refer to 2.8.9.2). The plasmid was then transformed into the chemically competent *E. coli* Top10 cells. However, very few (1-2) or no colonies had grown after multiple attempts, which suggested that there might have been an issue with the transformation efficiency. Further trials were carried out to optimise this method, by initially doubling both the amount of recombinant plasmid template and *Dpn*I. The parameters for transformation were also modified by; the addition of 10 µl of *Dpn*I treated sample to 50 µl competent cells instead of 1 µl, then plating out 150 µl of total sample instead of 100 µl and incubating for a longer period of time (20 hours instead of 16 hours). Nonetheless, all were unsuccessful and the results were inconclusive.

These results suggested that may have been caused by the lack of the newly synthesised DNA becoming circular plasmid and instead being linearized. Hence, a ligation reaction based on a previous protocol (Adereth Y. *et al.*, 2005) (Table 2.11) was carried out after *Dpn*I digestion to ensure that newly synthesised circular cDNA was reformed in order for transformation to be effective. Both ligation treated and non-ligation treated samples were transformed into competent cells to check whether this ligation step resulted in efficient transformation. The ligation step resulted in efficient transformation producing approximately 25 colonies in comparison to initial trials and non-ligated samples resulting in low transformation efficiency of 0-2 colonies. Colonies from the ligated treated plates were selected then the plasmids were isolated (refer to 2.7.3), and sequenced (refer to 2.8.8) confirming that the correct mutation was present (refer to 9.1.4).

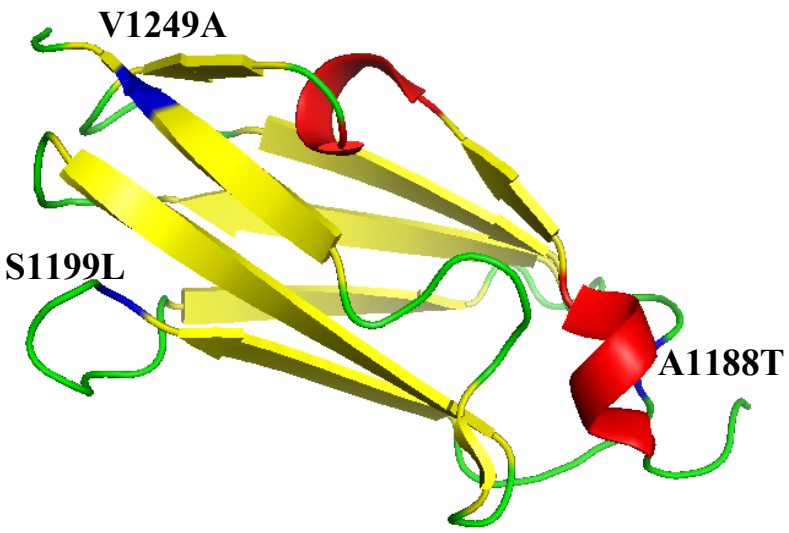

Figure 3.6 FLNA repeat 10 domain crystal structure.

Crystal structure of the FLNA repeat 10 domain with positions of mutations; V1249A, A1188T and S1199L identified. Displayed using PyMOL software (The PyMOL Molecular Graphics System, Version 1.3 Schrödinger, LLC), from FLNA repeat 10 structure coordinates (PBD-3RGH) (Page R.C. *et al.*, 2011).

3.5 Summary

Cloning of the FLNA repeat 10 cDNA into the *E. coli* expression vector pPROEX HTb was achieved providing a recombinant expression system. Two constructs; FLNAR10 1155 and 1158 were generated based on database domain boundary analysis to determine whether slight sequence differences leads to any differences in protein expression and solubility. OPD associated mutants were generated using an optimized whole plasmid PCR mutagenesis method, in order to assess whether they lead to any changes in the stability of the protein or affinity towards F-actin.

4. FLNA repeat 10 protein expression and purification

4.1 Introduction

The pPROEX HTb recombinant expression system enables the production of an N-terminal histidine-tagged recombinant FLNAR10 protein, which can be used in protein purification. Two steps were carried out to ensure pure protein of interest has been obtained, firstly; immobilised metal ion affinity chromatography (IMAC) using a column prepacked with Ni^{2+}-NTA ions that binds His-tagged proteins followed by, size exclusion chromatography (SEC) which further separates proteins based on their size. A high amount of pure FLNAR10 protein is required, in order to carry out *in vitro* biochemical tests.

4.2 Expression and solubility trials

The recombinant Wt FLNAR10 1155 and 1158 constructs were initially grown in *E. coli* BL21 (DE3) cells and the protein was then expressed by IPTG induction. The cultures were grown for 2, 4 or 18 hours to determine the optimum time for expression before being pelleted and subjected to sonication to achieve lysis. The lysed whole cell extract was then centrifuged to separate the soluble and insoluble fractions before being run on SDS-PAGE gels (refer to 2.9).

The SDS-PAGE gels revealed that a specific band running at approximately 14 kDa was only present after IPTG induction had occurred (indicated by the arrow in Figure 4.1). It was presumed that this 14 kDa protein was indeed the recombinant Wt FLNA repeat 10 protein based on the estimated molecular weight of FLNAR10 protein of 13.6 kDa calculated from its amino acid sequence using protparam software (refer to 2.5) and since this protein was not expressed in the uninduced fractions (lanes 2-7 of Figure 4.1).

The FLNAR10 protein band was observed to be predominantly expressed in the soluble fractions however, after incubation overnight the protein can be seen in both the soluble and insoluble fractions which could be a result of incomplete cell lysis, insufficient washing of the pellet or most likely inclusion bodies forming if overexpressed for longer periods of time. Expression of the FLNAR10 protein was shown to be optimal after 4 hours of incubation producing relatively high yields of soluble protein, therefore this condition was used in all further expression tests. The Wt FLNAR10 1155 protein construct seen in lanes 12 and 18 of Figure 4.1 seemed to be expressed with slightly higher yields of soluble protein in comparison to the other expressed Wt FLNAR10

1158 constructs leading to suggest that sequence differences may in fact affect protein expression and solubility (Figure 4.1). Therefore, the Wt FLNAR10 1155 construct was used for further later studies.

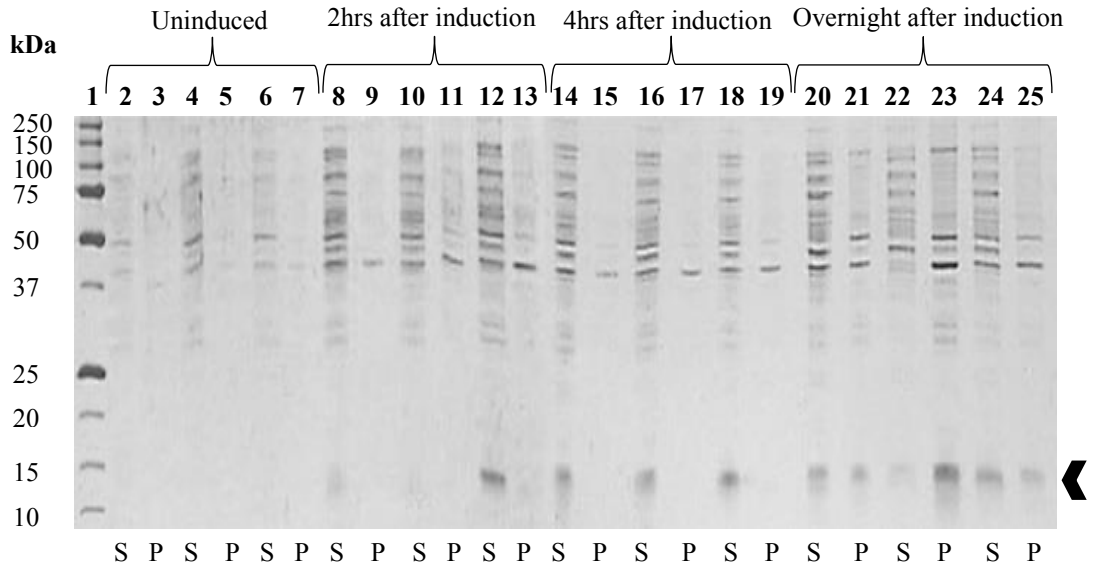

Figure 4.1 Wt FLNA repeat 10 protein expression trials.

Wt FLNAR10 protein expression trials ran on 15% SDS-PAGE gels at 200 V for approximately 50 minutes (refer to 2.2.2). Lane 1; Precision Plus™ unstained protein standard, Lanes 2-7; uninduced cells samples, Lanes 8-13; samples after 2 hours induction with IPTG, Lanes 14-19; samples after 4 hours induction with IPTG, Lanes 20-25; samples after overnight induction with IPTG. Lanes contain samples in the order of; construct Wt FLNAR10 1158 (originally derived from pFastBac-FLNA), construct Wt FLNAR10 1155 (originally derived from pFastBac-FLNA), then construct Wt FLNAR10 1158 (originally derived from pGEX-FLNAR10). Arrow represents FLNAR10 protein, samples loaded are represented by S = supernatant, P = pellet. Note; gel is a composite of two gels from lane 1-13 and 14-25.

4.3 Scaled up protein expression

In this study, a large amount of pure FLNAR10 protein was required to carry out biochemical studies. Initially, the FLNAR10 protein was obtained by first inoculating a single colony of the transformed *E. coli* BL21 into 50 ml of LB-amp. Protein expression was then induced by the addition of IPTG and the cultures were grown for a further 4 hours as previously determined by expression trials (refer to 4.2). The cells were harvested via centrifugation then lysed and analysed on SDS-PAGE gels (refer to 2.10.1 and 2.10.2). However, these trials produced low yields of soluble FLNAR10 protein. Therefore, the procedure was scaled up by using an initial 50 ml starter culture to 2 L of

LB-amp, while analysis using SDS-PAGE gels (refer to 2.2.2) revealed that relatively high yields of FLNAR10 protein were produced (refer to 2.10.1)..

4.4 Purification of FLNA R10 proteins

The resulting cellular extract was purified by means of chromatographic techniques. Purification was carried out in two steps in order to purify the histidine-tagged recombinant FLNAR10 protein. Firstly, immobilised metal ion affinity chromatography (IMAC) using a HisTrap FF column prepacked with Ni^{2+}-NTA ions followed by size exclusion chromatography (SEC). The Wt FLNAR10 1155 protein was initially expressed and purified in order to act as reference for the expected result and as a comparison for the mutant FLNAR10 proteins. Originally, three mutants were expressed, however, due to time constraints only two were selected for further use. These were the A1188T and V1249A FLNAR10 1155 mutations which were chosen as they are located at opposite ends in reference to the FLNAR10 crystal structure (Figure 3.6) and lead to slightly different OPD disorders; MNS and FMD, respectively (Page R.C. *et al.*, 2011, Robertson S.P. *et al.*, 2006, Robertson S.P. *et al.*, 2003).

The immobilized metal ion affinity chromatography (IMAC) is a protein purification technique that exploits the specific interaction between metal ions (such as Co^{2+}, Cu^{2+}, Ni^{2+}, and Zn^{2+}) to histidine. Pre-charged columns with metal ions are attached on a stationary support matrix allowing proteins with a His-tag to bind which can then be eluted with increasing concentrations of imidazole, which will out compete the His-tag interaction with the matrix ions. Size exclusion chromatography (SEC) involves the separation of proteins in solution based on their size. Proteins enter pores within the column resin and elute at different rates depending on size; large proteins elute first, while small proteins make their way through the pores, evidently delaying their elution. Proteins in chromatograms are measured by absorbance readings at 280 nm, which are represented as peaks.

4.5 Affinity chromatography

An initial small-scale binding assay to Nickel (Ni^{2+}-NTA) resin was carried out to study the characteristics of the recombinant proteins affinity towards Ni^{2+}-NTA. The column was first equilibrated with 2 ml of lysis buffer containing 25 mM of imidazole (buffer A, refer to 2.10.3), following centrifugation the soluble protein was then equilibrated onto the resin. The resin was then washed with buffer A to remove any unbound protein

then, the immobilized proteins were sequentially eluted using lysis buffer containing either 250 mM or 500 mM imidazole (refer to 2.10.3) to determine the required condition for the protein of interest to become unbound from the column resin. Elution samples were examined on an SDS-PAGE gel, revealing that the protein of interest does in fact bind to Ni^{2+}-NTA specifically through its His-tag. The protein of interest is seen to elute mostly under 250 mM imidazole concentration with some protein further eluting using the 500 mM imidazole buffer (not shown).

Larger scale purifications were then carried out using an ÄKTA protein purification system (GE Healthcare) through a pre-equilibrated Ni^{2+}-NTA Histrap FF column with buffer A containing 25 mM imidazole. The cells were initially lysed in buffer A containing 25mM imidazole (refer to 2.10.3) and also containing cOmplete EDTA-free protease inhibitor cocktail mix, then lysed by French-press and sonicated to ensure that complete lysing of the cells had occurred. The lysate mix was centrifuged, then the supernatant was filtered and injected onto the pre-equilibrated column running pre-programmed ÄKTA software that increases through a linear gradient between 25-400 mM of imidazole at a flow rate of 1.5 ml/min. Sample fractions were then collected and analysed on SDS-PAGE gels in reference to the chromatogram.

The protein of interest (FLNAR10) was determined based on the size derived using the protparam software (refer to 2.5) and by comparing to the uninduced sample which did not contain the protein of interest as expected. Initially, it was essential to go through various iterations to optimise running conditions of IMAC to produce pure soluble His-tagged Wt FLNAR10 protein.

Most unbound protein was removed in initial washing stages seen by the large peak produced between fractions A1-A10 in Figure 4.2. Two peaks were observed in the Wt FLNAR10 chromatogram, the first of which was a minor peak with a very low absorbance eluting at approximately 100 mM of imidazole concentration and a well-resolved peak with a very high absorbance eluting at approximately 230 mM imidazole concentration located between fractions B9-C4 (Figure 4.2). SDS-PAGE gels revealed that the first minor peak contained contaminating *E. coli* proteins whereas the second peak corresponded to the protein of interest, Wt FLNAR10 (Figure 4.3) producing a band of approximately 14 kDa in size as estimated previously (refer to 2.5) and was also

consistent with the earlier small scale purification trials that eluted at 250 mM imidazole concentration.

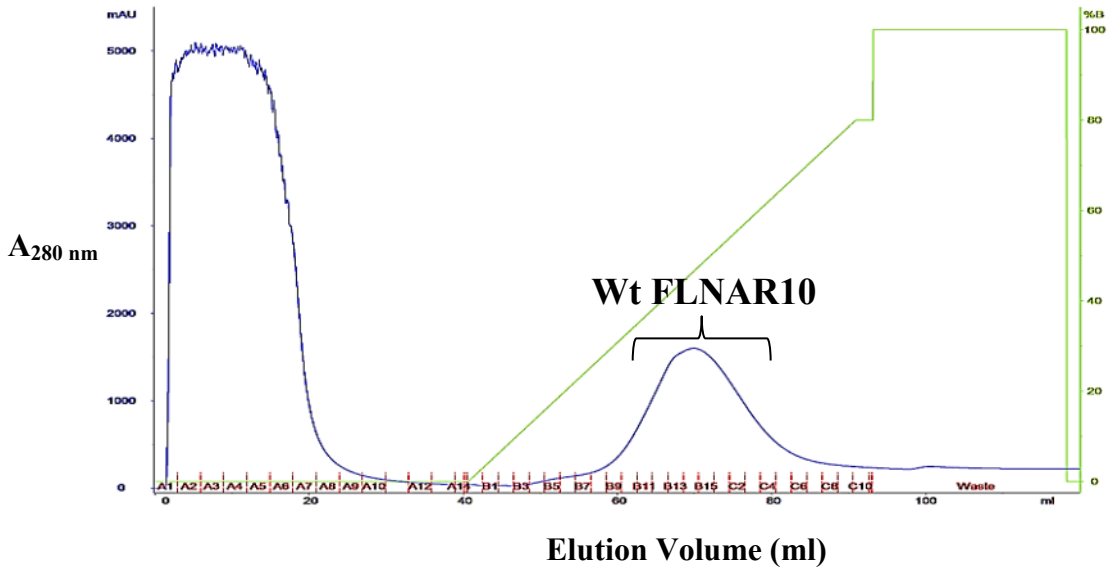

Figure 4.2 Wt FLNAR10 IMAC protein purification.

IMAC chromatogram using 5 ml Histrap FF column. Gradient increasing linearly between 25-400 mM imidazole (0-100% B) at a flow rate of 1.5 ml/min. Blue line measuring absorbance at 280 nm, Green line; gradient between 0-100% of imidazole buffer.

However, during purification of Wt FLNAR10 protein it became apparent that a recurrent secondary band seemed to elute at approximately 8 kDa along with the protein of interest (Figure 4.3). This was an unexpected result, which may have arisen based on multiple scenarios such as; not fully reduced non-native disulphide bonds, another contaminating his-tagged protein, or possibly protein degradation of the FLNAR10 protein. Initially this was thought to be a contaminating *E. coli* protein that had not been washed off, hence the fractions were pooled together and subjected to IMAC multiple times in order to remove and get better resolution of the peaks. IMAC was run either with the same conditions (refer to 2.10.3) or by doubling the elution gradient length (from 10 to 20 column volumes (CV)) and the amount of column washing steps (from 5 to 10 CV). The chromatogram revealed that only a single peak was present this was analysed using SDS-PAGE gel confirming that the secondary band was still present and was not removed (not shown). This led to multiple tests in order to either identify or remove this protein (refer to 4.4.3 secondary band issue).

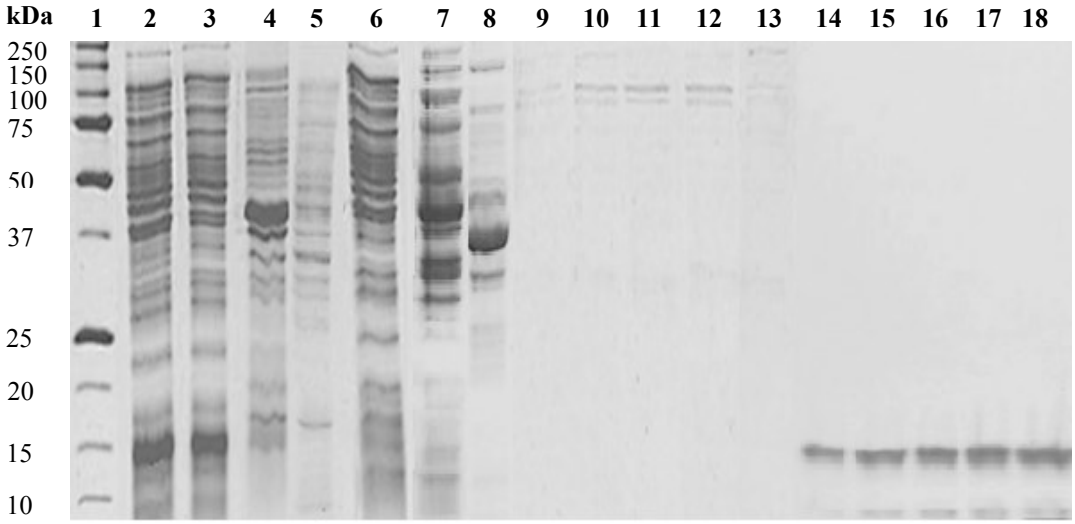

Figure 4.3 Wt FLNAR10 IMAC protein purification SDS-PAGE gel.

Wt FLNAR10 protein purification fractions ran on 12.5% SDS-PAGE gels at 200 V for approximately 40 minutes (refer to 2.2.2). Lane 1; Precision Plus™ unstained protein standard, Lane 2; cell lysate, Lane 3; supernatant, Lane 4; pellet, Lane 5; uninduced cell sample, Lane 6-18; fractions collected A3, A5, A7, A9, A12, B3, B5, B7, B10, B12, B14, C1, and C3 respectively. Note; gel is a composite of two gels from lane 1-12 and 13-18.

In both the FLNAR10 mutant (V1249A and A1188T) IMAC purifications, the chromatograms presented two main peaks as previously seen for the Wt FLNAR10 IMAC protein purification. However, initial purification resulted in overlap between the two peaks leading to some contaminating *E. coli* proteins to be present within the FLNAR10 protein fractions. Therefore, these peaks were resolved by increasing the elution gradient length from 10 to 20 CVs, and further increasing the number of column washes from 5 to 8 CVs. As previously seen in the Wt FLNAR10 IMAC protein purification (Figure 4.2 and 4.3) the first peak eluting at approximately 100 mM imidazole concentration contained contaminating *E. coli* proteins. While, the second peak eluting at approximately 230 mM imidazole concentration located between fractions C10-D7 corresponded to the FLNAR10 protein (Figures 4.4-4.7).

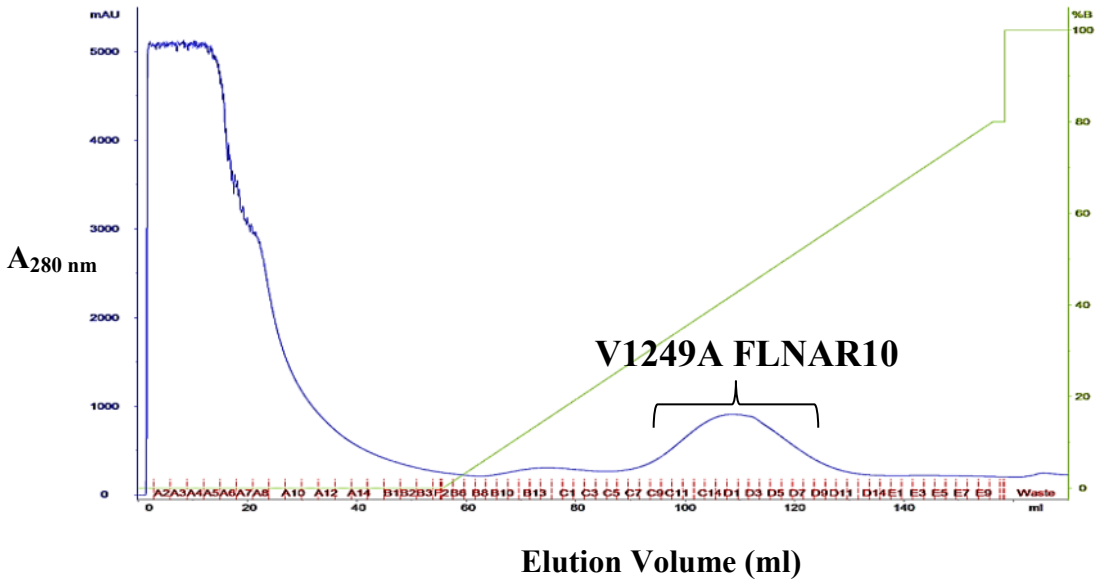

Figure 4.4 V1249A FLNAR10 IMAC protein purification.

IMAC chromatogram using 5 ml Histrap FF column. Gradient increasing linearly between 25-400 mM imidazole (0-100% B) at a flow rate of 1.5 ml/min. Blue line measuring absorbance at 280 nm, Green line; gradient between 0-100% of imidazole buffer.

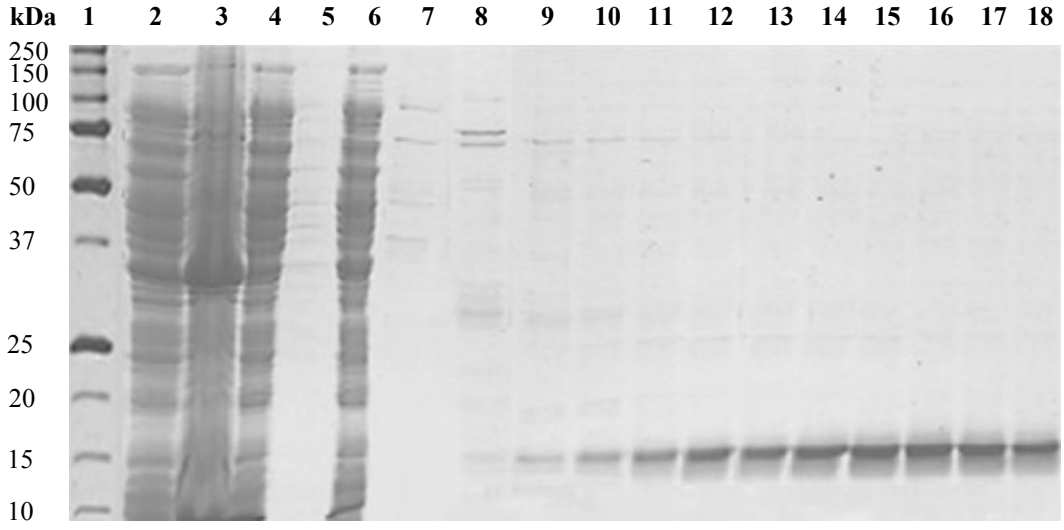

Figure 4.5 V1249A FLNAR10 IMAC protein purification SDS-PAGE gel.

V1249A FLNAR10 protein purification fractions ran on 12.5% SDS-PAGE gels at 200 V for approximately 40 minutes (refer to 2.2.2). Lane 1; Precision Plus™ unstained protein standard, Lane 2; cell lysate, Lane 3; pellet, Lane 4; supernatant, Lane 5; uninduced cell sample, Lane 6-18; fractions collected A4, A12, C1, C3, C5, C7, C9, C12, C14, D1, D3, D5, and D7 respectively. Note; gel is a composite of two gels from lane 1-7 and 8-18.

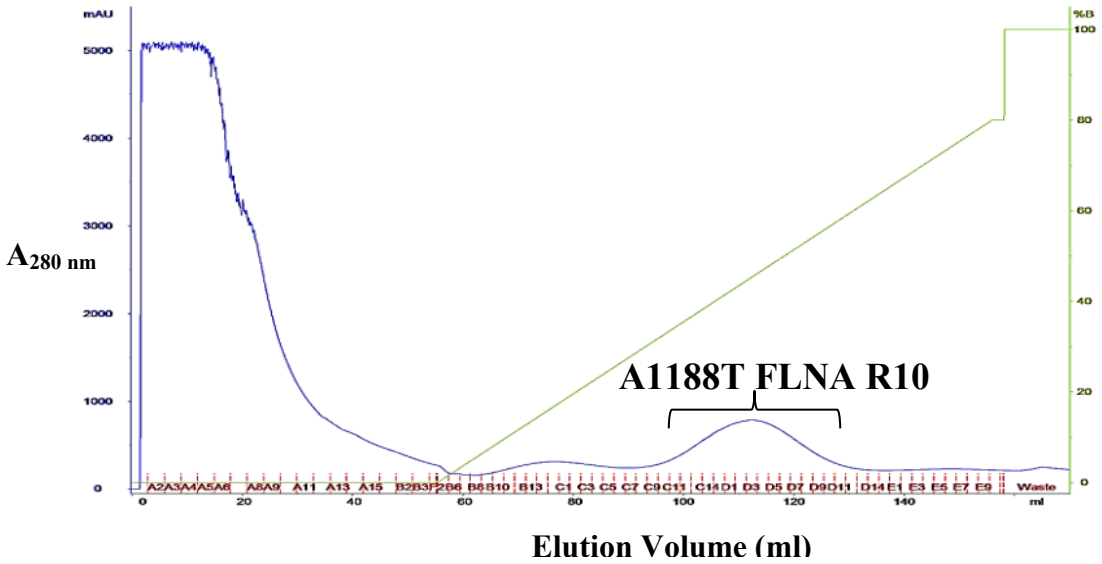

Figure 4.6 FLNAR10 A1188T IMAC protein purification

IMAC chromatogram using 5 ml Histrap FF column. Gradient increasing linearly between 25-400 mM imidazole (0-100% B) at a flow rate of 1.5 ml/min. Blue line measuring absorbance at 280 nm, Green line; gradient between 0-100% of imidazole buffer.

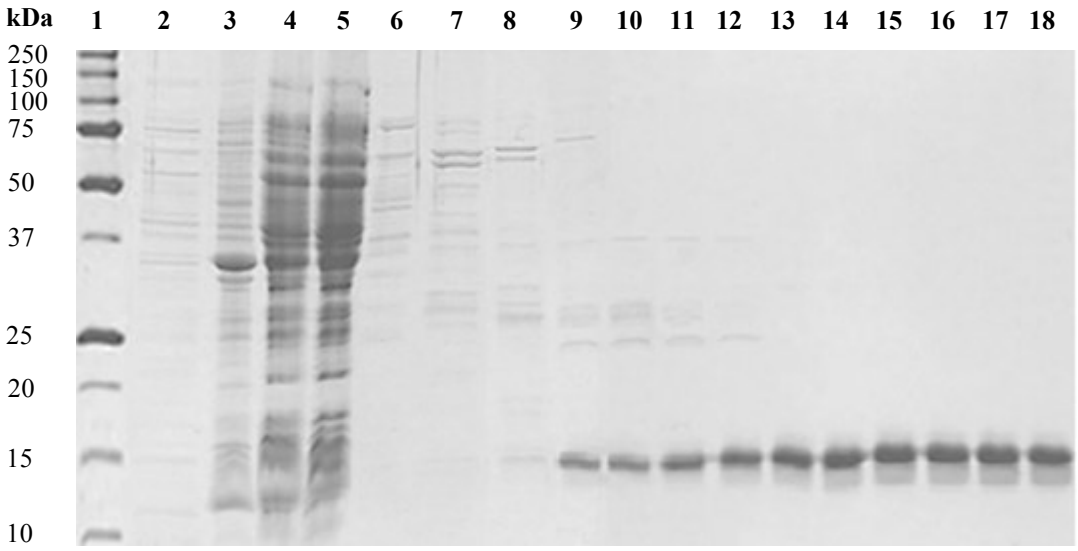

Figure 4.7 A1188T FLNAR10 IMAC protein purification SDS-PAGE gel.

A1188T FLNAR10 protein purification fractions run on 12.5% SDS-PAGE gels at 200 V for approximately 40 minutes (refer to 2.2.2). Lane 1; Precision Plus™ unstained protein standard, Lane 2; Uninduced cell sample, Lane 3; pellet, Lane 4; cell lysate, Lane 5; supernatant, Lane 6-18; fractions collected A11, B12, B14, C1, C5, C7, C11, C13, C15, D1, D3, D5, and D7 respectively. Note; gel is a composite of two gels from lane 1-7 and 8-18.

Interestingly, the IMAC chromatogram of Wt FLNAR10 protein was expressed and purified at higher yields in comparison to both mutants V1249 and A1188T FLNAR10 proteins. Which maybe a result of a number of scenarios such as the mRNA might not be translated as efficiently, the single amino acid mutations are causing changes to structure, the protein may not be fully folded, or the protein is unstable. Purification of both mutants resulted in relatively pure fractions containing the protein of interest at 14 kDa however, there was no apparent secondary band seen at 8 kDa as was present in the Wt FLNAR10 purification sample (Figure 4.3). This suggested that the secondary band maybe the result of degradation or co-elution of a bound protein (refer to 4.4.3 secondary band issue).

4.6 Size Exclusion Chromatography

Size exclusion chromatography (SEC) was carried out to further ensure pure FLNAR10 protein was obtained using a pre-equilibrated Superdex 75 10/300 GL column with SEC buffer (refer to 2.10.4) through an ÄKTA protein purification system (GE Healthcare). The pooled concentrated FLNAR10 protein sample from IMAC was loaded onto the pre-equilibrated column and was run through the pre-programmed ÄKTA software at a flow rate of 0.5 ml/min (refer to 2.10.4).

Multiple peaks were observed during SEC, which further separated out the FLNAR10 proteins from any remaining *E. coli* contaminating proteins that were detected faintly in IMAC SDS-PAGE gels (Figures 4.3, 4.5, and 4.7). In reference to the chromatograms and analysis using SDS-PAGE gels, the FLNAR10 protein (in all samples) eluted after 12 ml of SEC buffer between fractions A12-A13 (Figures 4.8, 4.10 and 4.12). However, the absorbance (A_{280} nm) of the peak representing the FLNAR10 protein was saturated due to the overloading of the column. This peak was analysed on SDS-PAGE gels and was revealed to contain relatively pure FLNAR10 protein represented as a band of approximately 14 kDa in size (Figures 4.9, 4.11 and 4.13).

Conversely, analysis of the purified Wt FLNAR10 protein on an SDS-PAGE gel revealed that the fractions contained the secondary band of 8 kDa, as previously seen after IMAC purification still remained (Figure 4.3 and 4.9). This secondary band was thought to be a contaminating protein, therefore in order to separate out this recurring

protein band, the Wt FLNAR10 protein fractions (A12-A13) were pooled together and run through SEC once more. Despite this, no further separation was observed on both the chromatogram and the SDS-PAGE gels (not shown).

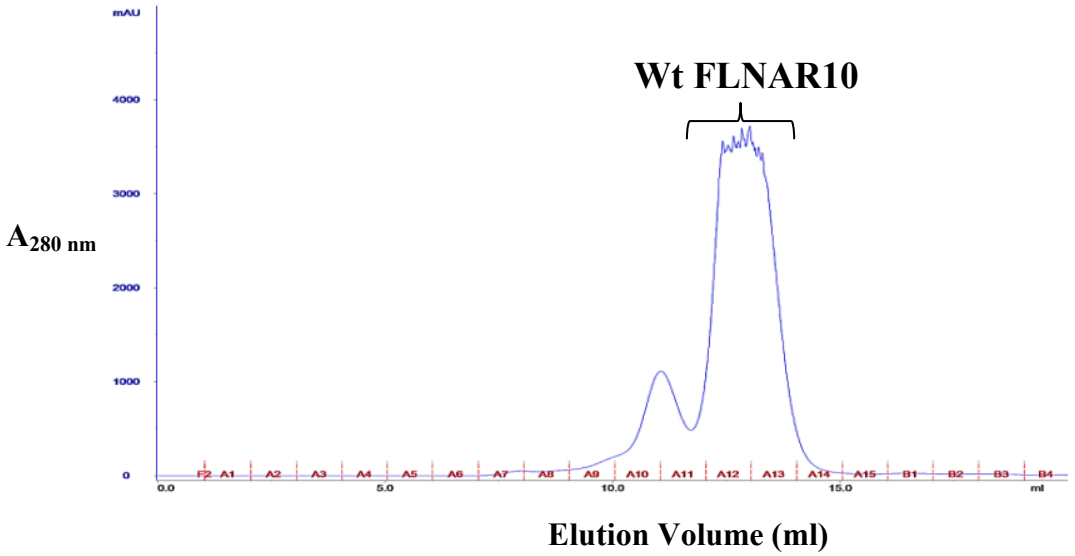

Figure 4.8 Wt FLNAR10 size exclusion protein purification using Superdex 75 10/300 GL column.

Concentrated pooled Wt FLNAR10 protein sample from IMAC purification was run at a flow rate of 0.5 ml/min through a Superdex 75 10/300 GL column. Blue line measures absorbance at 280 nm.

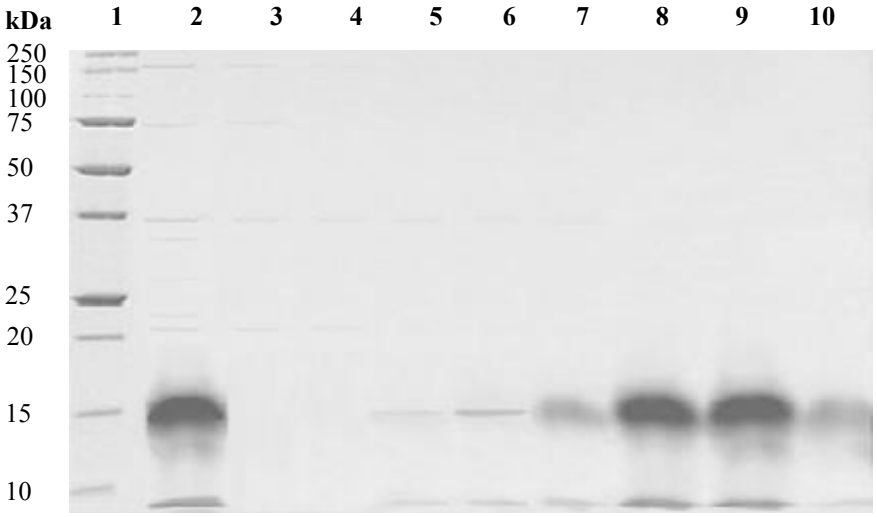

Figure 4.9 Wt FLNAR10 SEC protein purification SDS-PAGE gel.

Wt FLNA R10 protein purification fractions run on a 12.5% SDS-PAGE gel at 200 V for approximately 40 minutes (refer to 2.2.2). Lane 1; Precision Plus™ unstained protein standard, Lane 2; Pooled concentrated Wt FLNAR10 sample from IMAC, Lane 3; fraction A7, Lane 4; fraction A8, Lane 5; fraction A9, Lane 6; fraction A10, Lane 7; fraction A11, Lane 8; fraction A12, Lane 9; fraction A13, Lane 10; fraction A14.

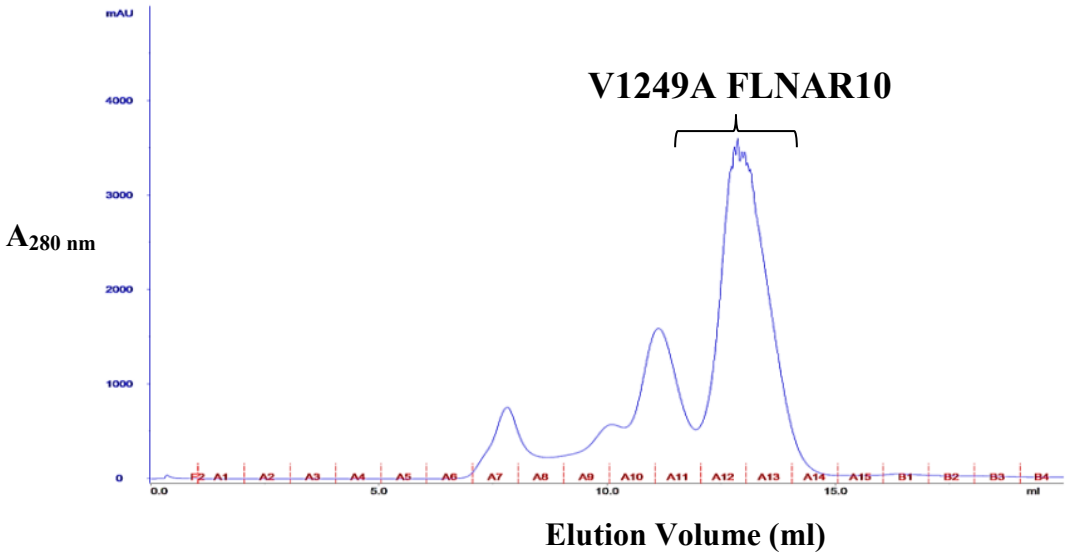

Figure 4.10 V1249A FLNAR10 size exclusion protein purification using Superdex 75 10/300 GL column.

Concentrated pooled V1249A FLNAR10 protein sample from IMAC purification was run at a flow rate of 0.5 ml/min through a Superdex 75 10/300 GL column. Blue line measures absorbance at 280 nm.

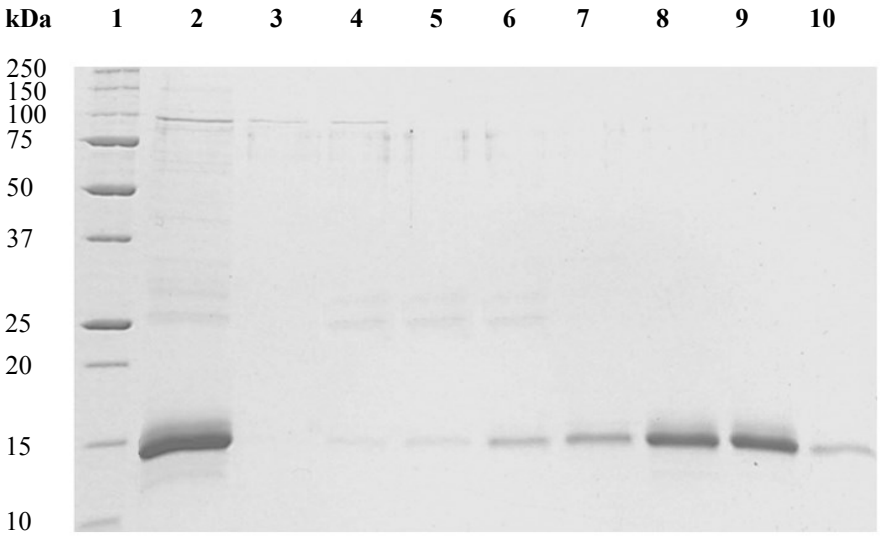

Figure 4.11 V1249A FLNAR10 SEC protein purification SDS-PAGE gel.

V1249A FLNAR10 protein purification fractions run on a 12.5% SDS-PAGE gel at 200 V for approximately 40 minutes (refer to 2.2.2). Lane 1; Precision Plus™ unstained protein standard, Lane 2; Pooled concentrated V1249A FLNAR10 sample from IMAC, Lane 3; fraction A7, Lane 4; fraction A8, Lane 5; fraction A9, Lane 6; fraction A10, Lane 7; fraction A11, Lane 8; fraction A12, Lane 9; fraction A13, Lane 10; fraction A14.

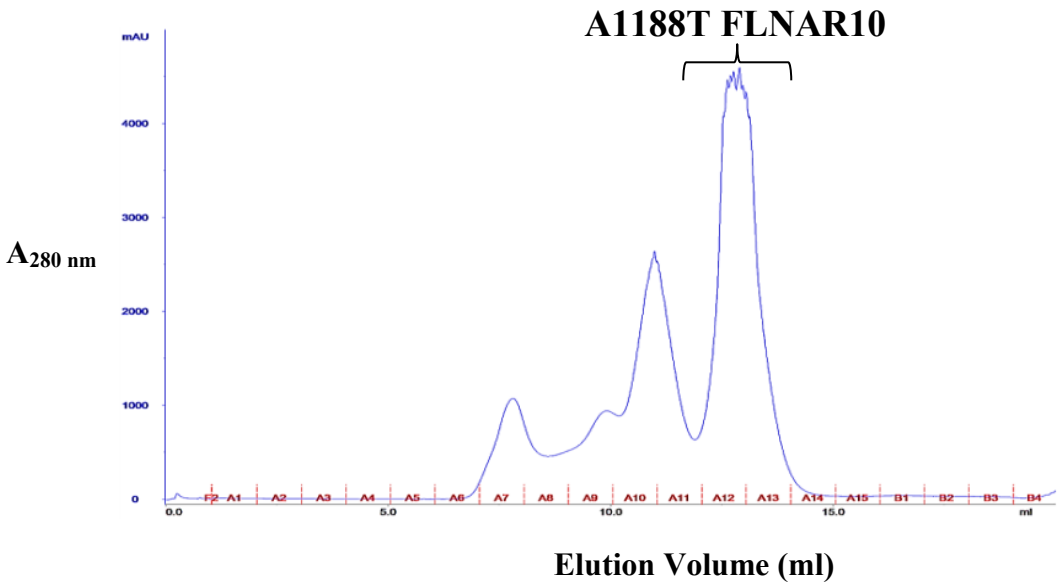

Figure 4.12 A1188T FLNAR10 size exclusion protein purification using Superdex 75 10/300 GL column.

Concentrated pooled A1188T FLNAR10 protein sample from IMAC purification was run at a flow rate of 0.5 ml/min through a Superdex 75 10/300 GL column. Blue line measures absorbance at 280 nm.

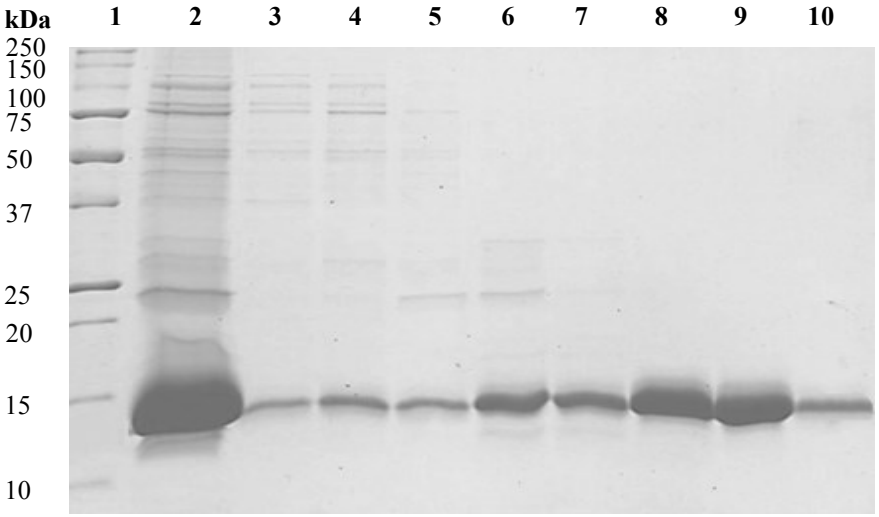

Figure 4.13 A1188T FLNAR10 SEC protein purification SDS-PAGE gel.

A1188T FLNAR10 protein purification fractions run on a 12.5% SDS-PAGE gel at 200 V for approximately 40 minutes (refer to 2.2.2). Lane 1; Precision Plus™ unstained protein standard, Lane 2; Pooled concentrated A1188T FLNAR10 sample from IMAC, Lane 3; fraction A7 , Lane 4; fraction A8, Lane 5; fraction A9, Lane 6; fraction A10, Lane 7; fraction A11, Lane 8; fraction A12, Lane 9; fraction A13, Lane 10; fraction A14.

4.7 Secondary band issue

During purification of the FLNAR10 protein, it became apparent that a second band at approximately 8 kDa was present along with the Wt FLNAR10 protein even after multiple purification steps. This recurrent secondary band was initially thought to have been expressed during early protein expression. Therefore, examining the SDS-PAGE gels (Figure 4.3 and 4.9) comparisons between the uninduced, pellet, supernatant and lysate samples with the purified FLNAR10 protein were made, which revealed that no apparent second band was present. Furthermore, 1 mM DTT and 2 mM EDTA were added to the SEC buffer in order to reduce any possible disulfide bonds and chelate metals to inhibit metallo protease activity, respectively, however, no difference was observed on expression of the second band (refer to 2.10.4).

The secondary band was then thought to have occurred due to proteolytic degradation, hence, a cocktail protease inhibitor tablet (cOmplete EDTA-free) was added to the lysis buffer to ensure no further degradation ensues once cells are lysed, yet again no significant difference was detected on the secondary band.

Separation of the two protein bands (at 14 kDa and 8 kDa) was then attempted through HPLC using a Jupiter C18 column (refer to 2.12). Though, separation was unsuccessful resulting in multiple split shoulder peaks eluting between 12-19 minutes (Figure 4.14 and appendix 9.3.1) that were confirmed on an SDS-PAGE gel to contain both the FLNAR10 (14 kDa) and the unknown secondary (8 kDa) protein bands (Figure 4.15). Other smaller peaks were also present with higher and lower retention times that are possibly due to buffer contaminants, salt or small molecules as no protein bands were observed on the SDS-PAGE gel corresponding to these peaks (Lanes 2-3, and 8-9 in Figure 4.15).

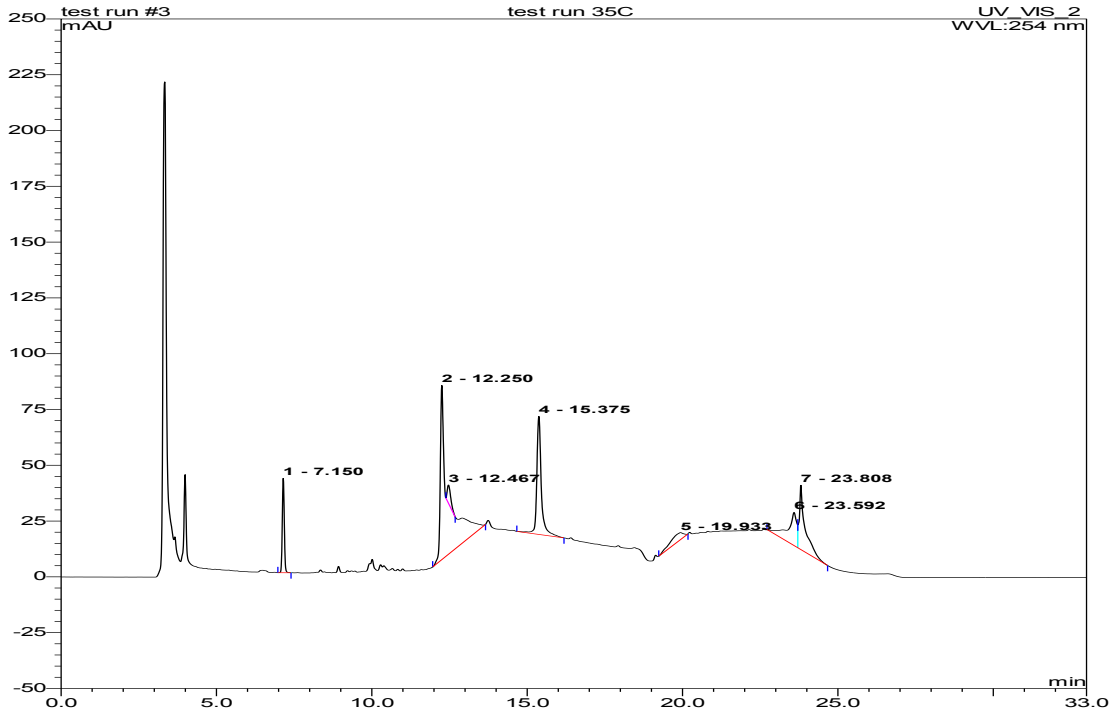

Figure 4.14 HPLC chromatogram of Wt FLNAR10 protein sample.

HPLC of Wt FLNAR10 protein run on Jupiter C18 column (4.6×250 mm 5um 300A, Phenomenex, USA) with an Ultimate 3000 analytical HPLC system (Dionex, USA) running along a gradient from 0.1% TFA/water (% A) into 0.08% TFA/70% MeCN/water (% B) in 16 min at a flow rate of 1 ml/min at wavelengths 254 nm.

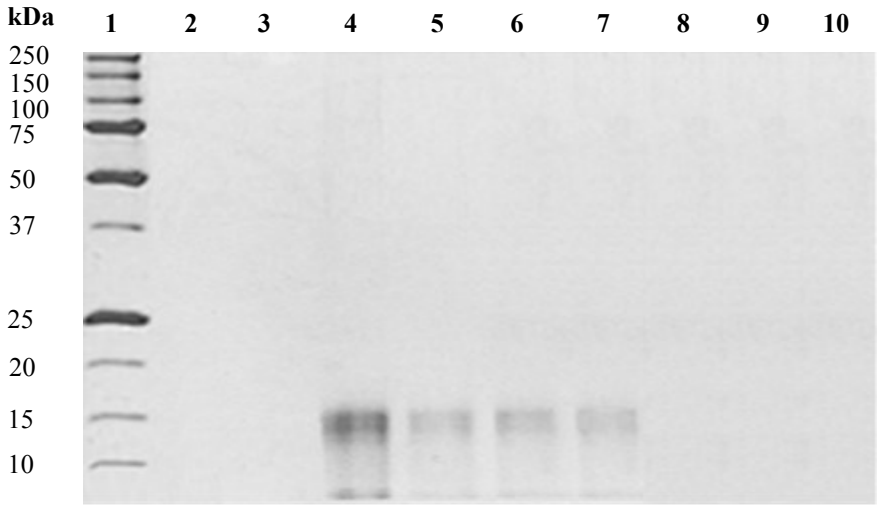

Figure 4.15 HPLC of Wt FLNAR10 protein samples SDS-PAGE gel.

SDS-PAGE gel of Wt FLNAR10 HPLC fractions run on 12.5% SDS-PAGE gel at 200 V for approximately 40 minutes. Lane 1; Precision Plus™ unstained protein standard, Lane 2; Initial peak, Lane 3; peak 1, Lane 4; peak 2, Lane 5; peak 3, Lane 6; peak 4, Lane 7; peak 5, Lane 8; peak 6, Lane 9; peak 7.

As HPLC was unable to separate the two bands, it was alleged that the secondary band might have occurred due to a co-eluting protein, a His-tagged protein, instability, or proteolytic degradation. To determine whether this secondary band had occurred as a result of temperature instability of the Wt FLNAR10 protein, the Wt FLNAR10 protein samples were incubated overnight at a range of temperatures -20, 4, 20, and 37℃ and analysed on SDS-PAGE gels (refer to 2.13). The Wt FLNAR10 protein was also treated with rTEV protease to target the removal of the His-tag then analysed on an SDS-PAGE gel (refer to 2.14). The SDS-PAGE gel revealed that digestion using the rTEV protease produced a product of 11 kDa in size suggesting, that the 8 kDa secondary band seen was not due to the removal of the His-tag. On the other hand, at higher incubation temperatures of 37℃, slightly increased amounts of the secondary band were observed (lane 5, Figure 4.16). A further increase in temperature or incubation time may have revealed a better result. Nevertheless, this suggested that the 8 kDa band seen during purification may potentially be the result of a degradation effect on the protein which consequentially leads to a truncated form of the FLNAR10 protein.

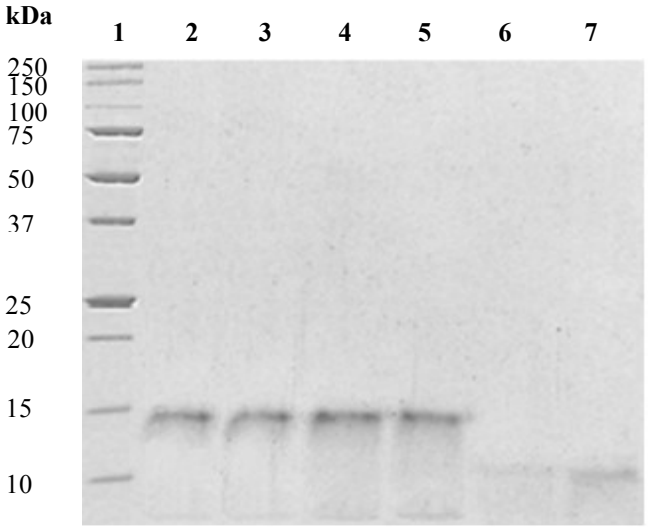

Figure 4.16 SDS-PAGE gel of temperature instability analysis and His-tag removal of Wt FLNAR10 protein samples.

Wt FLNAR10 protein ran on a 12.5% SDS-PAGE gel at 200 V for approximately 40 minutes (refer to 2.2.2). Temperature (refer to 2.13) or rTEV protease (refer to 2.14) incubated Wt FLNAR10 protein samples. Lane 1; Precision Plus™ unstained protein standard, Lane 2; Incubated at 4℃ as control, Lane 3; Incubated at -20℃, Lane 4; Incubated at 20℃, Lane 5; Incubated at 37℃, Lane 6; Incubated with rTEV 1:1 ratio, Lane 7; Incubated with rTEV 1:2.

Following the assumption that the secondary band maybe a truncated form of the FLNAR10 protein, the two protein bands (14 kDa and 8 kDa) were subjected to in-gel tryptic digests followed by mass spectroscopy using ESI-QUAD-TOF (refer to 2.11). The mass spectroscopy data was analysed using Mascot NCBI non-redundant protein data base peptide software to characterise the protein bands from the purified Wt FLNAR10 sample. Peptide scores of individual ions scored greater than 43 indicated identity or extensive homology ($p<0.05$).

In both bands analysed, some peptide sequence identity to FLNA were identified with peptide scores over 43 observed in non-shaded region of Figure 4.17A. Analysis revealed that the 14 kDa band was in fact the FLNA repeat 10 protein, while the second band seen at 8 kDa revealed that it had some FLNA repeat 10 sequence identity mainly near the C-terminal end, suggesting that digestion of the protein may indeed be occurring (Figure 4.17). However, as only a few peptides had statistically scored over the threshold level (Figure 4.17) may imply that the mass spectroscopy data may not be considerable. This analysis may be due to contamination of other proteins or inefficient tryptic digests.

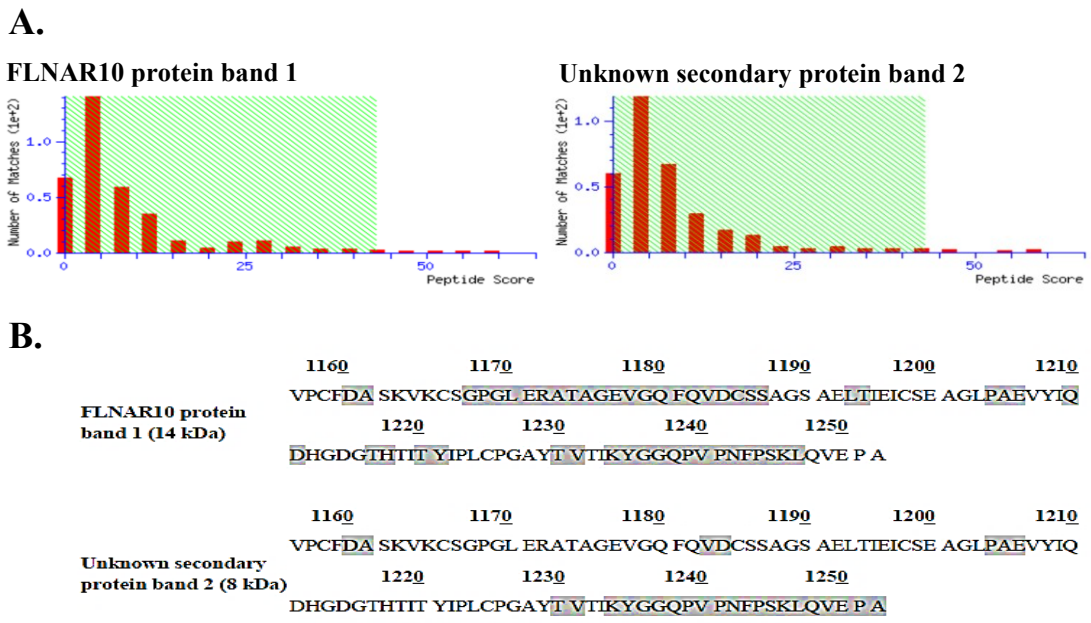

Figure 4.17 Wt FLNA repeat 10 protein Mass spectroscopy analysis of bands.

Wt FLNA repeat 10 protein mass spectroscopy analysis using Mascot software. **A.** Peptide scores of individual ions score greater than 43 indicate identity or extensive homology ($p<0.05$). Green shading not significant peptide sequence identity. **B.** Wt FLNA repeat 10 sequence mass spectroscopy peptide alignments. Highlighting reflects peptides identified.

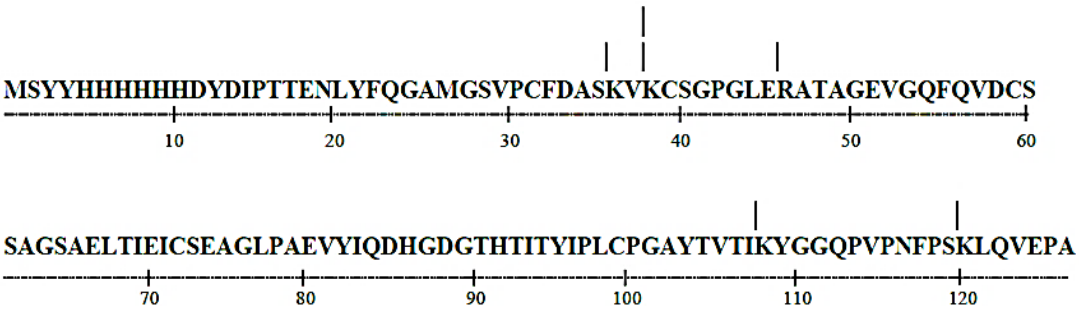

Figure 4.18 Map of possible trypsin cleavage sites. For His-tagged for Wt FLNAR10.

Wt FLNA R10 domain protein map of possible cleavage sites of trypsin adapted from peptide cutter (ExPASY). Vertical dashed lines represent potential trypsin cleavage sites.

Accordingly, *in silico* cleavage of the Wt FLNAR10 protein using trypsin was carried out using peptide cutter (ExPASY) software, which revealed that there were only five possible cleavage sites (Figure 4.18) within the FLNAR10 protein. This may reflect the digestion pattern seen previously for mass spectroscopy (Figure 4.17) to be insufficient or inaccessible due to the hydrophobic fold shown in the crystal structure of FLNAR10 (Figure 3.6) .

The fact that both A1188T and V1249A mutant FLNAR10 proteins had no obvious second band present in contrast to the Wt FLNAR10 during protein purification appeared to be intriguing. Perhaps this maybe a consequence of amino acid substitutions leading to slight changes in the structure caused by differences in the folding of the protein. On the other hand, maybe caused by local folding that is affected by external factors such as temperature, molecular crowding, or restriction of space during *E. coli* expression.

Looking at the crystal structure of FLNAR10 (Figure 3.6) there seems to be unstructured regions at both the N- and C- terminal ends that perhaps could be targeted by proteases, therefore leading to a truncated form of the protein. This notion maybe likely as suggested by the evidence obtained, but unfortunately the results did not yield adequate evidence and further studies would need to be performed. However, due to time constraints in this project this was unable to be carried out. Regardless, *in vitro* biochemical tests were carried out using this purified Wt FLNAR10 protein.

4.8 Summary

Expression of the pPROEX HTb-FLNAR10 recombinant constructs was able to produce soluble Wt and mutant FLNAR10 proteins. Pure FLNAR10 protein for further studies was obtained using a two-step purification system, IMAC Ni^{2+}-NTA chromatography followed by SEC. However, during Wt FLNAR10 protein purification a secondary eluting protein (8 kDa) was present in the Wt FLNAR10 fractions, which was supposedly caused by degradation or digestion of the FLNAR10 protein.

5. In vitro biochemical studies of Wildtype and mutant FLNA repeat 10 domains

5.1 Introduction

In vitro biochemical studies were used to study the effects of mutations in FLNA repeat 10 domain with respect to stability, secondary structure, and affinity towards F-actin of FLNA R10 proteins. A combination of proteolysis, circular dichroism (CD) spectroscopy and CD thermal denaturation were used to assess the structural stability, folding state and secondary structure of the FLNAR10 domain proteins. CD spectroscopy is based on the differential ability of a protein to absorb polarised light depending on its secondary structure. An important role for the filamin proteins is to crosslink F-actin to regulate the actin cytoskeleton to function in maintaining cell shape, cell migration, differentiation, and division. Intact full length FLNA has been shown to bind moderately to F-actin (Kd ~1.7×10^{-8} M) which was originally considered to be through the actin binding domain (ABD) alone, however, the ABD of FLNA alone has a relatively lower affinity towards F-actin (Kd ~1.7×10^{-5} M) (Nakamura F. *et al.*, 2007, Nakamura F. *et al.*, 2011). Consequently, FLNA repeat 10 domain was identified to contribute in binding to F-actin allowing the overall stronger interaction observed towards F-actin (Suphamungmee W. *et al.*, 2012, Nakamura F. *et al.*, 2007). Actin co-sedimentation binding assays were carried out to assess whether mutations in FLNA repeat 10 domain lead to any differences in the affinity towards F-actin which may correlate with an altered or gain-of-function phenotype that could lead to their respective disorders MNS or FMD.

5.2 Resistance to proteolytic cleavage

Controlled proteolysis to compare digestion sensitivity and structural stability of the FLNA repeat 10 domain proteins was carried out. If a protein is more easily digested it suggests that the protein maybe in a less well folded or in a more disordered state (Heiring C. and Muller Y.A., 2001). Wt, A1188T, and V1249A FLNAR10 protein samples were subjected to proteolysis to see whether there were any differences in their resistance to proteolytic digestion. Initially a trial was carried out on the Wt FLNAR10 protein sample using the enzymes; chymotrypsin, trypsin, subtilisin, and papain from the floppy choppy kit (JBS Jena Bioscience) at different ratios (w/w) of 100:1, 300:1, and 800:1 of FLNAR10 protein to enzyme, to define whether digestion of the protein occurs. Trials were also carried out to optimize the digestion temperature, and time for each enzyme. These trials revealed that the 300:1 ratio was optimal and only the

chymotrypsin and subtilisin enzymes were able to partially digest the protein, while the other enzymes were inefficient in these conditions (data not shown).

Digestions were then carried out on FLNAR10 Wt and mutant protein samples using either chymotrypsin or subtilisin at a ratio of 300:1 (w/w) incubated at room temperature. Samples were taken after an incubation time of 0, 60, 300 minutes and overnight for chymotrypsin, while subtilisin treated samples were taken after 0, 15, 180 minutes and overnight incubation periods and then samples were run on SDS-PAGE gels (refer to 2.15). These conditions were optimized based on the enzyme activity to determine a pattern for the digestion sensitivity of the FLNA repeat 10 domain proteins.

There appeared to be no significant difference between the protease treated Wt and mutant FLNAR10 proteins (Figure 5.1 and 5.2). Nevertheless, the imperviousness of all samples to partial digestion suggests that the protein seems to be tightly folded consistent with the FLNA repeat 10 domain structure (Figure 3.6) with minor accessibility to protease digestion. This suggests that the FLNAR10 protein appears to be stable owing the formation of the compact β-sandwich structure in line with its tight hydrophobic packing. Partial digestion is possibly caused by the digestion of the unstructured termini regions of the FLNA repeat 10 domain seen in the crystal structure (Figure 3.6).

Interestingly though, both the chymotrypsin and subtilisin proteases appeared to initially cleave the FLNAR10 protein producing a product of approximately 8 kDa in size (Figure 5.1 and 5.2). This may have been a coincidence, but seems to match the size of the secondary band that was present observed after purification of the Wt FLNAR10 protein. This may support a hypothesis of initial degradation of the Wt FLNAR10 protein producing a truncated form of the protein as previously suggested (refer to 4.4.3). The Wt FLNAR10 protein might in this case be slightly more susceptible to proteases in comparison to the mutant FLNAR10 proteins although, this was not observed in this case and remains to be resolved. However, noted that the size of the protein bands lower than 10 kDa maybe estimated values based on the calculation from an extrapolated MW calibration curve carried out using GelAnalyzer software, therefore may differ slightly so cannot be definite about matching the size of the secondary band.

Protease treated protein samples products were also compared to rTEV protease treated FLNAR10 protein samples, which cleaves the His-tag at a specific site (refer to 2.14). This revealed that a different sized band was observed of approximately 11 kDa in size was produced suggesting that both proteases (chymotrypsin and subtilisin) do not directly cleave off the His-tag alone, therefore signifying that there is no tag interference.

The SDS-PAGE gels reveal that subtilisin (Figure 5.1) seems to cleave the FLNAR10 protein to a greater extent in comparison to the chymotrypsin treated samples (Figure 5.2) which may occur as a result of greater access to the cleavage sites or the greater enzyme activity. Initially, the 8 kDa band is observed, but seems to be further digested which is apparent by its disappearance over higher incubation periods (Figure 5.1).

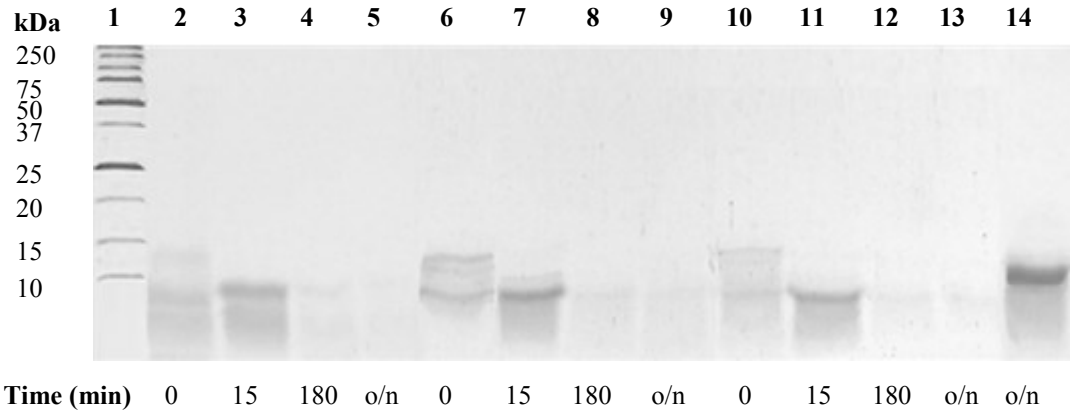

Figure 5.1 SDS-PAGE gel of subtilisin resistance trials.

FLNAR10 protein samples digestion by subtilisin run on 15% SDS-PAGE gels at 200 V for approximately 50 minutes (refer to 2.2.2 and 2.15). Lane 1; Precision Plus™ unstained protein standard, Lanes 2-5; Wt FLNAR10 treated samples, Lanes 6-9; V1249A FLNAR10 treated samples, Lanes 10-13; A1188T FLNAR10 treated samples, Lane 14; Wt FLNAR10 treated with rTEV at a 1:2 (w/w) ratio (refer to 2.14). Samples were taken after 0, 15, 180 minutes and overnight (o/n) incubation treatment respectively. Note; gel is a composite of two gels from lanes 1-9 and 10-14.

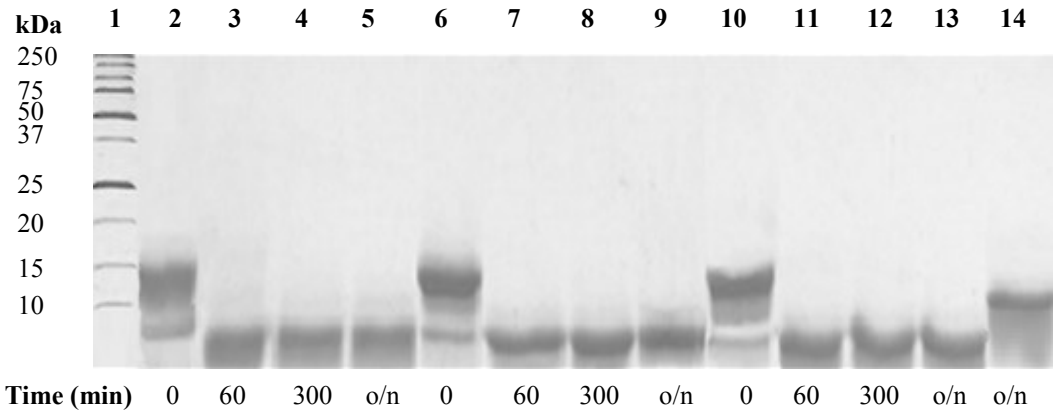

Figure 5.2 SDS-PAGE gel of chymotrypsin resistance trials.

FLNAR10 protein samples after chymotrypsin digestion run on 15% SDS-PAGE gels at 200 V for approximately 50 minutes (refer to 2.2.2 and 2.15). Lane 1; Precision Plus™ unstained protein standard, Lanes 2-5; Wt FLNAR10 treated samples, Lanes 6-9; V1249A FLNAR10 treated samples, Lanes 10-13; A1188T FLNAR10 treated samples, Lane 14; Wt FLNAR10 treated with rTEV at a 1:2 (w/w) ratio (refer to 2.14). Samples were taken after 0, 60, 300 minutes and overnight (o/n) incubation treatment respectively. Note; gel is a composite of two gels from lanes 1-10 and 11-14.

The FLNAR10 sequence was *in silico* cleaved using chymotrypsin (subtilisin was unavailable) using peptide cutter (ExPASY) software, resulting in approximately 25 possible cleavage sites that were mapped to the amino acid sequence (Figure 5.3). Comparing the cleavage sites to the crystal structure of FLNAR10 (Figure 3.6), reveals that most cleavage sites are situated near the termini ends of the FLNAR10 protein, which are consistently more likely to be cleaved. However, other cleavage sites will likely be within the hydrophobic core, which will likely make them inaccessible. Therefore, in reference to the SDS-PAGE gels, the bands produced after cleavage seems to fit the argument of the unstructured termini regions of the protein to be cleaved. Further analysis using mass spectroscopy could be used to analyse individual bands in order to classify the identity of the fragments produced, but due to time constrains in this project this was not carried out.

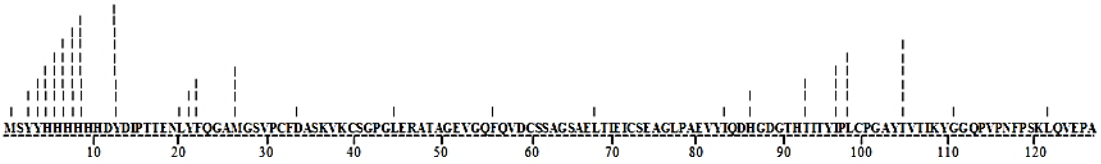

Figure 5.3 Map of possible chymotrypsin cleavage sites.

FLNAR10 Wt domain protein sequence showing possible cleavage sites of chymotrypsin adapted from peptide cutter (ExPASY). Vertical dashed lines represent potential chymotrypsin cleavage site, where number of dashes represent more predicted targeted regions.

5.3 Secondary structure analysis

Initial analysis of the amino acid sequence of FLNA repeat 10 was performed to identify the secondary structural elements within the protein. The secondary structure of FLNA repeat 10 was predicted using online servers; JPred (http://www.compbio.dundee.ac.uk/www-jpred/), PredictProtein (https://www.predictprotein.org/), PsiPred (http://bioinf.cs.ucl.ac.uk/psipred/), and also by comparing to the secondary structure from the previously determined crystal structure (Page R.C. *et al.*, 2011) (Figure 5.4). All programs predicted that the protein largely contains β-strands and random coil, with mostly conserved structure predictions between the programs and crystal structure analysis. However, comparison of the predictions from the programs to the secondary structure of the crystal structure further revealed that the protein coils consist of additional β-turns, β-bulge, and α-turns.

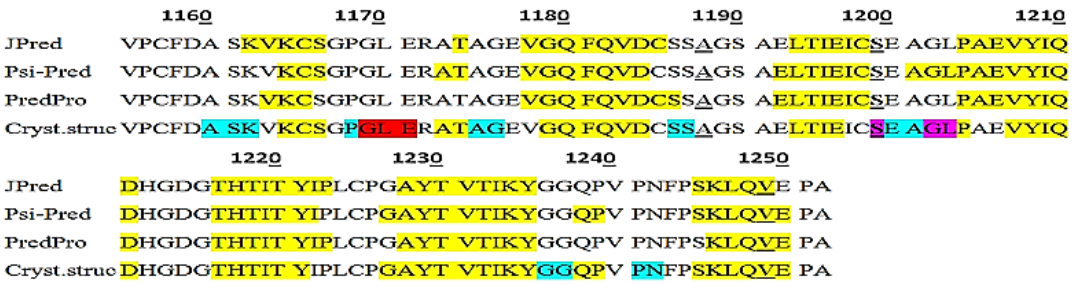

Figure 5.4 Secondary structure predictions for FLNA repeat 10 domain.

Analysis of FLNAR10 secondary structure analysis using JPred, Psi-Pred, PredictProtein programs and crystal structure data derived from Protein data bank (PDB-3RGH) (Page R.C. *et al.*, 2011) (numbers refer to full length FLNA). FLNA repeat 10 domain sequence with defined secondary structure. β-strand in yellow, α-helix in red, β-turn in cyan, β-bulge in pink, mutations in blue.

5.4 Circular dichroism (CD) spectroscopy

In order to examine whether mutations in the FLNAR10 domain protein cause any changes in the secondary structure or folding state of the FLNAR10 protein, Far-UV circular dichroism (CD) was performed. Far UV CD is based on the ability of a protein to differentially absorb polarised light depending on the secondary structural folding content present within the protein (Johnson W.C., 1990). Protein secondary structure elements (α-helix, β-sheet, β-turn, or random coil) absorb polarised light differently leading to different CD spectra patterns represented by model in Figure 5.5.

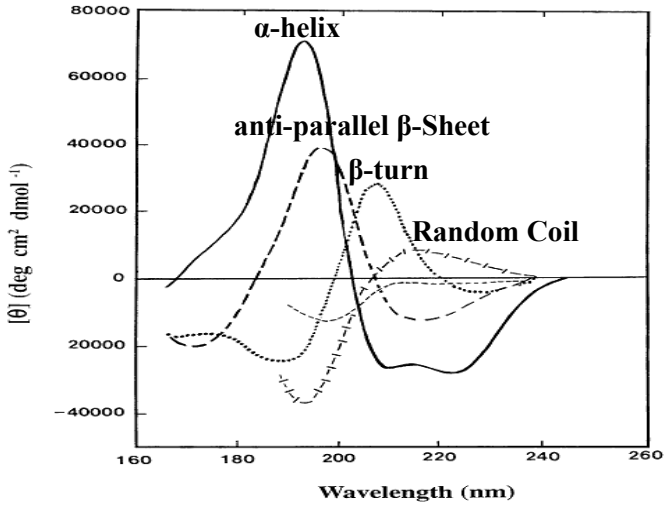

Figure 5.5 Far-UV CD spectra of associated types of secondary structure.

Far-UV CD spectra representing secondary structure types α-helix, anti-parallel β-sheet, β-turn, and random coil. Adapted from (Kelly S.M. *et al.*, 2005).

CD spectra were measured in the far-UV region in a 1 mm path cell cuvette between 180-260 nm using a Chirascan CD spectrometer (Applied Biophysics) with 1 nm readings taken every second. The CD spectra obtained were adjusted by initially averaging and smoothing the spectrum data, then by subtracting the baseline, which corresponds to buffer only. Conversion of the data from CD units of millidegrees into mean residue ellipticity units was carried out in order to adjust for the concentration and the size of the protein (refer to 2.16). Deconvolution of the CD spectra was performed using CDNN software and then analysed using CAPITO and K2d3 software, which contain algorithms and datasets to allow calculation of the likely secondary structure present in protein.

Initially, 0.1 mg/ml of lysozyme protein sample from chicken egg white (Sigma) was run as a positive control for the CD instrument. The lysozyme CD spectrum was compared to previously published CD spectra (Greenfield N.J., 2006, Tanaka F. *et al.*, 1975), revealing to have the same general pattern (Figure 5.6), therefore suggesting that the native structure had been obtained.

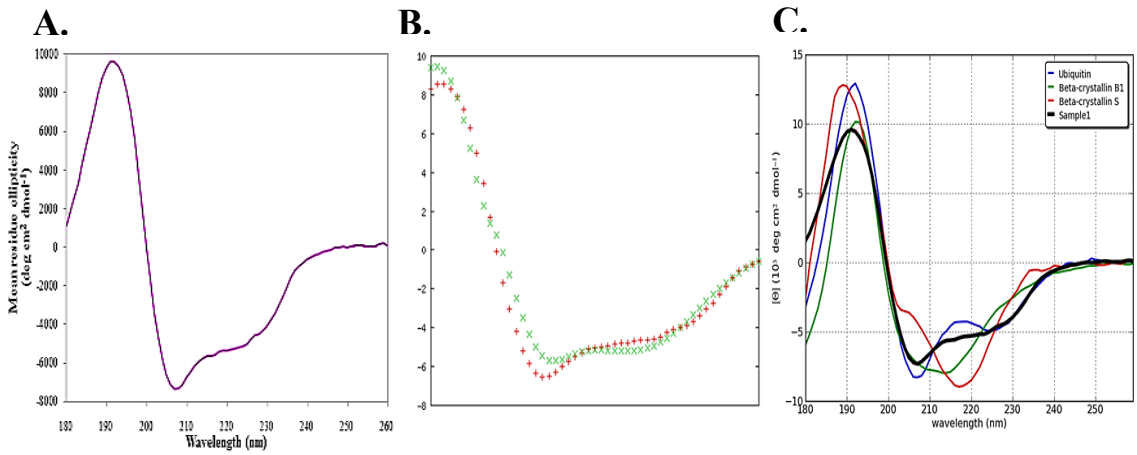

Figure 5.6 CD spectrum analysis of the lysozyme protein sample.

Analysis of the lysozyme CD spectrum **A**. Far-UV CD spectrum of 0.1 mg/ml lysozyme protein sample measured at wavelengths between 180-260 nm, at 1 nm readings taken every 1 second. **B.** analysis of the lysozyme spectrum through K2D3 server, green represents predicted spectrum, red represents input spectrum. **C.** Analysis of the lysozyme spectrum using the CAPITO server, black line represents input spectrum.

Multiple iterations of CD spectroscopy were initially carried out to optimize the concentration of the FLNAR10 protein samples needed to obtain appropriate CD spectra, which was determined to be 0.07 mg/ml. The CD spectra of the FLNAR10 protein samples (Wt and mutants) generally had the same CD spectra pattern. However, the spectra signal data between 180-190 nm was quite scattered in all the samples possibly due to some absorption of buffer ions in this region (refer to appendix 9.2.1). Therefore, only CD data between wavelengths 190-260 nm was considered to be suitable for further analysis and to acquire an improved estimate of the secondary structure in the FLNAR10 protein samples.

The FLNAR10 CD spectra were at first compared to the Far-UV CD spectra secondary structure model (Figure 5.5) in order initially determine the secondary structure and folding pattern of the FLNAR10 protein samples. The FLNAR10 protein samples

appeared to mostly, contain β secondary structure (β-turns and antiparallel β-sheet) and random coil, consistent with previous secondary structure analysis (refer to 5.3 and Figure 5.4). A characteristic β-secondary structure pattern are observed at a minima of ~ 219 nm, and a maxima of ~ 206 nm, while a minima at ~ 196 nm reflects random coil (Figure 5.7).

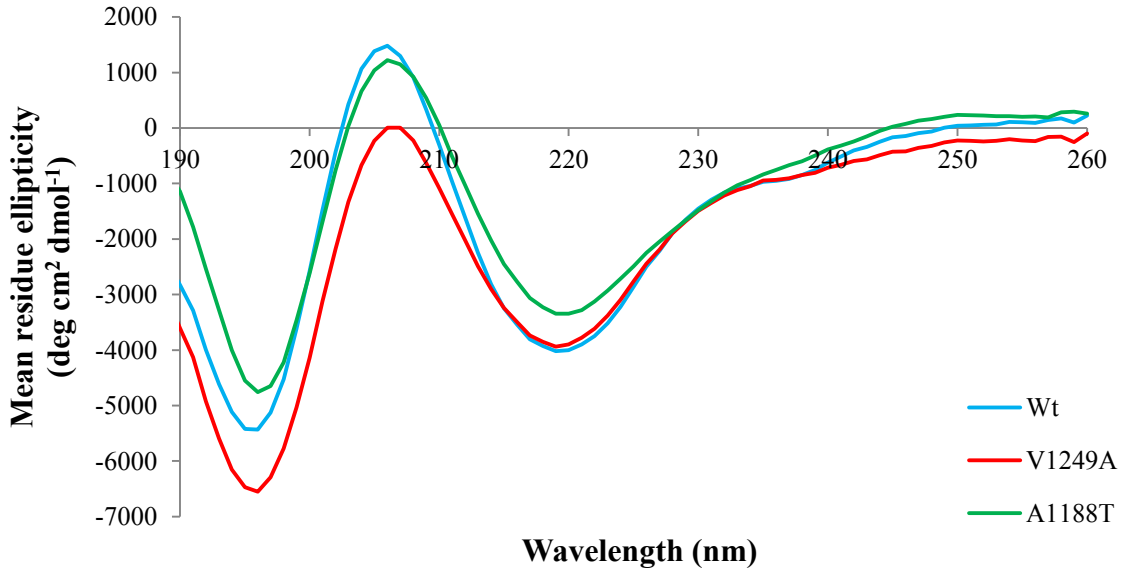

Figure 5.7 Far-UV CD spectra of FLNAR10 domain protein.

Far-UV CD spectra of 0.07 mg/ml Wt, V1249A, and A1188T FLNAR10 protein samples measured at wavelengths between 190-260 nm, at 1 nm readings taken every 1 second.

Deconvulation using the CDNN software, gives an estimate of the proportions of secondary structure present within a protein based on the CD spectra, by comparing and matching the spectra of the protein to known protein structures in its database (Andrade M. *et al.*, 1993). The CDNN algorithm revealed that the FLNAR10 protein samples consisted of approximately 11% α-helix, 42% β-sheet, 15% β-turn, and 32% random coil (Table 5.1), these values are largely consistent with the previously determined X-ray crystal structure and secondary structure sequence analysis (Figure 5.4) (Page R.C. *et al.*, 2011). However, it is significant to realise that CD analysis only gives an estimate of the proportions of secondary structure and the general CD spectrum trend exhibited by most proteins may not always hold for other proteins, therefore their estimations may not always be completely accurate (Kelly S.M. *et al.*, 2005).

Table 5.1 Deconvolution of the CD spectrum of FLNAR10 protein using. CDNN software.

Analysis of Wt FLNAR10 CD spectrum through CDNN software, determining the proportion of each secondary structure type. Adjusted proportion to 100%.

Secondary structure component	Proportion of secondary structures (%)	Adjusted proportion of secondary structures (%)
Helix	16%	12%
Antiparallel	45%	32%
Parallel	13%	10%
Beta-Turn	21%	15%
Random Coil	44%	31%
Total Sum	139%	100%

CAPITO and K2d3 online servers enable the estimation of the proteins secondary structure from its CD spectra based on closely structurally related proteins within their databases. Analysis of the FLNAR10 protein samples using CAPITO or K2d3 software revealed that the CD spectra of this protein had a relatively poor fit to the predicted CD spectra within the database (Figure 5.8). While analysis of the lysosome control sample using these servers, resulted in small deviations and a relatively good fit to the predicted CD spectra within the databases (Figure 5.6). Analysis using lysozyme as a control protein suggests that a true fit to the predicted CD spectra within the database was obtained, which was possibly achieved due to the known common structural fold of lysozyme in the database in comparison to the less known fold of FLNAR10 protein.

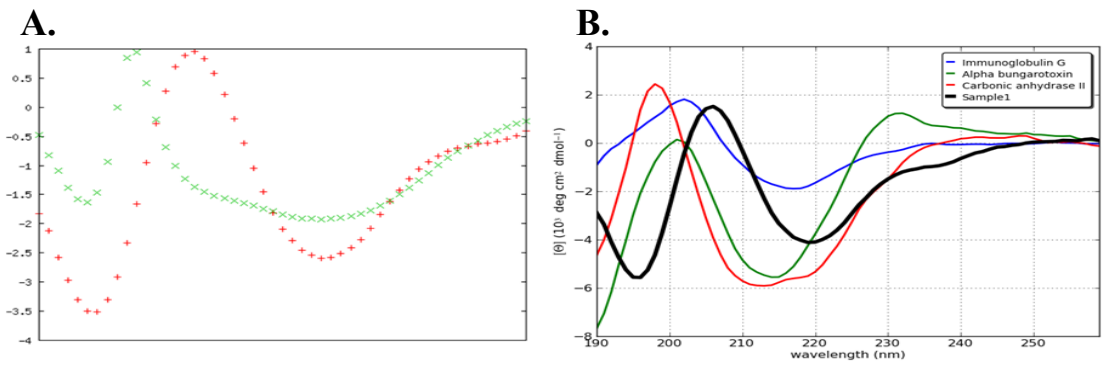

Figure 5.8 CD spectrum analysis of the Wt FLNAR10 protein sample.

A. Analysis of the Wt FLNAR10 protein spectrum through K2d3 server, green represents predicted spectrum, red represents input spectrum. **C.** Analysis of the Wt FLNAR10 protein spectrum using the CAPITO server, black line represents input spectrum.

However, the large deviation and ill-fitting analysis of the FLNAR10 protein samples seemed to be caused by a slight shift to the right of the CD spectra in comparison to the predicted spectra. In reference to the secondary structure model (Figure 5.5) the CD spectra pattern for the FLNAR10 protein sample appears to fit with the β-turn pattern to a better extent than the predicted β-sheet pattern, suggesting that analysis from CAPITO and K2d3 may have not considered this or their respective databases did not contain this protein folding pattern. Nonetheless, the spectra were comparable with the previously reported CD spectra for repeat domains in filamin C (Himmel M. *et al.*, 2003, Pudas R. *et al.*, 2005, Vorgerd M. *et al.*, 2005) with a minima at ~ 219 nm, and a maxima at ~ 206 nm, suggesting that the FLNAR10 protein domains have the correct native structure folding patterns (Figure 5.9).

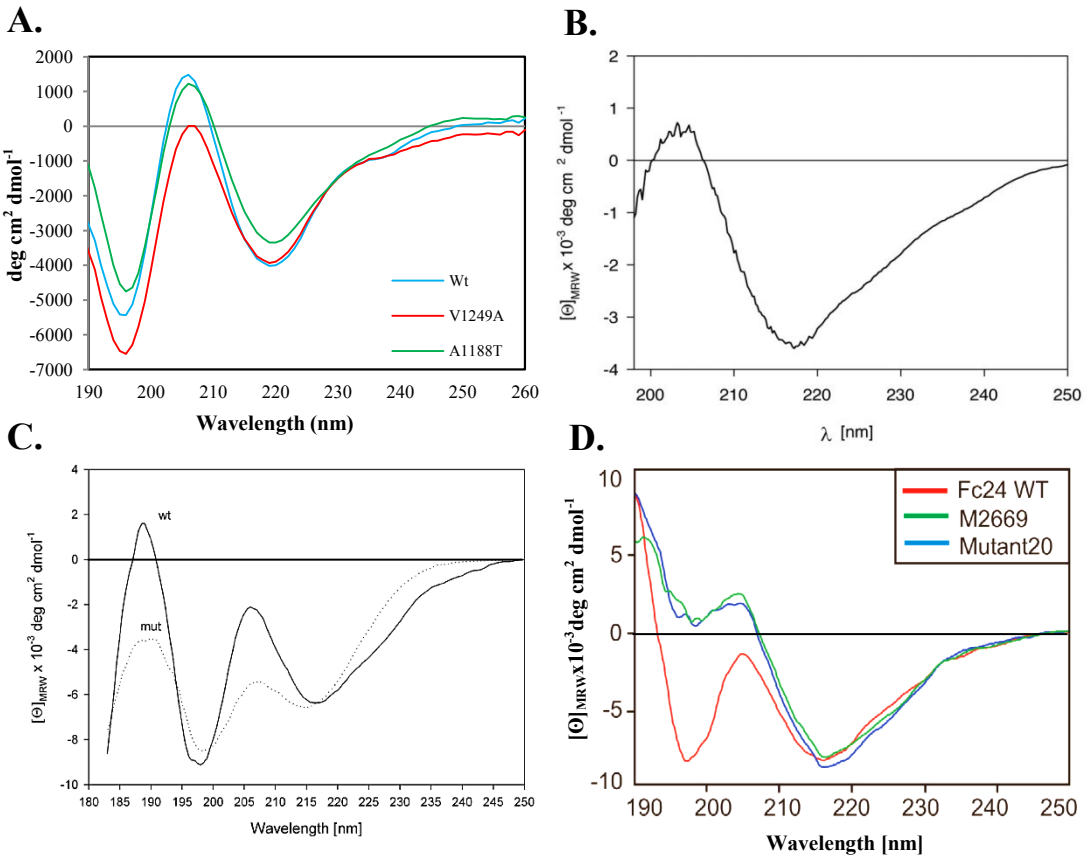

Figure 5.9 Filamin repeat domains CD spectra.

CD spectra of filamin repeat domains. **A.** CD spectra of FLNAR10 (this study), **B.** CD spectrum of FLNC repeat 23-24 domain, adapted from (Himmel M. *et al.*, 2003), **C.** CD spectra of FLNC repeat 24 domain, adapted from (Vorgerd M. *et al.*, 2005), **D.** CD spectra of FLNC repeat 24 domain, adapted from (Pudas R. *et al.*, 2005).

The CD spectra of the FLNAR10 protein samples were assessed to determine whether mutations leading to the OPD spectrum disorders MNS and FMD produced any changes in the structure or stability of the protein. The FLNAR10 purified protein samples (Wt, V1249A, and A1188T) showed no significant difference in the CD spectra overall folding pattern suggesting that no direct changes in the secondary structure occur upon introduction of the mutation. However, both mutant FLNAR10 domain samples (A1188T and V1249A) displayed slightly lower signal intensity in comparison to the Wt protein sample (Figure 5.7). This possibly signifies that changes in the conformation or partial unfolding of the FLNAR10 structure may have occurred resulting in slightly less stable proteins as previously suggested in the literature (Pudas R. *et al.*, 2005, Vorgerd M. *et al.*, 2005), although further evidence is needed to confirm this notion. In order to take into consideration any discrepancies, the protein samples CD spectra were all treated the same and the data was subtracted from a baseline corresponding to buffer only. Additionally, the data was converted from the CD units of millidegrees into mean residue ellipticity units to take into account the concentration and the size of the protein.

As the mutant V1249A FLNAR10 protein spectrum seemed to have slightly lower signal intensity in comparison to the two other protein samples Wt and the A1188T FLNAR10 protein (Figure 5.7), indicating that slight differences in the stability between the proteins may exist. The indicative slight instability from these missense mutations may hold the key to the mechanisms that are involved in leading to the OPD disorders. However, additional evidence is needed to support this theory.

5.5 CD Thermal Denaturation

Initially CD spectroscopy analysis presented the secondary structural pattern of the FLNAR10 protein, but also revealed slight differences between the Wt and mutant FLNAR10 protein samples suggested to be caused due to differences in stability. Therefore, CD thermal denaturation was performed to determine the thermal stability of the FLNAR10 protein. Where, thermal unfolding of the protein monitored by CD spectroscopy to evaluate the differences in protein stability based on changes in the secondary structure. Parameters were the same as previously described for CD spectroscopy, however, measurements were instead taken every 5℃ between 5-90℃ with 60 seconds equilibration time at each temperature. The spectra were analysed by

deconvolution of the CD spectra through CDNN software then the data was normalised and further fitted to a sigmoidal denaturation model using GraphPad Prism software (refer to 2.16).

As the temperature increases the protein starts to unfold, while the spectra of the FLNAR10 domain protein samples appear to change shape signifying a change in the structure. The minima characteristic of β-sheet observed at ~ 219 nm appears to slightly decrease in signal intensity, whereas the maxima at ~ 206 nm seems to shift to a lower wavelength (~ 200 nm) marginally, while adopting a minima peak (Figures 5.10-5.12). Analysing the spectra using CDNN software over the course of denaturation, reveals that the β-sheet content is reduced by approximately 16%, and this decrease is compensated by adopting an increase of 22% in random coil structure, which is consistent with the protein becoming unfolded. Comparing between the FLNAR10 protein samples, revealed that both mutants unfolded at slightly lower temperatures in contrast to the Wt protein, implying that they may be slightly unstable or less tightly packed (Figures 5.10-5.12) as previously hypothesised by Page R.C. *et al*., 2011.

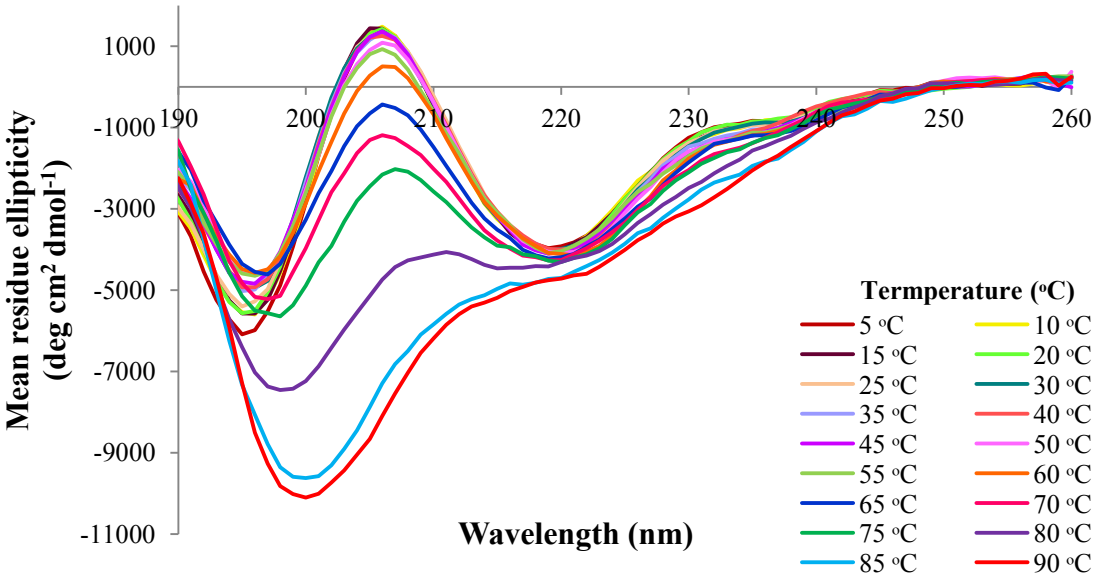

Figure 5.10 CD thermal denaturation spectra of Wt FLNAR10 domain protein.

Far-UV CD spectra of 0.07 mg/ml thermal denaturation of Wt FLNAR10 domain protein sample measured at wavelengths between 190-260 nm, at 1 nm readings taken every 1 second. Measurements were taken every 5℃ between 5-90℃ with 60 seconds equilibration time at each temperature.

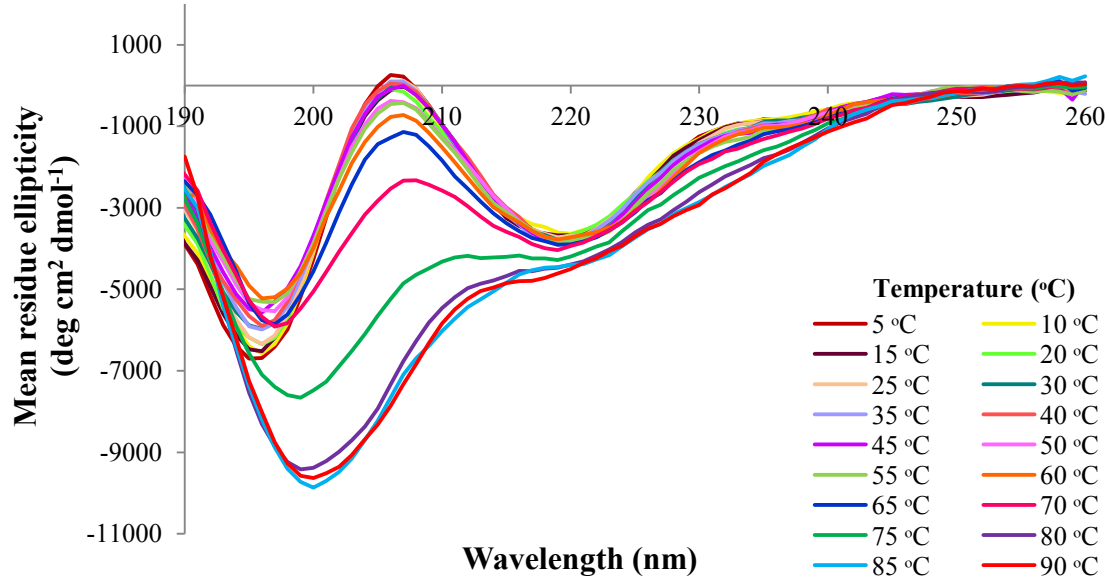

Figure 5.11 CD thermal denaturation spectra of V1249 FLNAR10 domain protein.

Far-UV CD spectra of 0.07 mg/ml thermal denaturation of V1249A FLNAR10 domain protein sample measured at wavelengths between 190-260 nm, at 1 nm readings taken every 1 second. Measurements were taken every 5℃ between 5-90℃ with 60 seconds equilibration time at each temperature.

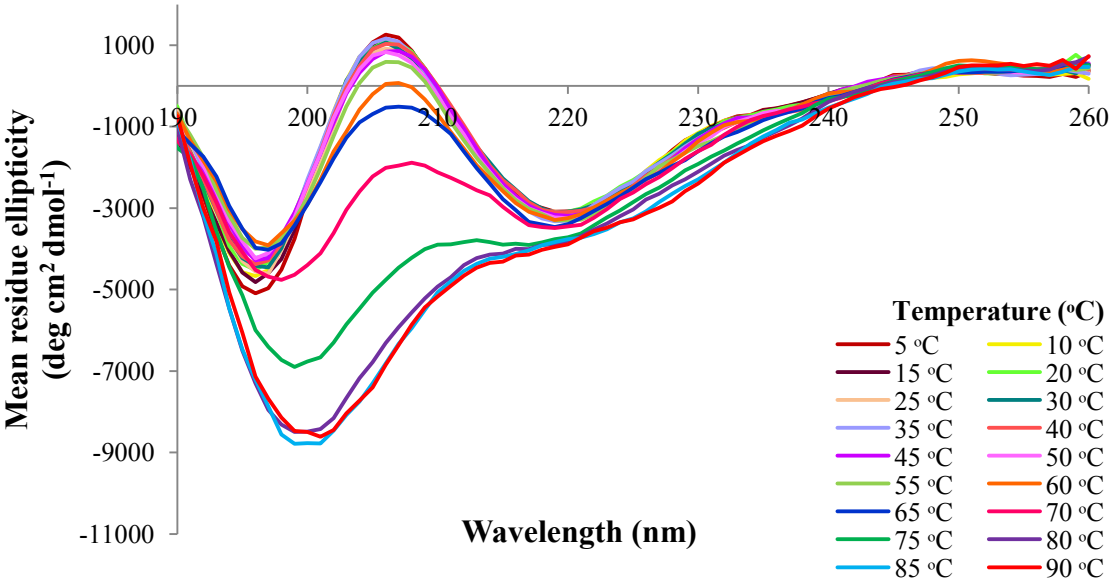

Figure 5.12 CD thermal denaturation spectra of A1188T FLNAR10 domain protein.

Far-UV CD spectra of 0.07 mg/ml thermal denaturation of A1188T FLNAR10 domain protein sample measured at wavelengths between 190-260 nm, at 1 nm readings taken every 1 second. Measurements were taken every 5℃ between 5-90℃ with 60 seconds equilibration time at each temperature.

In order to determine the melting temperature (Tm) of the protein, the CD data was normalised by taking the percentage of the total change in signal at one wavelength and was plotted against the temperature. A large change in the folding pattern was observed at wavelength ~ 206 nm, therefore this wavelength was selected to analyse the unfolding pattern between the Wt and mutant samples and to determine their Tm. The normalised graph at wavelength ~ 206 nm with respect to temperature achieved a sigmoidal plot, suggesting that the protein changes from a folded to an unfolded state presuming a two-state transition (Gupta R. and Ahmad F., 1999). However, thermal denaturation was determined to be irreversible, when the spectra was remeasured at 20℃ after the melt, the spectra remained the same as at the end of the melt (at 90℃), therefore the free energy change cannot be determined (not shown).

The normalised data was further fit to the Boltzmann sigmoid model through GraphPad Prisim software to estimate the Tm of the FLNAR10 protein samples (Figure 5.13). The point of inflection is represented when a protein transitions from a folded to an unfolded state (at 50%), which also reflects the Tm assuming a two-state model. The sigmoidal model had a relatively good fit to the data reflected by an R-square value of approximately 0.99. The Tm of FLNA R10 proteins were determined to be as follows; Wt; 76 ± 1.20℃, V1249A; 72 ± 0.44℃, and A1188T; 70 ± 0.45℃ (Table 5.2 and Figure 5.13). The Tm determined for the purified FLNAR10 protein seems to be relatively high in comparison to previous studies of the ABD of FLNA and FLNB, which had Tm of approximately 40℃ (Clark A.R. *et al.*, 2009, Sawyer G.M. *et al.*, 2009) and Ig18 which had a Tm of 57℃. This implies that the FLNAR10 protein is highly stable, possibly due to its tightly folded structure. Even after the FLNAR10, protein is denatured at 90℃, some secondary structure remains that again suggest its high stability.

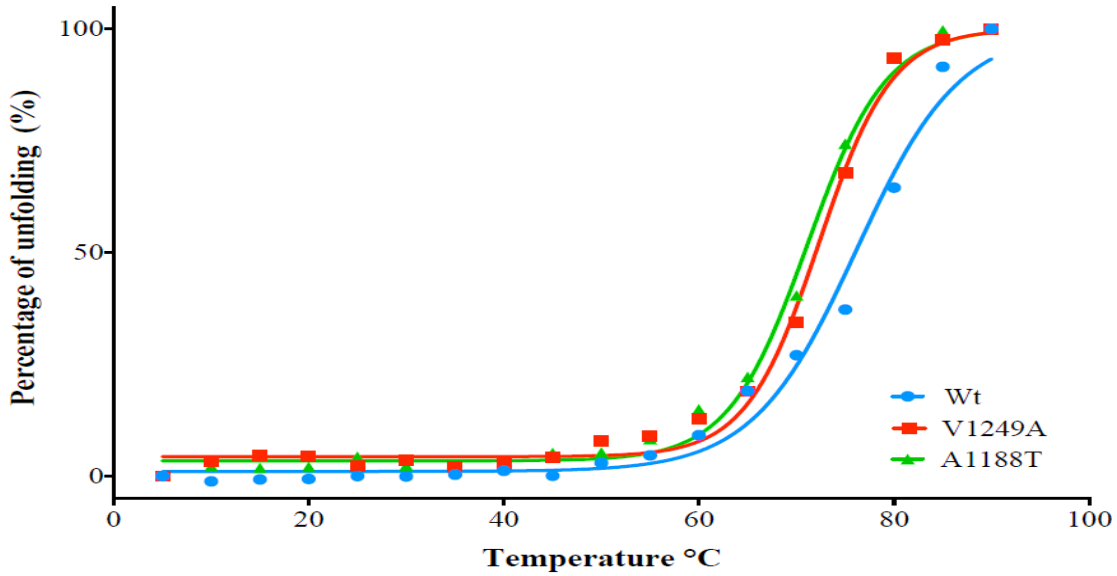

Figure 5.13 Normalised CD spectra of FLNAR10 domain proteins at 206 nm fitted to Boltzmann sigmoid model.

Normalised Far-UV CD spectra at absorbance at wavelength ~ 206 nm of FLNAR10 protein samples; Wt, V1249A and A1188T. (Normalised; the percentage of the total decrease in signal plotted against the temperature), Boltzmann sigmoid model fitted to the data using GraphPad Prism software (version 6.00 for Windows, GraphPad Software).

Table 5.2 Analysis of the Boltzmann sigmoid model to the normalised unfolding data at 206 nm.

FLNA repeat 10 protein samples analysis of fitting the Boltzmann sigmoid model to the normalised unfolding data at wavelength ~ 206 nm.

	Wt % unfolded	**V1249A % unfolded**	**A1188T % unfolded**
Best-fit values			
Bottom	1.04 ± 1.35	4.35 ± 0.89	3.41 ± 0.88
Top	~ 100.0	~ 100.0	~ 100.0
V50	76.14 ± 1.20	72.32 ± 0.44	71.12 ± 0.45
Slope	5.30 ± 0.86	3.74 ± 0.37	4.05 ± 0.38
Goodness of Fit			
R square	0.99	0.99	0.99
Absolute Sum of Squares	263.50	122.00	113.60
Standard deviation of residuals	4.34	2.95	2.85

Differences seen in the Tm and the rate of unfolding between the mutant and Wt FLNAR10 protein samples conclude that the mutant proteins are marginally less stable than Wt protein sample. Mutant domains are possibly slightly less stable due to minor changes in the tertiary structure caused by the amino acid substitutions. Any changes however, are unobserved in Far-UV secondary structure analysis. These slight differences between the mutant and Wt FLNAR10 domains may demonstrate a possible mechanism to alter the FLNA functions (refer to 5.6) which may in turn lead to the OPD group of disorders MNS and FMD. However, due to small differences between the melting temperatures additional evidence is needed to support this theory.

5.6 FLNAR10 and F-actin binding

Earlier studies have presented that the full-length FLNA dimer binds with reasonably strong affinity towards F-actin of K_d ~1.7×10^{-8} M, while the affinity of the FLNA ABD alone towards F-actin is relatively weak with a K_d ~1.7×10^{-5} M. These observations suggested that an additional region within the molecule may contribute to the overall binding affinity towards F-actin as seen in the full-length FLNA (Nakamura F. *et al.*, 2007, Nakamura F. *et al.*, 2011). The FLNA repeat 10 domain was identified to bind to F-actin, indicating in being the contributing region in the full-length FLNA to allow the overall binding affinity towards F-actin seen in the full-length FLNA (Suphamungmee W. *et al.*, 2012, Nakamura F. *et al.*, 2007). However, the affinity of the FLNAR10 region towards F-actin was not assessed previously, therefore actin co-sedimentation assays were carried out in this study to determine the affinity, and also to assess whether mutations in the FLNA repeat 10 domain lead to changes in the affinity towards F-actin, which may alter the functions of the FLNA protein. These changes may correlate towards a better understanding of the OPD disorders.

Assays were set up by mixing the polymerised actin (F-actin) (10 μM) with purified FLNA repeat 10 protein samples of different concentrations, then subjecting this mix to high speed ultracentrifugation in order to pellet the F-actin bound proteins. The supernatant and pellet samples were run on SDS-PAGE gels and the bands were quantified by densitometry (refer to 2.17). The data was then analysed by calculating the ratio of FLNAR10 protein bound to F-actin and fitted to binding models using GraphPad Prism software. Both FLNAR10 and F-actin alone were run as controls and to take into consideration any FLNAR10 pelleting on its own when analysing the data.

If binding occurs between the FLNAR10 protein and F-actin co-sedimentation of these proteins will occur resulting in these proteins to be present in the pellet sample.

Initially, trial actin binding assays were conducted to determine whether binding occurs between the purified FLNAR10 protein samples and F-actin. The SDS-PAGE gels confirmed the presence of bands representing both the F-actin and FLNAR10 proteins within the pellet sample, in comparison to the supernatant sample, which only contains unbound FLNAR10 protein. This reflects that binding of the FLNAR10 proteins to F-actin occurs, as they are able to co-sediment (Figure 5.14).

To establish the pattern of binding, the FLNAR10 protein samples concentration was varied, while F-actin concentration was fixed. Initial analysis of the actin co-sedimentation assays revealed that the FLNAR10 protein appeared to bind weakly towards F-actin (Figure 5.14) in comparison to the previously published filamin ABD (Clark A.R. *et al.*, 2009, Duff R.M *et al.*, 2011, Sawyer G.M. *et al.*, 2009, Nakamura F. *et al.*, 2007). This appears to be consistent with the suggested function of the FLNA repeat 10 domain in contributing to the overall binding affinity towards F-actin (Suphamungmee W. *et al.*, 2012) by possibly positioning the rod domain near F-actin (Figures 1.3-1.5), however further evidence is needed to resolve this mechanism. Interestingly, the secondary band at 8 kDa apparent in the Wt FLNAR10 protein sample seemed to co-sediment along with the F-actin, consistent with the analysis (refer to 4.7) of being part of the FLNAR10 protein. To keep analysis of the data reliable, the secondary band observed in the Wt FLNAR10 protein SDS-PAGE gels (Figure 5.14) was taken into consideration during densitometry calculations.

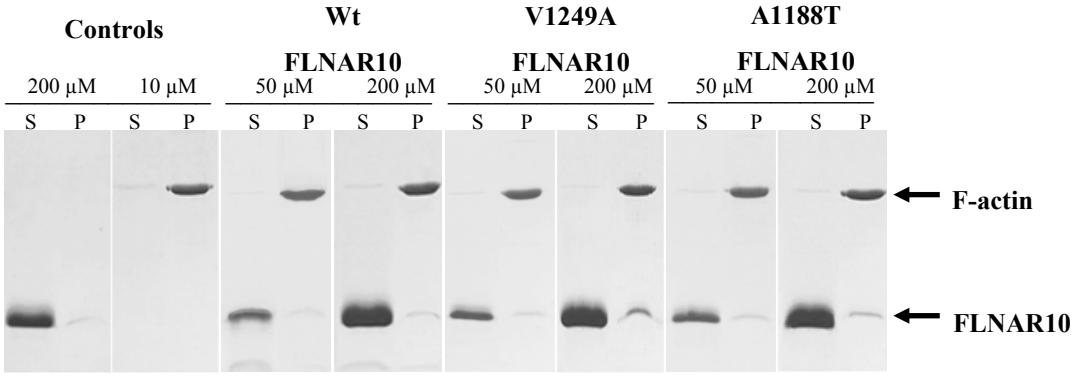

Figure 5.14 Example actin co-sedimentation assay.

Example of an actin co-sedimentation assay, samples were run on a 15% SDS-PAGE gels at 200 V for approximately 50 minutes (refer to 2.2.2 and 2.17). Ratio of 10 µM F-actin to either 50 µM or 200 µM FLNA R10 protein. Controls 200 µM referring to FLNAR10 and 10 µM F-actin, S= supernatant, P = Pellet.

Previous co-sedimentation studies of the filamin ABD or myosin binding to F-actin have been observed to follow a 1:1 binding models (Duff R.M *et al.*, 2011, Sawyer G.M. *et al.*, 2009, Clark A.R. *et al.*, 2009, Várkuti B.H. *et al.*, 2012). Therefore, based on these observations the data was fit to a 1:1 binding model using GraphPad prisim, however, upon assessment the FLNAR10 data was unable to fit this binding model. Owing to the lack of curvature and saturation of F-actin, the data was difficult and unsuccessful to fit this model (Figure 5.15). This may have occurred due to weak binding, or non-specific binding occurring once the primary sites on F-actin are occupied.

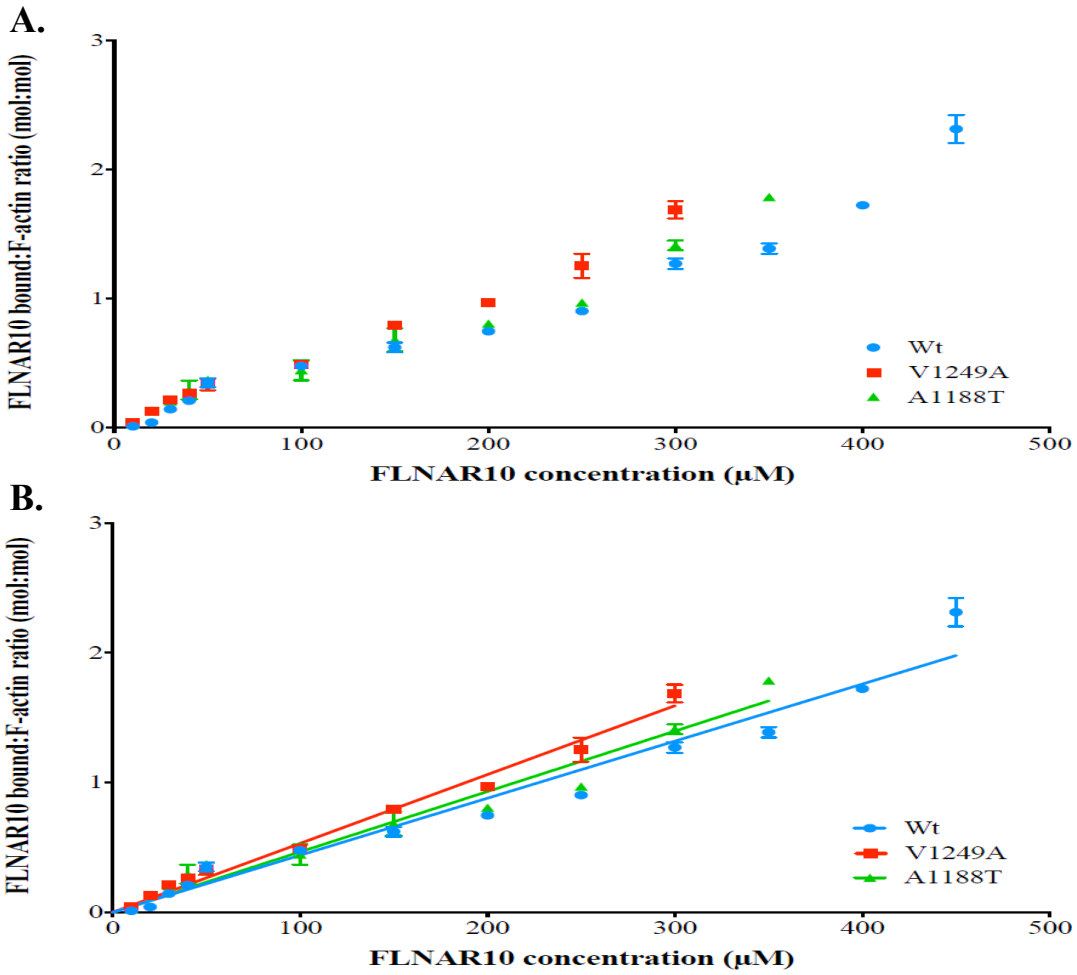

Figure 5.15 Actin co-sedimentation assay data.

A. Actin co-sedimentation assay data was analysed by densitometry. The ratio of FLNAR10 protein bound to F-actin was plotted against FLNAR10 concentrations from 0-450 µM. **B.** Fitting of actin co-sedimentation data using one site binding (hyperbola) model. Graphs were made using GraphPad Prism software (version 6.00 for Windows, GraphPad Software).

The literature has previously shown that protein concentrations used in actin co-sedimentation trials did not exceed 200 μM and produced the typical hyperbolic relationship of bound to free protein in full-length FLNA and myosin (Duff R.M *et al.*, 2011, Clark A.R. *et al.*, 2009, Nakamura F. *et al.*, 2007, Várkuti B.H. *et al.*, 2012). Therefore, based on observation the 1:1 binding model was fit to the data between 10 - 200 μM of FLNAR10 protein to assess whether a hyperbolic curve is observed. The data initially seemed to have a tolerable fit to this model producing a hyperbolic shape, suggesting that at lower concentrations of FLNAR10 protein specific binding to F-actin maybe occurring that eventually becomes non-specific owing to arbitrary binding or to pelleting non-specifically with F-actin at higher concentrations (Figure 5.14 and 5.16). In order to compensate for any non-specific pelleting controls of FLNAR10 protein samples alone were run (Figure 5.14) and were then subtracted off from the sample data. In retrospect, the Kd was unable to be accurately estimated from this model as no saturation of F-actin was able to be achieved, which suggested that this model did not fit accurately as originally estimated. The 1:1 binding model seemed to overestimate the fit of the data resulting in an R squared value of approximately 0.95, but was not considered significant (refer to 9.3.2).

As the typical 1:1 binding model was unable to fit this data range, an alternative model was attempted to fit the data. The Boltzmann sigmoid model was used to fit the data between 10 – 200 μM, as the data seemed to have an initial slight sigmoidal shape. The data seemed to generally fit this model to a better extent (Figure 5.16) with an R-squared value of approximately 0.98 however, resulted in a large confidence interval, standard error and again no saturation of F-actin was achieved (refer to 9.3.3). Therefore, the Kd value was again unable to be correctly estimated from this model, but provided a better fit.

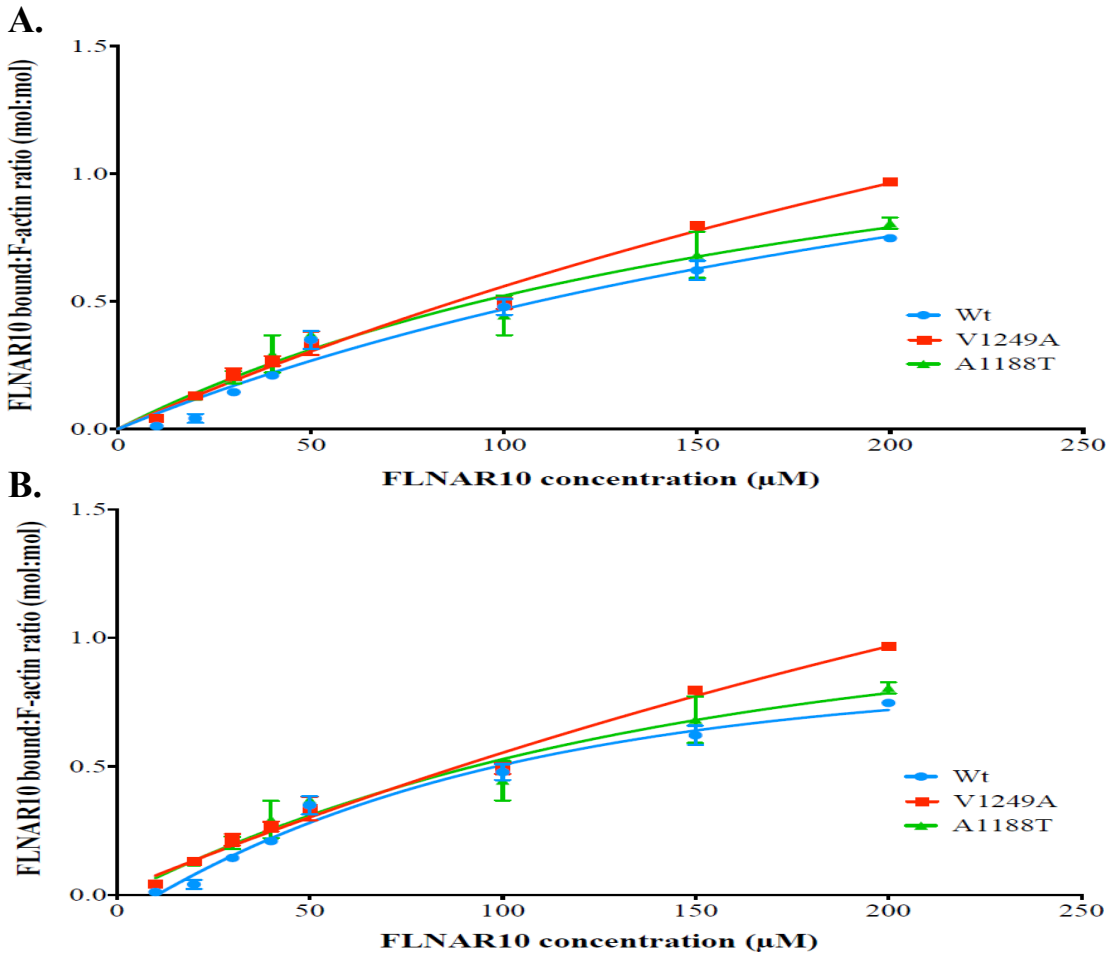

Figure 5.16 Actin co-sedimentation assays fitted with 1:1 binding model (0-200 µM FLNAR10 protein).

Actin co-sedimentation assay normalised data fitted with a 1:1 binding model (one site binding (hyperbola)) with FLNAR10 concentrations ranging from 0-200 µM. Using GraphPad Prism software (version 6.00 for Windows, GraphPad Software).

As these binding models did not typically fit the data in the case of the FLNAR10 protein analysed in this study, it is suggested that a different binding pattern may exist for this region within FLNA. Previously Nakamura *et al* (2007) used deletion constructs containing different regions of the FLNA protein, which demonstrated that the constructs did not all result in the typical 1:1 binding model observed for the full-length FLNA (Nakamura F. *et al.*, 2007). Interestingly, the constructs that contained both the FLNA ABD and repeat 10 domain resulted in a hyperbolic pattern at low FLNA concentrations, but were less hyperbolic in comparison to the full-length FLNA (Figure 1.6). This pattern was similar to the binding patterns observed in this study for the FLNAR10 protein (Figure 5.16), which may imply that at low concentrations of

FLNAR10 protein (0-50 μM) specific binding may occur that eventually becomes non-specific at higher concentrations of FLNAR10 protein. This theory suggests that an initial interaction between the FLNAR10 and F-actin protein may form that may further promote the ABD in full-length FLNA to bind to F-actin providing an overall stronger binding affinity towards F-actin. Different regions of the FLNA protein may fulfil specialised roles, which lead to different behaviours in binding to F-actin and other binding patterns. As the *in vitro* co-sedimentation assay revealed that the FLNA ABD and repeat 10 domain results in lower affinity towards F-actin suggested by the pattern of binding in comparison to the full-length FLNA protein, additional interactions between the domains or other factors that allow the overall interaction to F-actin may occur.

Notably, it was observed that small differences in affinity towards F-actin between the Wt and mutant samples existed. Both the mutant FLNAR10 protein samples (A1188T and V1249A) were detected to bind to F-actin with a slightly higher affinity in comparison to the Wt FLNAR10 protein (Figure 5.14 - 5.16, refer to 9.3.1), which appeared to be consistent with the previously proposed gain of function phenotype on OPD disorders (Robertson S.P. *et al.*, 2003). Interestingly, the V1249A FLNAR10 protein sample seemed to have a higher affinity towards F-actin in comparison to the other FLNAR10 protein samples (A1188T and Wt), however it is unclear why this difference occurs. This is evidently curious to compare as both these mutations lead to severe cases of OPD spectrum disorders, suggesting the possibility of changes to the structure allowing a larger interface to allow F-actin binding.

The crystal structure of the FLNA Repeat 10 domain (Page R.C. *et al.*, 2011) was modelled to fit within the N-terminus of the F-actin protein, but its orientation during binding remains unclear (Figure 1.8). This interaction has been suggested to occur through a conserved basic residue groove within the FLNAR10 domain with interaction specificity occurring through the assistance of residues neighbouring this basic groove. Using the FLNAR10 domain model (Page R.C. *et al.*, 2011) the recurrent mutations A1188T and V1249A leading to severe forms of OPD disorders (Robertson S.P. *et al.*, 2003, Robertson S.P. *et al.*, 2006) were mapped to sit near this basic groove (Figure 5.17) suggesting the possibility that these residues maybe involved indirectly in the interaction with F-actin. It is possible to suggest that these mutations may lead to

conformational changes allowing for a more open structure, which consequently leads to an increase in binding to F-actin as seen in this study. The A1188T mutation associated with MNS has been mapped to be located near the N-terminal region of FLNAR10 domain, while the V1249A mutation causing FMD is located near the C-terminus of FLNAR10 domain (Robertson S.P. *et al.*, 2003, Page R.C. *et al.*, 2011, Robertson S.P. *et al.*, 2006). This proposes that a specific single mechanism may lead to these severe OPD disorders through their increased affinity towards F-actin.

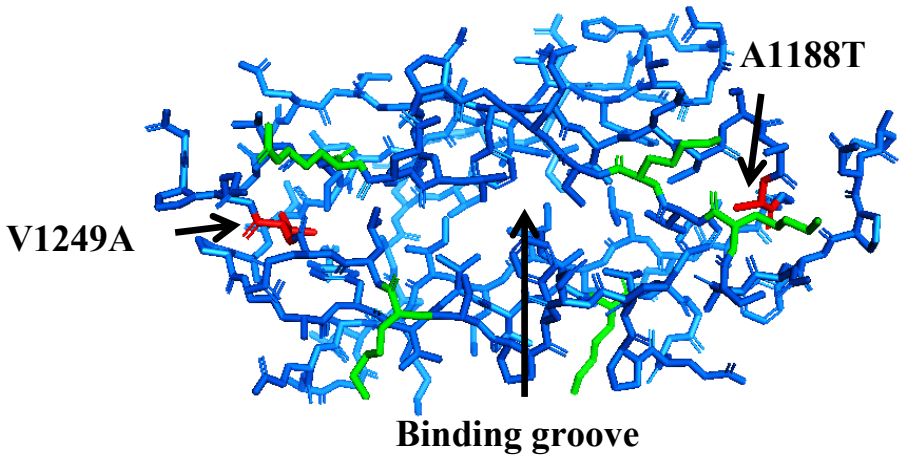

Figure 5.17 FLNAR10 domain structure showing possible F-actin binding groove.

FLNAR10 domain binding groove formed by conserved basic residues (Lys1162, Lys1164, Arg1172, Lys1234, and Lys1246) in green. Amino acids in red show mutation sites for V1249A and A1188T that, sit near the binding groove. Figure was made using PyMOL software (The PyMOL Molecular Graphics System, Version 1.3 Schrödinger, LLC) from the FLNA repeat 10 structure coordinates (PBD-3RGH) (Page R.C. *et al.*, 2011).

The amino acid Ala1188 sits on the BC loop allowing the hydrophobic packing of the β-sandwich to occur with a calculated solvent accessibility of 0.0 $Å^2$. On the other hand, Val1249 is buried within the hydrophobic core at the carboxy-terminal end of FLNAR10 with solvent exposure calculated as 0.6 $Å^2$. These mutations have been proposed to cause disruptions of the hydrophobic packing of the FLNAR10 domain. The structure of the FLNA protein containing either the A1188T or the V1249A mutation was modelled using pymol software (Figure 5.18). The A1188T mutation seems to result in the larger hydrophilic amino acid threonine causing clashes with the side chains of Val1163, Cys1185, and Tyr1235 leading to the proposed disruption of both the BC loop and the nearby CD loop (Page R.C. *et al.*, 2011). Peculiarly in contrast

to the A1188T mutation, the V1249A mutation does not lead to steric clashes as the hydrophobic amino acid valine is substituted with the smaller amino acid alanine. The substitution of valine to alanine possibly causes a cavity, which may lead to disruptions of the hydrophobic packing in this region (Figure 5.18), possibly by providing a more open structure allowing for the F-actin to bind to previously hidden basic residues, however, its mechanism remains unclear (Page R.C. *et al.*, 2011). These mutations imply the importance of hydrophobic packing on the structure and function of the FLNA repeat 10 domain, disruptions may alter the stability and impair folding of the FLNA protein.

The mutants in this study observed a slight increase in the affinity towards F-actin in comparison to the wild type FLNAR10 protein. Particularly the FLNAR10 V1249A mutation presented with a slightly higher affinity towards F-actin in comparison to the other mutant A1188T, this may have been caused by a larger change in the structure produced by the amino acid substitution of valine to alanine. The amino acids valine and threonine contain branched β-carbons that are attached to two non-hydrogen substitutes leading to restrictions in the conformation of the backbone (Betts M.J. and Russell R.B., 2003). When valine is substituted to alanine (a non-branched amino acid), it possibly causes a loss of restriction on the conformation of the backbone allowing for a more open structure. Whereas, a change from alanine to threonine not only causes steric clashes, but may also lead to some restriction on the conformation of the backbone. Consequently, this conformation leading to a greater freedom of movement may allow the higher affinity towards F-actin seen in the V1249A mutation; however, further enquiry is needed.

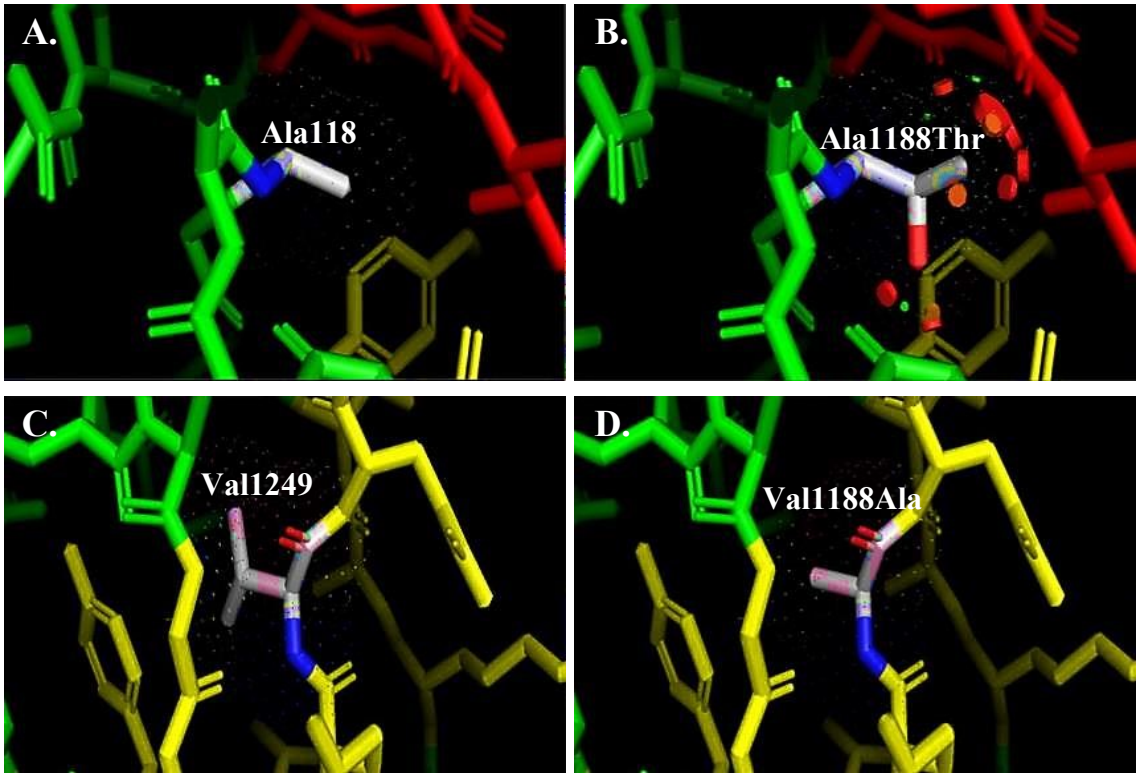

Figure 5.18 FLNAR10 domain mutations associated with severe OPD disorders effects on the FLNAR10 domain structure.

FLNAR10 domain alterations due to mutations A1188T and V1249A leading disruption of the hydrophobic packing. **A. & B.** A1188T mutation effects on the crystal structure of FLNAR10, proposed to lead to steric clashes with the other neighbouring amino acids shown by orange circles. **C. & D.** V1249A mutation effects on the crystal structure of FLNAR10, the V1249A mutation possibly leads to a cavity.. Figure was created using PyMOL software (The PyMOL Molecular Graphics System, Version 1.3 Schrödinger, LLC) from the FLNA repeat 10 structure coordinates (PBD-3RGH) (Page R.C. *et al.*, 2011).

Overall, these observations suggest that regions containing mutational hotspots within the FLNA repeat 10 domain may possibly be involved in indirectly allowing F-actin and other proteins to bind, therefore further investigation of exact binding location is needed. Effects of these mutations in leading to increased affinity towards F-actin are consistent with a gain-of-function mechanism of its respective skeletal disease in the OPD spectrum group of disorders as shown in previous ABD filamin studies (Sawyer G.M. *et al.*, 2009, Clark A.R. *et al.*, 2009). However, the underlying biochemical mechanism of OPD disorders and the cellular functions of FLNA remain to be investigated.

5.7 Summary

In vitro biochemical studies were carried out with the aim of comparing and contrasting the effects of mutations on the stability, secondary structure, and affinity towards F-actin of the FLNAR10 proteins. Initially, the secondary band seen during protein purification of Wt FLNAR10 protein sample was seen during protease digestion suggesting that it may have been caused by an initial degradation of the protein leading to the production of a truncated form of the protein, though this remains unclear. CD spectroscopy and proteolysis revealed that the overall fold and resistance to cleavage was almost equivalent between the Wt and mutant FLNAR10 protein samples with only minor differences. CD thermal denaturation further revealed that the FLNAR10 protein was stable resulting in a high Tm consistent with the tightly packed hydrophobic folding seen in the crystal structure. This is also consistent with the well-behaved protein during purification and storage. The FLNAR10 protein was shown to have a relatively weak binding affinity towards F-actin consistent with being an additional contributor towards the overall binding affinity of the FLNA to F-actin. Both mutants showed a slight increase in the affinity towards F-actin in comparison to the Wt FLNAR10 protein, which is consistent with their associated gain-of function diseases.

Particularly, the FLNAR10 V1249A mutation showed a slightly higher affinity towards F-actin and less thermostability than the A1188T mutation, which was proposed to be caused by a larger change in the structure due to the amino acid substitution. Overall, these results contribute towards a better understanding of the FLNA structure and function providing further evidence towards a gain-of function mechanism for the OPD disorders, FMD and MNS.

6. *Conclusions*

6.1 Introduction

The aim of this study was to examine the molecular properties of the Filamin A repeat 10 domain in reference to its associated X-linked OPD spectrum disorders MNS and FMD, to provide insight and a better understanding of the FLNA mechanisms during normal and disease states. Filamin sits at the centre of a complex and fine-tuned mechanism allowing the regulation of cell shape, cell migration, differentiation, and division by triggering the remodelling of the actin cytoskeleton through signal transductions. The FLNA protein allows the crosslinking of actin filaments (F-actin) into orthogonal networks through its amino-terminal actin binding domain (ABD) (Hartwig J.H. *et al.*, 1980), while other domains link to the cellular membrane and recruit signalling molecules involved in signal transduction (MacPherson M. and Fagerholm S.C., 2010, Hou L. *et al.*, 1990, Stossel T.P. *et al.*, 2001, Feng Y. and Walsh C.A., 2004, Popowicza G.M. *et al.*, 2006).

Interestingly, not only the ABD of FLNA binds to F-actin, but the repeat 10 domain of FLNA has also been structurally identified to bind to F-actin as well (Suphamungmee W. *et al.*, 2012). Coincidently, conserved mutations leading to severe OPD skeletal disorders have been demonstrated to cluster within the repeat 10 domain of FLNA (Robertson S.P. *et al.*, 2003) suggesting its functional importance for mediating the correct function of FLNA. However, the precise effects and mechanisms leading to these diseases are yet to be revealed. *In vitro* biochemical studies were used to compare the effects of these recurrent mutations in the FLNAR10 protein on its stability, secondary structure, and affinity towards F-actin, while also determining the binding affinity of the FLNAR10 protein to F-actin. Initial studies showed that the FLNAR10 protein was able to bind to F-actin, but with a relatively weak binding affinity in comparison to previous ABD (Clark A.R. *et al.*, 2009, Sawyer G.M. *et al.*, 2009, Nakamura F. *et al.*, 2007). Studies revealed that both the Wt and mutant FLNAR10 protein samples were relatively stable leading to a high melting temperature which is consistent with its tightly packed hydrophobic structure as determined through the crystal structure (Page R.C. *et al.*, 2011). Mutations within the FLNA repeat 10 led to an observation of a slightly increased affinity towards F-actin and reduced thermostability in comparison to the wild-type FLNA repeat 10, as previously seen for mutations within the ABD of FLNA (Clark A.R. *et al.*, 2009). Studies suggest that changes within the structure may lead to these observed differences in the increase in

binding to F-actin, which seems consistent with a gain-of-function mechanism for the OPD disorders (Page R.C. *et al.*, 2011, Clark A.R. *et al.*, 2009, Robertson S.P. *et al.*, 2003). Taken together these results contribute towards a gain-of function mechanism for the OPD spectrum disorders and provide a better understanding of the FLNA mechanism in binding to F-actin.

6.2 FLNA repeat 10 domain and F-actin

Previously the literature has identified that the repeat 10 domain of FLNA was able to bind to F-actin using co-sedimentation assays and TEM (Nakamura F. *et al.*, 2007, Nakamura F. *et al.*, 2011, Suphamungmee W. *et al.*, 2012), but its affinity towards actin was not evaluated. In this study, the FLNA repeat 10 domain proteins binding capacity was assessed using *in vitro* actin co-sedimentation assays and were then quantified using densitometry. The FLNAR10 protein revealed that it had a relatively weak binding capacity for F-actin, in comparison to the previously published actin binding results for filamin ABD (Clark A.R. *et al.*, 2009, Duff R.M *et al.*, 2011). This seemed to be consistent with the idea that the FLNAR10 domain acts as an additional contributor towards F-actin binding (Nakamura F. *et al.*, 2007, Suphamungmee W. *et al.*, 2012) by possibly stabilising the branched configuration of F-actin.

Binding of the FLNA repeat 10 protein to F-actin did not follow the 1:1 ratio binding models seen in previous actin binding proteins (Clark A.R. *et al.*, 2009, Duff R.M *et al.*, 2011, Várkuti B.H. *et al.*, 2012), suggesting that it may have a different binding mechanism compared to the ABD of FLNA. One model has suggested that an interface forms between regions of conserved basic residues that form a groove in the FLNA repeat 10 domain to allow binding to the complementary negatively charged amino acids on the N-terminus of F-actin leading to electrostatic interactions. (Page R.C. *et al.*, 2011). However, as other FLNA repeat domains contain these conserved residues yet contain a slightly varied amino acid sequence (Ithychanda S.S. *et al.*, 2009). It has been suggested that other neighbouring residues facilitate the interaction to F-actin (Nakamura F. *et al.*, 2007, Suphamungmee W. *et al.*, 2012, Page R.C. *et al.*, 2011), however, remains to be further examined.

A mechanism for the organisation of the actin cytoskeleton suggests that the weakly interacting ABD and repeat 10 domain of FLNA cooperatively promote FLNA binding to F-actin resulting in a stronger interaction, while allowing flexibility. Nearby

filaments cross-link to form a mechanically organised actin cytoskeleton network, which can be disrupted due to the weak interactions between FLNA and F-actin during cytoskeletal remodelling (Suphamungmee W. *et al.*, 2012). However, additional domains *in vivo* other than repeat 10 may favour or contribute to the F-actin interactions, which were not observed within *in vitro* conditions in this study.

6.3 Severe OPD Disorder mechanism and FLNA repeat 10

Previously the crystal structure of FLNA repeat 10 (Page R.C. *et al.*, 2011) was modelled to fit within the N-terminus of the F-actin however its orientation and polarity during binding remains vaguely understood. One mechanism suggests that binding occurs through a basic residue groove within FLNA repeat 10 with neighbouring residues allowing the specificity of interaction (Suphamungmee W. *et al.*, 2012). In this study two recurrent mutations A1188T and V1249A previously identified to lead to severe forms of OPD disorders with prenatal lethal males were examined (Robertson S.P. *et al.*, 2006, Robertson S.P. *et al.*, 2003). The A1188T and V1249A FLNA repeat 10 missense mutations were mapped to sit near the basic residue groove of the FLNA repeat 10 domain suggesting its importance in FLNA function. These mutations led to a slight increase in F-actin binding affinity in comparison to the wild-type FLNA repeat 10 protein observed in actin co-sedimentation assays, consistent with a gain-of-function disorder for OPD spectrum group of disorders as shown in actin binding FLNA ABD mutations (Clark A.R. *et al.*, 2009, Robertson S.P. *et al.*, 2003, Suphamungmee W. *et al.*, 2012). These results reinforce the proposed model where the neighbouring residues near the groove of the FLNA repeat 10 may play an important factor by influencing the interaction between FLNA repeat 10 and F-actin, suggesting that it must be sequence dependent.

Examining the crystal structure, of FLNA repeat 10 it is possible to suggest that these mutations may lead to conformational changes allowing for a more open structure, which consequently leads to an increase in affinity towards F-actin. The A1188T mutation associated with MNS physically sits near the N-terminal, while the V1249A mutation causing FMD is located near the C-terminus of repeat 10 (Robertson S.P. *et al.*, 2003, Page R.C. *et al.*, 2011, Robertson S.P. *et al.*, 2006) suggesting that a specific single mechanism leads to these disorders. The mutated residues of these severe disorders are buried with a predicted minimal side-chain solvent exposure. The A1188T

has been proposed to lead to disruptions of the BC loop of FLNA repeat 10 causing clashes with the side chains of nearby residues leading to disruption of the hydrophobic packing (Page R.C. *et al.*, 2011). On the other hand, the V1249A mutation does not lead to steric clashes with other residues as it is substituted by a smaller amino acid, but is suggested to cause a loosely packed hydrophobic region, however, its mechanism remains unclear (Page R.C. *et al.*, 2011). These mutations imply the importance of hydrophobic packing and structure in FLNA repeat 10 domain, suggesting that mutations within FLNA repeat 10 domain may possibly reduce the stability and impair folding as the structure is disrupted. This was observed with slightly reduced stability in both mutants however, the secondary structure did not dramatically change.

In this study, differences in expression of the FLNA repeat 10 protein were observed, the wild-type FLNA repeat 10 protein was expressed at much higher yields in *E. coli* than both mutant FLNA repeat 10 which could be caused by inefficient translation of mRNA or the amino acid substitutions lead to an unstable protein. CD thermal denaturation revealed that the isolated FLNA repeat 10 protein is relatively stable. However, both mutant proteins showed slightly reduced stability, consistent with previously assessed ABD of FLNA (Clark A.R. *et al.*, 2009) and FLNB (Sawyer G.M. *et al.*, 2009). This establishes a connection between the stability of a protein and function leading to OPD causing mutations. Although the underlying biochemical mechanism of OPD and the cellular functions of FLNA remains unclear. Nonetheless, additional studies are required to define how these disease-causing mutations affect the structure of the FLNA repeat 10 during binding to F-actin. Further understanding of mutations within FLNA will provide new insights into the complex molecular mechanism of FLNA and its human disorders.

6.4 FLNA repeat 10 importance

FLNA is an important building block of the larger complex network of the actin cytoskeleton mediating the organisation of the actin filaments in response to cell signals. The F-actin branching and cross-linking previously suggested that dimerization of the FLNA monomers at the C-terminus and an intact ABD are needed to mediate rigid perpendicular branching of F-actin to withstand cell stress (Nakamura F. *et al.*, 2007, Stossel T.P. *et al.*, 2001, Gorlin J.B. *et al.*, 1990, Weihing R.R., 1988). In contrast to the usual lethal form of PH, a few rare cases of males with mild PH were identified

(Sheen V.L. *et al.*, 2001, Parrini E. *et al.*, 2004, Van Kogelenberg M., 2010). This resulted from a loss of dimerisation of the FLNA monomers, however, the FLNA had partial function remaining (Van Kogelenberg M., 2010). This partial loss-of-function observed proposes that FLNA dimerisation may not be as important as originally thought for F-actin cross-linking, suggesting either an alternative dimerisation mechanisms or maybe an alternate actin binding mechanism unaffected by dimerisation to compensate for this effect. As previously identified and shown in this study that the FLNA repeat 10 domain binds to F-actin *in vitro* (Suphamungmee W. *et al.*, 2012, Nakamura F. *et al.*, 2007), this interaction may provide a possible mechanism to compensate for the binding of F-actin and lead to the partial function seen in the mild form of PH *in vivo*. However, further examination of this theory is required to determine whether FLNA repeat 10 domain can compensate for the binding of F-actin *in vivo*.

Interactions between the FLNA repeat domains and membrane receptors have been identified through structural analysis, revealing that rod 1 generally binds to small proteins such as signalling molecules (Nakamura F. *et al.*, 2006). On the other hand, the FLNA repeat 10 domain, which is part of rod 1 has one of the least characterized binding partners, but it is a mutational hotspot for the severe OPD disorders suggesting its importance. Nonetheless, it has been shown previously and in this study to be able to bind to F-actin (Nakamura F. *et al.*, 2007, Suphamungmee W. *et al.*, 2012) and to also interact with the T-cell receptor CD4 at the cytoplasmic domain leading to an important role in the human immunodeficiency virus entry into the immune cells (Jimenez-Baranda S. *et al.*, 2007). However, no defining mechanism has been established into how this specific repeat domain leads to these severe disorders. Clark *et al* showed that mutations within the CH1 of the ABD of FLNA resulted in an increased affinity towards F-actin and a reduced stability of the protein due to disruptions of a conserved salt bridge similar to results seen in this study. However, a unique calmodulin-binding site within the CH1 of ABD binding to calcium-activated calmodulin competes with F-actin to permit the dissociation of the FLNA-F-actin interactions allowing regulation of this interaction (Nakamura F. *et al.*, 2005). On the other hand, phosphorylated hinge regions led to a decrease in actin binding allowing regulation of interactions with integrins and glycoproteins (Chen M. and Stracher A., 1989, Ohta Y. and Hartwig J.H., 1995, Goldmann W.H. *et al.*, 1997, Gorlin J.B. *et al.*,

1990). This suggests that a mutation within these regions leads to the loss of regulation, which may also contribute to the disorders seen *in vivo*. Consequently, the same mechanism whereby additional regulatory binding partners maybe involved for the repeat 10 domain of FLNA, where mutations in this domain may in turn lead to a loss of regulation inducing cellular consequences and subsequently develop the gain-of-function OPD disorders.

6.5 Conclusion

The overall secondary structure of FLNA repeat 10 protein is typical for filamin repeat domains previously determined. The FLNA repeat 10 protein determined to be stable with a high melting point and resistance to cleavage, consistent with a packed hydrophobic β-sandwich structure. While the mutations associated with FMD and MNS, V1249A and A1188T respectively, were observed to have a slightly reduced thermostability implying slight instability in comparison to the wild-type FLNA repeat 10 protein. FLNAR10 was revealed to have a relatively weak binding affinity towards F-actin consistent with previous observations. While the FLNAR10 mutants showed a slight increase in affinity towards F-actin in comparison to the wild type FLNA protein, particularly the FLNAR10 V1249A mutation, which may cause a larger change in the structure due to its amino acid substitution.

Overall, these data provide the first biochemical evidence of FLNAR10 binding affinity to F-actin and its recurrent mutations towards a gain-of function mechanism, therefore contributing towards a better understanding of the FLNA structure and function. However, it remains unclear how these mutations alter the structure of FLNA leading to these OPD disorders, but suggests the importance of the FLNA repeat 10 domain in the function of FLNA

7. *Future Directions*

As mentioned earlier, this study provides the first biochemical evidence of FLNAR10 binding affinity to F-actin and its recurrent mutations towards a gain-of function mechanism, therefore contributing towards a better understanding of the FLNA structure and function. However, it remains unclear how these mutations alter the structure of FLNA leading to these OPD disorders, but suggests the importance of the FLNA repeat 10 domain in the function of FLNA

By further defining the structure of the FLNA repeat 10 domain, while interacting with F-actin *in vitro* using crystallography, will allow the binding interface, orientation, and specificity of this interaction to be resolved. In addition will determine any structural changes associated with the FLNA repeat 10 mutations, while binding to F-actin. Actin crosslinking studies using a transmission electron microscopy would provide evidence of intramolecular interactions between FLNA repeat 10 and actin networks. Moreover, would allow to compare whether any differences between the wild-type and mutant FLNA repeat 10 occur as suggested by this study.

As proposed in previous studies (Suphamungmee W. *et al.*, 2012, Nakamura F. *et al.*, 2007, Page R.C. *et al.*, 2011), the interaction between FLNA repeat 10 and F-actin has been suggested to occur through a conserved basic residue groove within the FLNAR10 domain with interaction specificity occurring through the assistance of residues neighbouring this basic groove. In this study, the mutation sites were mapped to sit near the basic groove this supported the proposed idea that these residues maybe involved indirectly in the interaction with F-actin. Mutations in these sites lead to changes in affinity towards F-actin, which was suggested to cause conformational changes to the FLNAR10 structure due to the size of the amino acid. Therefore, by examining whether mutating these specific sites or residues near the basic groove in the FLNAR10 with alternative larger or smaller amino acids may reveal differences in binding affinity towards F-actin, which will further support the previously mentioned theory.

This study focused specifically on the interaction between the FLNA repeat 10 domain protein and F-actin *in vitro*. Further studies are needed to determine whether this interaction is consistent with full-length FLNA. *In vivo* studies focusing on modifications of the motility or adhesion of cells between mutant and wild-type FLNA repeat 10 containing cells would offer additional insight into the FLNA functions in living organisms.

Within the FLNAR10 sequence, phosphorylation sites were determined to be present, which has been suggested to allow regulation of FLNA. Phosphorylation has been suggested to neutralize the clusters of positive charges in specific repeats causing the structure to become more compact as subunits bind together (Gorlin J.B. *et al.*, 1990). By examining whether phosphorylating these regions affects the FLNAR10 structure, as previously proposed to regulate interactions in other regions of FLNA or lead to differences in binding to F-actin will allow for regulation of interactions. Regulation through phosphorylation may provide a mechanism to control FLNA to F-actin interactions in FLNA associated with mutations leading to disorders, which may suggest a mechanism to counteract effects of interaction with F-actin. In addition, by identifying proteins that directly interact with regions of the FLNA protein may provide regulation of the FLNA structure and function.

Overall, these experiments proposed will further uncover a better understanding of the FLNA structure and function during the disease and normal state.

8. *Bibliography*

Adereth Y., Champion K.J., Hsu T. & Dammai V. 2005. Site-directed mutagenesis using Pfu DNA polymerase and T4 DNA ligase. *Biotechniques,* 38**,** 864-868.
Alenghat F.J. & Ingber D.E. 2002. Mechanotransduction: all signals point to cytoskeleton, matrix, and integrins. *Sci STKE***,** pe6.
Andrade M., Chacon P., Merelo J. & Moran F. 1993. Evaluation of secondary structure of proteins from UV circullar dichroism spectra using an unsupervised learning neural network. *Protein Engineering,* 6**,** 383-390.
Berndt M.C., Gregory C., Kabral A., Zola H., Fournier D. & Castaldi P.A. 1985. Purification and preliminary characterization of the glycoprotein Ib complex in the human platelet membrane. *J Biochem,* 151**,** 637-649.
Betts M.J. & Russell R.B. 2003. Amino Acid Properties and Consequences of Substitutions. *Bioinformatics for Geneticists,* eds M. R. Barnes and I. C. Gray**,** ch14.
Burridge K. & Chrzanowska-Wodnicka M. 1996. Focal adhesions, contractility, and signaling. *Ann Rev Cell Dev Biol,* 12**,** 463-518.
Calderwood D.A., Huttenlochert A., Kiosses W.B., Rose D.M., Woodside D.G., Schwartz M.A. & Ginsberg M.H. 2001. Increased filamin binding to β-integrin cytoplasmic domains inhibits cell migration. *Nat Cell Biol,* 3**,** 1060-1068.
Calderwood D.A., Shattil S.J. & Ginsberg M.H. 2000. Integrins and actin filaments: reciprocal regulation of cell adhesion and signaling. *J Biol Chem,* 275**,** 22607-22610.
Chen M. & Stracher A. 1989. In situ phosphorylation of platelet actinbinding protein by cAMP-dependent protein kinase stabilizes it against proteolysis by calpain. . *J. Biol. Chem.,* 264**,** 14282-14289.
Clark A.R., Sawyer G.M., Robertson S.P. & Sutherland-Smith A.J. 2009. Skeletal dysplasias due to filamin A mutations result from a gain-of function mechanism distinct from allelic neurological disorders. *Hum Mol Genet,* 24**,** 4791-4800.
Cunningham C.C., Gorlin J.B., Kwiatkowski D.J., Hartwig J.H., Janmey P.A., Byers H.R. & Stossel T.P. 1992. Actin-binding protein requirement for cortical stability and efficient locomotion. *Science,* 255**,** 325-327.
Cunningham J.G., Meyer S.C. & Fox J.E. 1996. The cytoplasmic domain of the alpha-subunit of glycoprotein (GP) Ib mediates attachment of the entire GP Ib-IX complex to the cytoskeleton and regulates von Willebrand factor-induced changes in cell morphology. *J Biol Chem,* 271**,** 11581-11587.
D'addario M., Arora P.D., Fan J., Ganss B., Ellen R.P. & Mcculloch C.A. 2001. Cytoprotection against mechanical forces delivered through beta 1 integrins requires induction of filamin A. *J Biol Chem,* 276**,** 31969–31977.
Didonna B.A. & Levine A.J. 2007. Unfolding cross-linkers as rheology regulators in F-actin networks. *Phys Rev E Stat Nonlin Soft Matter Phys,* 75**,** 041909.
Dixon, R. D. S., Arneman, D. K., Rachlin, A. S., Sundaresan, N., Costello, J. M., Campbell, S. L. & Otey, C. A. 2008. Palladin is an actin crosslinking protein that uses immunoglobulin-like domains to bind filamentous actin. *J. Biol. Chem. ,* 283**,** 6222–6231.
Dos Remedios C.G., Chhabra D., Kekic M., Dedova I.M., Tsubakihara M., Berry D.A. & N.J., N. 2003. Actin binding proteins: regulation of cytoskeletal microfilaments. . *Phys Rev,* 83**,** 433-473.
Dudding B.A., Gorlin R.J. & Langer L.O. 1967. The oto-palato-digital syndrome. A new symptom-complex consisting of deafness, dwarfism, cleft palate, characteristic facies, and a generalized bone dysplasia. . *Am J Dis Child,* 113**,** 214-221.

Duff R.M, Tay V., Hackman P., Ravenscroft G., Mclean C., Kennedy P., Steinbach A., Schoffler W., Van Der Ven P.F.M, Furst D.O., Song J., Djinovic-Carugo K., Penttila¨ S., Raheem O., Reardon K., Malandrini A., Gambelli S., Villanova M., Nowak K.J., Williams D.R., Landers J.E., Brown Jr. R.H., Udd B. & Laing N.G. 2011. Mutations in the N-terminal Actin-Binding Domain of Filamin C Cause a Distal Myopathy. *The American Journal of Human Genetics,* 88**,** 729–740.

Ehrlicher A.J, Nakamura F., Hartwig J.H., Weitz D.A. & Stossel T.P. 2011. Mechanical strain in actin networks regulates FilGAP and integrin binding to filamin A. *Nature,* 478**,** 260-263.

Feng, Y., Chen M.H., Moskowitz I.P., Mendonza A.M., Vidali L., Nakamura F., Kwiatkowski D.J. & Walsh C.A. 2006. Filamin A (FLNA) is required for cell-cell contact in vascular development and cardiac morphogenesis. *Proc. Natl. Acad. Sci. USA. ,* 103**,** 19836–19841.

Feng Y. & Walsh C.A. 2004. The many faces of filamin: a versatile molecular scaffold for cell motility and signalling. *Nat Cell Biol,* 6**,** 1034-1038.

Fitch N., Jequier S. & Gorlin R. 1983. The oto-palato-digital syndrome, proposed type II. *Am J Med Genet,* 15**,** 655– 664.

Fox J.E. 1985a. Identification of actin-binding protein as the protein linking the membrane skeleton to glycoproteins on platelet plasma membranes. *J Biol Chem,* 260**,** 11970-11977.

Fox J.E. 1985b. Linkage of a membrane skeleton to integral membrane glycoproteins in human platelets. Identification of one of the glycoproteins as glycoprotein Ib. *J Clin Inv,* 76**,** 1673-1683.

Fox J.E., Aggerbeck L.P. & Berndt M.C. 1988. Structure of the glycoprotein Ib.IX complex from platelet membranes. *J Biol Chem,* 263**,** 4882-4890.

Fox J.W., Lamperti E.D., Eksioglu Y.Z., Hong S.E., Feng Y., Graham D.A., Scheffer I.E., Dobyns W.B., Hirsch B.A., Radtke R.A., Berkovic S.F., Huttenlocher P.R. & Walsh C.A. 1998. Mutations in filamin 1 prevent migration of cerebral cortical neurons in human periventricular heterotopia. *Neurons,* 21**,** 1315-1325.

Gardel M.L., Nakamura F., Hartwig J.H., Crocker J.C., Stossel T.P. & Weitz D.A. 2006. Prestressed F-actin networks cross-linked by hinged filamins replicate mechanical properties of cells. *Proc. Natl. Acad. Sci. ,* 103**,** 1762–1767.

Gargiulo A., Auricchio R., Barone M.V., Cotugno G., Reardon W., Milla P.J., Ballabio A., Ciccodicola A. & Auricchio A. 2007. Filamin A is mutated in X-linked chronic idiopathic intestinal pseudo-obstruction with central nervous system involvement. *J Human Genet,* 80**,** 751-758.

Glogauer M., Arora P., Chou D., Janmey P.A., Downeyi G.P. & Mcculloch C.A.G. 1998. The role of actin-binding protein 280 in integrin-dependent mechanoprotection. *J Biol Chem,* 273**,** 1689-1698.

Goldmann W.H., Tempel M., Sprenger I., Isenberg G. & Ezzell R.M. 1997. Viscoelasticity of actin-gelsolin networks in the presence of filamin. *J Biochem,* 246**,** 373–379.

Gorlin J.B., Yamin R., Egan S., Stewart M., Stossel T.P., Kwiatkowski D.J. & Hartwig J.H. 1990. Human endothelial actin-binding protein (ABP-280, nonmuscle filamin): a molecular leaf spring. *J Cell Biol,* 111**,** 1089-1105.

Gorlin R.J. & Cohen M.M. 1969. Frontometaphyseal dysplasia: a new syndrome. *Am J Dis Child,* 118**,** 487-494.

Gorlin R.J., Poznanski A.K. & Hendon I. 1973. The oto-palato-digital (OPD) syndrome in females. *Oral Surg Oral Med Oral Pathol,* 35**,** 218– 224.

Greenfield N.J. 2006. Using circular dichroism collected as a function of temperature to determine the thermodynamics of protein unfolding and binding interactions. *Nature,* 1**,** 2527-2535.
Guerrini R., Mei D., Sisodiya S., Sicca F., Harding B., Takahashi Y., Dorn T., Yoshida A., Campistol J., Krämer G., Moro F., Dobyns W.B. & Parrini E. 2004. Germline and mosaic mutations of FLN1 in men with periventricular heterotopia. *Neurology,* 63**,** 51-56.
Gupta R. & Ahmad F. 1999. Protein Stability: Functional Dependence of Denaturational Gibbs Energy on Urea Concentration. *Biochem,* 38**,** 2471-2479.
Hart A.W., Morgan J.E., Schneider J., West K., Mckie L., Bhattacharya S., Jackson I.J. & Cross S.H. 2006. Cardiac malformations and midline skeletal defects in mice lacking filamin A. . *Hum. Mol. Genet.,* 15**,** 2457–2467.
Hartwig J.H. & Stossel T.P. 1981. Structure of macrophage actin-binding protein molecules in solution and interacting with actin filaments. *J Mol Biol,* 145**,** 563-581.
Hartwig J.H., Tyler J. & Stossel T.P. 1980. Actin-binding protein promotes the bipolar and perpendicular branching of actin filaments. *J Cell Biol,* 87**,** 841-848.
Heikkinen O.K., Ruskamo S., Konarev P.V., Svergun D.I., Iivanainen T., Heikkinen S.M., Permi P., Koskela H., Kilpeläinen I. & Ylänne J. 2009. Atomic structures of two novel immunoglobulin-like domain pairs in the actin cross-linking protein filamin. *J. Biol. Chem.,* 284**,** 25450-25458.
Heiring C. & Muller Y.A. 2001. Folding screening assayed by proteolysis: application to various cystine deletion mutants of vascular endothelial growth factor. *Protein Engineering,* 14**,** 183-188.
Himmel M., Van Der Ven P.F., Stocklein W. & Furst D.O. 2003. The limits of promiscuity: isoformspecific dimerization of filamins. *Biochem,* 42**,** 430-439.
Hou L., Luby-Phelps K. & Lanni F. 1990. Brownian motion of inert tracer macromolecules in polymerized and spontaneously bundled mixtures of actin and filamin. *J Cell Biol,* 110**,** 1645-1654.
Huttenlocher A., Ginsberg M.H. & Horwitz A.F. 1996. Modulation of cell migration by integrin-mediated cytoskeletal linkages and ligand-binding affinity. *J Cell Biol,* 134**,** 1551-1562.
Hynes R.O. 1992. Integrins: versatility, modulation and signaling in cell adhesion. *Cell,* 69**,** 11-25.
Ithychanda S.S., Hsu D., Li H., Yan L., Liu D., Das M., Plow E.F. & Qin J. 2009. Identification and Characterization of Multiple Similar Ligand-binding Repeats in Filamin. Implication on filamin-mediated receptor clustering and cross-talk. *J Biol Chem,* 284.
Janmey P.A, Hvidt S., Lamb J. & Stossel T.P. 1990. Resemblance of actin-binding protein/actin gels to covalently crosslinked networks. *Nature,* 345**,** 89-92.
Jimenez-Baranda S., Gomez-Mouton C., Rojas A., Martínez-Prats L., Mira E., Ana Lacalle R., Valencia A., Dimitrov D.S., Viola A., Delgado R., Martínez-a C. & Manes S. 2007. Filamin-A regulates actin-dependent clustering of HIV receptors. *Nat. Cell Biol. ,* 9**,** 838–846.
Johnson W.C. 1990. Protein secondary structure and circular dichroism: A practical guide. . *Proteins: Structure, Function, and Bioinformatics,* 7**,** 205-214.
Kasza K.E., Broedersz C.P., Koenderink G.H., Lin Y.C., Messner W. & Millman E.A. 2010. Actin filament length tunes elasticity of flexibly cross-linked actin networks. *Biophys J,* 99**,** 1091-1100.

Kasza K.E., Nakamura F., Hu S., Kollmannsberger P., Bonakdar N. & Fabry B. 2009. Filamin A is essential for active cell stiffening but not passive stiffening under external force. *Biophys J,* 96**,** 4326-4335.

Kelly S.M., Jess T.J. & Price N.C. 2005. How to study proteins by circular dichroism. *Biochimica et Biophysica Acta* 1751 119– 139.

Kesner B., Ding F., Temple B. & Dokholyan N. 2009. N-terminal strands of filamin Ig domains act as a conformational switch under biological forces. *Proteins,* 78**,** 12-24.

Kyndt F., Gueffet J-P., Probst V., Jaafar P., Legendre A., Le Bouffant F., Toquet C., Roy E., Mcgregor L., Lynch S.A., Newbury-Ecob R., Tran V., Young I., Trochu J-N., Le Marec H. & Schott J-J. 2007. Mutations in the Gene Encoding Filamin A as a Cause for Familial Cardiac Valvular Dystrophy. *Circulation journal of the American heart association,* 115**,** 40-49.

Lad Y., Kiema T., Jiang P., Pentikainen O.T., Coles C.H., Campbell I.D., Calderwood D.A & Ylänne J. 2007. Structure of three tandem filamin domains reveals autoinhibition of ligand binding. *EMBO,* 17**,** 3993-4044.

Laemmli U.K. 1970. Cleavage of Structural Proteins during the Assembly of the Head of Bacteriophage T4. *Nature,* 227**,** 680-685.

Li X. E., Tobacman L.S., Mun J.Y., Craig R., Fischer S. & Lehman W. 2011. Tropomyosin position on F-actin revealed by EM reconstruction and computational chemistry. . *Biophys J,* 100**,** 1005-1013.

Macpherson M. & Fagerholm S.C. 2010. Filamin and filamin-binding proteins in integrin-regulation and adhesion. Focus on: "FilaminA is required for vimentin-mediated cell adhesion and spreading". *J Cell Physiol,* 298**,** C221-236.

Maestrini E., Patrosso C., Mancini M., Rivella S., Rocchi M. & Repetto M. 1993. Mapping of two genes encoding isoforms of the actin binding protein ABP-280, a dystrophin like protein, to Xq28 and to chromosome 7. *Hum Mol Genet,* 2**,** 761–766.

Mccoy A.J., Fucini P., Noegel A.A. & Stewart M. 1999. Structural basis for dimerization of the Dictyostelium gelation factor (ABP120) rod. . *Nat. Struct. Biol.,* 6**,** 836–841

Mcgough A. 1998. F-actin-binding proteins. *Curr Opin Struct Biol,* 8**,** 166-176.

Melnick J.C. & Needles C.F. 1966. An undiagnosed bone dysplasia. A 2 family study of 4 generations and 3 generations. *Am J Roentgenol Radium Ther Nucl Med* 97**,** 39– 48.

Meyer S.C., Zuerbig S., Cunningham C.C., Hartwig J.H., Bissell T., Gardner K. & Fox J.E.B. 1997. Identification of the region in actin-binding protein that binds to the cytoplasmic domain of glycoprotein Ibalpha. *J Biol Chem,* 272**,** 2914-2919.

Moro F., Carrozzo R., Veggiotti P., Tortorella G., Toniolo D., Volzone A. & Guerrini R. 2002. Familial periventricular heterotopia: missense and distal truncating mutations of the FLN1 gene. . *Neurology,* 58**,** 916–921.

Nakamura F., Hartwig J.H., Stossel T.P. & Szymanski P.T. 2005. Ca2+ and calmodulin regulate the binding of filamin A to actin filaments. *J. Biol. Chem. ,* 280**,** 32426–32433.

Nakamura F., Osborn T.M., Hartemink C.A., Hartwig J.H. & Stossel T.P. 2007. Structural basis of filamin A functions. *J Cell Biol,* 179**,** 1011-1025.

Nakamura F., Pudas R., Heikkinen O., Permi P., Kilpelainen I. & Munday A.D. 2006. The structure of the GPIb-filamin A complex. *Blood,* 107**,** 1925-1932.

Nakamura F., Stossel T.P. & Hartwig J.H. 2011. The filamins Organizers of cell structure and function. *Cell Adhesion & Migration,* 5**,** 160-169.

Ohta Y. & Hartwig J.H. 1995. Actin filament cross-linking by chicken gizzard filamin is regulated by phosphorylation in vitro. *Biochem,* 34**,** 6745–6754.

Ohta Y., Hartwig J.H. & Stossel T.P. 2006. FilGAP, a Rho- and ROCK-regulated GAP for Rac binds filamin A to control actin remodelling. *Nat. Cell Biol.,* 8**,** 803-814.

Ohta Y., Suzuki N., Nakamura S., Hartwig J.H. & Stossel T.P. 1999. The small GTPase RalA targets filamin to induce filopodia. *Proc. Natl. Acad. Sci. ,* 96.

Ono, K., Yu, R., Mohri, K. & Ono, S. 2006. Caenorhabditis elegans kettin, a large immunoglobulin-like repeat protein, binds to filamentous actin and provides mechanical stability to the contractile apparatuses in body wall muscle. *Mol. Biol. Cell,* 17**,** 2722–2734.

Page R.C., Clark J. G. & Misra S. 2011. Structure of filamin A immunoglobulin-like repeat 10 from Homo sapiens. *Acta Crystallogr Sect F Struct Biol Cryst Commun,* 67**,** 871-876.

Parrini E., Mei D., Wright M., Dorn T. & Guerrini R. 2004. Mosaic mutations of the FLN1 gene cause a mild phenotype in patients with periventricular heterotopia. *Neurogenet,* 5**,** 191-196.

Parrini E., Ramazzotti A., Dobyns W.B., Mei D., Moro F., Veggiotti P., Marini C., Brilstra E.H., Dalla Bernardina B., Goodwin L., Bodell A., Jones M.C., Nangeroni M., Palmeri S., Said E., Sander J.W., Striano P., Takahashi Y., Van Maldergem L., Leonardi G., Wright M., Walsh C.A. & Guerrini R. 2006. Periventricular heterotopia: phenotypic heterogeneity and correlation with Filamin A mutations. *Brain,* 129**,** 1892-1906.

Pentikainen U. & Ylanne J. 2009. The regulation mechanism for the auto-inhibition of binding of human filamin A to integrin. *J. Mol. Biol* 393**,** 644–657.

Popowicza G.M., Müllerb R., Noegelb A.A., Schleicherc M., Hubera R. & Holaka T.A. 2004. Molecular Structure of the Rod Domain of Dictyostelium Filamin. *J Mol Biol,* 342**,** 1637-1646.

Popowicza G.M., Schleicher M, Noegel Aa & Ta., H. 2006. Filamins: promiscuous organizers of the cytoskeleton. *Trends in Biochem Sci,* 31**,** 411-419.

Pudas R. 2006. *Structural and interaction studies on the carboxy-terminus of filamin, an actin-binding protein.* PhD Thesis, University of Oulu.

Pudas R., Kiema T-R., Butler P.J.G., Stewart M. & Ylanne J. 2005. Structural basis for vertebrate filamin dimerization. *Structure,* 13**,** 111-119.

Robertson S.P. 2005. Filamin A: phenotypic diversity. *Curr. Opin. Genet. Dev.,* 15**,** 301– 307.

Robertson S.P. 2007. Otopalatodigital syndrome spectrum disorders:otopalatodigital syndrome types 1 and 2, frontometaphyseal dysplasia and Melnick-Needles syndrome. *European Journal of Human Genetics, Nature,* 15**,** 3-9.

Robertson S.P., Jenkins Z.A., Morgan T., Ades L., Aftimos S., Boute O., Fiskerstrand T., Garcia-Minaur S., Grix A., Green A., Kaloustian V.D., Lewkonia R., Mcinnes B., Van Haelst M.M., Macini G., Ille´S T., Mortier G., Newbury-Ecob R., Nicholson L., Scott C.I., Ochman K., Brozek I., Shears D.J., Superti-Furga A., Suri M., Whiteford M., Wilkie A.O.M. & Krakow D. 2006. Frontometaphyseal Dysplasia: Mutations in FLNA and Phenotypic Diversity. *J Med Genet,* 140A**,** 1726–1736.

Robertson S.P., Twigg S.R., Sutherland-Smith A.J., Biancalana V., Gorlin R.J., Horn D., Kenwrick S.J., Kim C.A., Morava E., Newbury-Ecob R., Orstavik K.H., Quarrell O.W., Schwartz C.E., Shears D.J., Suri M., Kendrick-Jones J. & Wilkie A.O. 2003. Localized mutations in the gene encoding the cytoskeletal protein filamin A cause diverse malformations in humans. *Nat Genet,* 33**,** 487-491.

Robertson S.P., Walsh S., Oldridge M., Gunn T., Becroft D. & Wilkie A.O. 2001. Linkage of otopalatodigital syndrome type 2 (OPD2) to distal Xq28: evidence for allelism with OPD1. *Am J Hum Genet* 69**,** 223– 227.

Ruskamo S. & Ylanne J. 2009. Structure of the human filamin A actin-binding domain. *Acta Crystallogr D Biol Crystallogr,* 65**,** 1217-1221.

Sawyer G.M., Clark A.R., Robertson S.P. & Sutherland-Smith A.J. 2009. Disease-associated substitutions in the filamin B actin binding domain confer enhanced actin binding affinity in the absence of major structural disturbance: Insights from the crystal structures of filamin B actin binding domains. *J Mol Biol,* 390**,** 1030-1047.

Sells M.A., Boyd J.T. & Chernoff J. 1999. p21-activated kinase 1 (Pak1) regulates cell motility in mammalian fibroblasts. *J Cell Biol,* 145**,** 837-849.

Sells M.A., Knaus U.G., Bagrodia S., Ambrose D.M., Bokoch G.M. & Chernoff J. 1997. Human p21- activated kinase (Pak1) regulates actin organization in mammalian cells. *Curr Biol,* 7**,** 202-210.

Seo M.D., Seok S.H., Im H., Kwon A.R., Lee S.J., Kim H.R., Cho Y., Park D. & Lee B.J. 2008. Crystal structure of the dimerization domain of human filamin A. *Proteins,* 75**,** 258-263.

Shaffer J.F., Kensler R.W. & Harris S.P. 2009. The myosin-binding protein C motif binds to F-actin in a phosphorylation-sensitive manner. . *J. Biol. Chem.,* 284**,** 12318–12327.

Sheen V.L., Dixon P.H., Fox J.W., Hong S.E., Kinton L., Sisodiya S.M., Duncan J.S., Dubeau F., Scheffer I.E., Schachter S.C., Wilner A., Henchy R., Crino P., Kamuro K., Dimario F., Berg M., Kuzniecky R., Cole A.J., Bromfield E., Biber M., Schomer D., Wheless J., Silver K., Mochida G.H., Berkovic S.F., Andermann F., Andermann E., Dobyns W.B., Wood N.W. & Walsh C.A. 2001. Mutations in the X-linked filamin 1 gene cause periventricular nodular heterotopia in males as well as in females. *Hum Mol Genet,* 10**,** 1775-1783.

Sheen V.L., Feng Y., Graham D., Takafuta T., Shapiro S.S. & Walsh C.A. 2002. Filamin A and Filamin B are co-expressed within neurons during periods of neuronal migration and can physically interact. *Hum Mol Genet,* 11**,** 2845-2854.

Shizuta Y., Shizuta H., Gailo M., Davies P. & Pastan I. 1976. Purification and Properties of Filamin, an Actin Binding Protein from Chicken Gizzard. *J Biol Chem,* 251**,** 6562-6567.

Stossel T.P., Condeelis J., Cooley L., Hartwig J.H., Noegel A. & Schleicher M. 2001. Filamins as integrators of cell mechanics and signalling. *Nat Rev Mol Cell Biol,* 2**,** 138-145.

Stossel T.P. & Hartwig J.H. 1975. Interactions of actin, myosin, and a new actin-binding protein of rabbit pulmonary macrophages. II. Role in cytoplasmic movement and phagocytosis. *J Biol Chem,* 250**,** 5706-5712.

Suphamungmee W., Nakamura F., Hartwig J. H. & Lehman W. 2012. Electron Microscopy and 3D Reconstruction Reveals Filamin Ig Domain Binding to F-Actin. *J Mol Biol,* 424**,** 248–256.

Sutherland-Smith A.J., Moores C.A., Norwood F.L., Hatch V., Craig R., Kendrick-Jones J. & Lehman W. 2003. An atomic model for actin binding by the CH domains and spectrin-repeat modules of utrophin and dystrophin. *J. Mol. Biol,* 329**,** 15–33.

Tanaka F., Forster L.S., Pal P.K. & Rupley J. A. 1975. The circular dichroism of lysozyme. *J Biol Chem,* 250**,** 6977-6982.

Tyler J.M., Anderson J.M. & Branton D. 1980. Structural comparison of several actin-binding macromolecules. *J Cell Biol,* 85**,** 489-495.

Vadlamudi R.K., Li F., Adam L., Nguyen D. & Ohta Y. 2002. Filamin is essential in actin cytoskeletal assembly mediated by p21-activated kinase 1. *Nat Cell Biol,* 4**,** 681-690.

Van Kogelenberg M. 2010. *Studies into the Underlying Aetiology of Periventricular Heterotopia.* PhD Thesis University of Otago.

Várkuti B.H., Yang Z., Kintses B., Erdélyi P., Bárdos-Nagy I., Kovács A.L., Hári P., Kellermayer M., Vellai T. & Málnási-Csizmadia A. 2012. A novel actin binding site of myosin required for effective muscle contraction. *Nature Structural & Molecular Biology,* 19**,** 299–306.

Vorgerd M., Van Der Ven P.F.M., Bruchertseifer V., Lowe T., Kley R.A., Schroder R., Lochmuller H., Himmel M., Koehler K., Furst D.O. & Huebner A. 2005. A Mutation in the Dimerization Domain of Filamin C Causes a Novel Type of Autosomal Dominant Myofibrillar Myopathy. *Am. J. Hum. Genet. ,* 77**,** 297–304.

Weihing R.R. 1988. Actin-binding and dimerization domains of HeLa cell filamin. Biochemistry. *Biochem,* 27**,** 1865-1869.

Weiss W., Weiland F. & Görg A. 2009. Protein detection and quantitation technologies for gel-based proteome analysis *Methods in Molecular Biology,* 564**,** 59-82.

Xu W., Xie Z., Chung D.W. & Davie E.W. 1998. A novel human actin-binding protein homologue that binds to platelet glycoprotein Iba. *Blood,* 92**,** 1268-1276.

9. *Appendices*

9.1 Cloning

Primer name	Sequence 5` → 3`	Restriction enzyme
FLNAR10 1155 Forward	AAAGGATCCGTTCCCTGCTTTGACGCAT	BamHI
FLNAR10 1158 Forward	AAAGGATCCTTTGACGCATCCAAAGTCAA	BamHI
FLNAR10 1252 Reverse	AAAGTCGACTTACGCAGGTTCCACCTGCAGCT	SalI
pPROEX HTb Rus (Forward)	TTCTCTCATCCGCCAAAACAGC	-
M13-48 Rev F (Reverse)	AGGGGATAACAATTTCACACAGG	-
FLNA R10 A1188T Forward	ACTGCTCGAGCACGGGCAGCGCG	-
FLNA R10 A1188T Reverse	CGCGCTGCCCGTGCTCGAGCAGT	-
FLNA R10 V1249A Forward	CAGCAAGCTGCAGGCGGAACCTGCGTAAG	-
FLNA R10 V1249A Reverse	CTTACGCAGGTTCCGCCTGCAGCTTGCTG	-
FLNA R10 S1199L Forward	TGACCATTGAGATCTGCTTGGAGGCGGGGC	-
FLNA R10 S1199L Reverse	GCCCCGCCTCCAAGCAGATCTCAATGGTCA	-

Appendix 9.1.1 Primers used for cloning.

Primers listed were used for cloning, whole plasmid PCR mutagenesis, and sequencing. Underlined regions reflect restriction enzyme site.

Construct name	FLNA R10 Amino acid Sequence N→C terminal
Wt FLNA 1155	VPCFDASKVKCSGPGLERATAGEVGQFQVDCSSAGSAELTIE ICSEAGLPAEVYIQDHGDGTHTITYIPLCPGAYTVTIKYGGQP VPNFPSKLQVEPA
Wt FLNA 1158	FDASKVKCSGPGLERATAGEVGQFQVDCSSAGSAELTIEICS EAGLPAEVYIQDHGDGTHTITYIPLCPGAYTVTIKYGGQPVP NFPSKLQVEPA
A1188T FLNA 1155	VPCFDASKVKCSGPGLERATAGEVGQFQVDCSS**A**GSAELTIE ICSEAGLPAEVYIQDHGDGTHTITYIPLCPGAYTVTIKYGGQP VPNFPSKLQVEPA
A1188T FLNA 1158	FDASKVKCSGPGLERATAGEVGQFQVDCSS**A**GSAELTIEICS EAGLPAEVYIQDHGDGTHTITYIPLCPGAYTVTIKYGGQPVP NFPSKLQVEPA
V1249A FLNA 1155	VPCFDASKVKCSGPGLERATAGEVGQFQVDCSSAGSAELTIE ICSEAGLPAEVYIQDHGDGTHTITYIPLCPGAYTVTIKYGGQP VPNFPSKLQ**V**EPA
V1249A FLNA 1158	FDASKVKCSGPGLERATAGEVGQFQVDCSSAGSAELTIEICS EAGLPAEVYIQDHGDGTHTITYIPLCPGAYTVTIKYGGQPVP NFPSKLQ**V**EPA
S1199L FLNA 1155	VPCFDASKVKCSGPGLERATAGEVGQFQVDCSSAGSAELTIE IC**S**EAGLPAEVYIQDHGDGTHTITYIPLCPGAYTVTIKYGGQP VPNFPSKLQVEPA
S1199L FLNA 1158	FDASKVKCSGPGLERATAGEVGQFQVDCSSAGSAELTIEIC**S** EAGLPAEVYIQDHGDGTHTITYIPLCPGAYTVTIKYGGQPVP NFPSKLQVEPA

Appendix 9.1.2 FLNA repeat 10 sequence constructs.

FLNA repeat 10 sequence constructs used. FLNA constructs with N-terminus at either amino acid 1155 or 1158, to the C-terminus amino acid 1252. Mutants were created by whole plasmid PCR mutagenesis (refer to 2.8.9). Amino acids highlighted represent mutation sites.

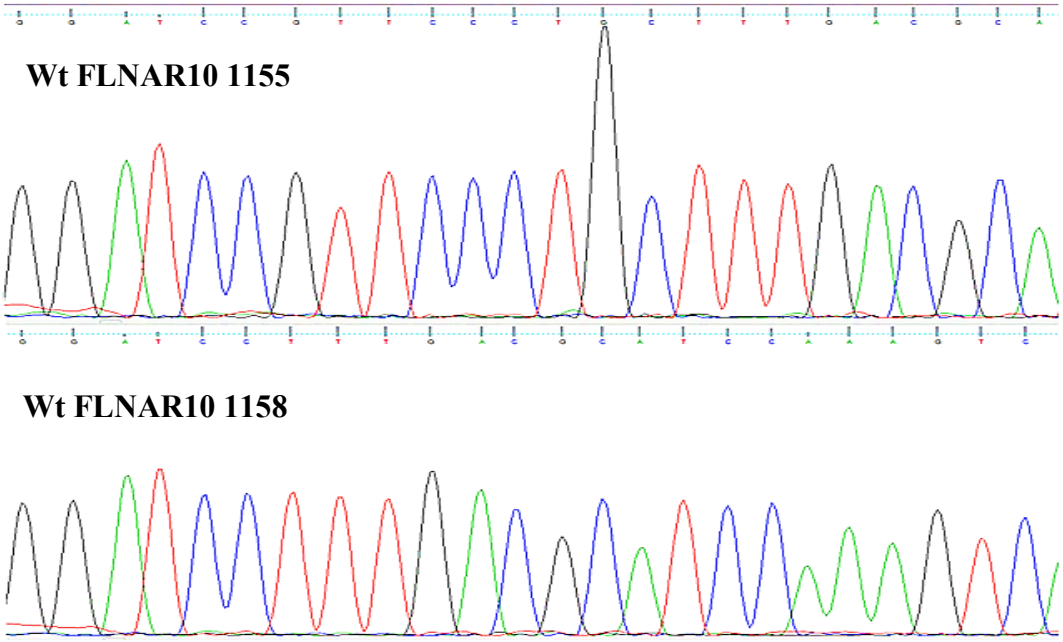

Appendix 9.1.3 FLNA repeat 10 sequencing different constructs.

FLNA repeat 10 1155 or 1158 constructs sequencing viewed using FinchTV. Nucleotides represented as A; green, T; red, C; black, G; blue.

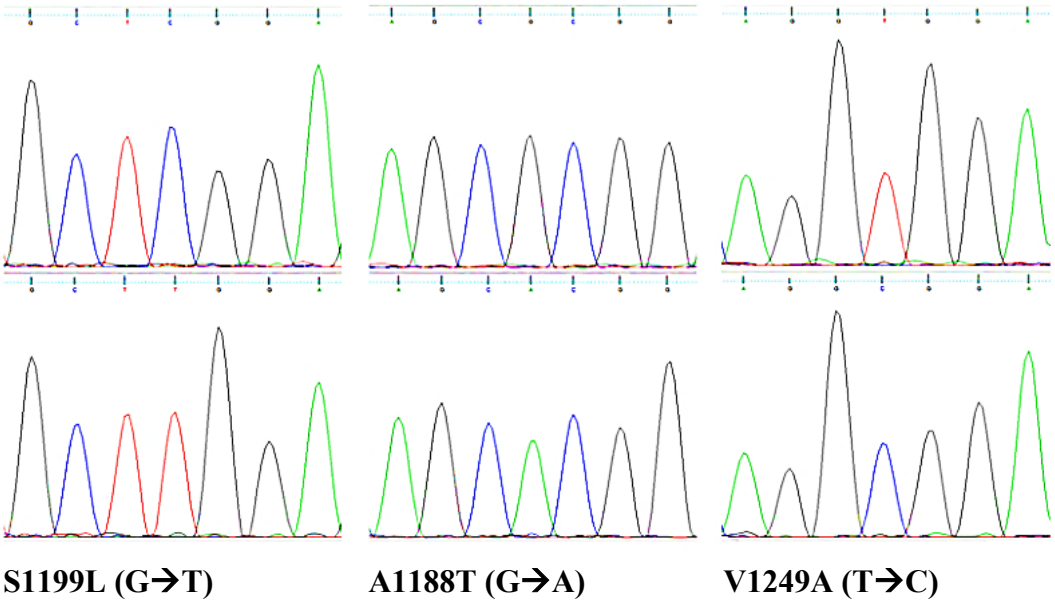

Appendix 9.1.4 FLNA repeat 10 sequencing of mutants.

FLNA repeat 10 mutant constructs V1249A, A1188T, and S1199L sequenced then viewed using FinchTV. Nucleotides represented as A; green, T; red, C; black, G; blue..

9.2 CD spectroscopy analysis

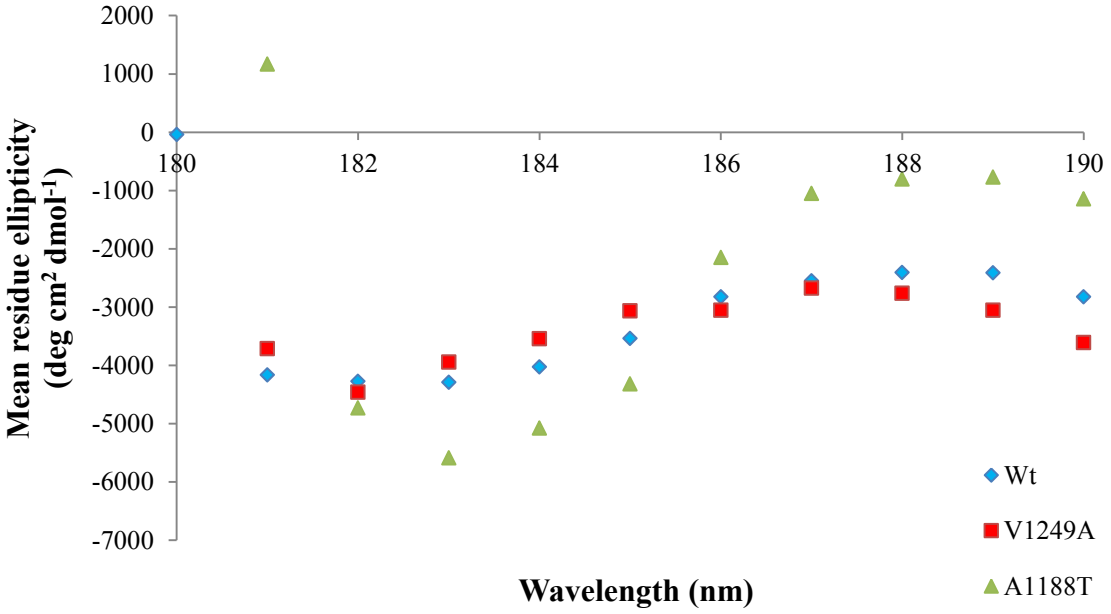

Appendix 9.2.1 Far-UV CD spectrum of FLNAR10 180-190nm.

Far-UV CD spectrum of 0.07 mg/ml of FLNAR10 protein samples measured at wavelengths between 180-190 nm, at 1 nm readings taken every 1. Wavelengths from 180-190 nm were scattered so were not considered.

9.3 Actin Co-sedimentation assay

	FLNAR10: bound to F-actin ratio (mol:mol)		
Filamin concentration (μM)	**Wt**	**V1249A**	**A1188T**
10	0.01	0.04	0.03
20	0.04	0.13	0.13
30	0.14	0.22	0.20
40	0.21	0.27	0.29
50	0.35	0.34	0.37
100	0.48	0.49	0.44
150	0.62	0.80	0.68
200	0.75	0.97	0.81
250	0.90	1.25	0.97
300	1.27	1.69	1.41
350	1.39	-	1.79
400	1.72	-	-
450	2.31	-	-

Appendix 9.3.1 Actin co-sedimentation assay data.

Averaged data of actin co-sedimentation assays using a ratio of 10uM F-actin to varying concentration of FLNA R10 protein samples compared for Wt and mutant constructs.

	Wt	V1249A	A1188T
Best-fit values			
Bmax	1.93	3.47	1.63
Kd	310.40	521.30	211.60
Standard Error			
Bmax	0.40	0.75	0.29
Kd	91.75	143.40	61.70
95% Confidence Intervals			
Bmax	1.09 to 2.76	1.88 to 5.07	0.99 to 2.26
Kd	119.60 to 501.20	213.80 to 828.80	79.27 to 343.90
Goodness of Fit			
Degrees of Freedom	21	14	14
R square	0.96	0.99	0.95
Absolute Sum of Squares	0.06	0.02	0.05
Sy.x	0.05	0.04	0.06
Number of points analysed	23	16	16

Appendix 9.3.2 Analysis of actin co-sedimentation assay normalised data range 10-200 µM fitted to one site binding (hyperbola) model.

Analysis of one site binding (hyperbola) model fitted to the data range between 10-200 µM of FLNR10 protein, through GraphPad Prism software (version 6.00 for Windows, GraphPad Software).

	Wt	V1249A	A1188T
Best-fit values			
Bottom	~ -395.10	~ -199.70	~ -472.90
Top	0.84	~ 2.33	1.02
V50	~ -584.60	~ -1665.00	~ -833.70
Slope	~ 96.66	~ 373.40	~ 136.00
Standard Error			
Bottom	~ 175030	~ 121471	~ 622974
Top	0.18	~ 9.55	0.78
V50	~ 43378	~ 243433	~ 181618
Slope	~ 94.42	~ 4009.00	~ 421.80
95% Confidence Intervals			
Bottom	(Very wide)	(Very wide)	(Very wide)
Top	0.46 to 1.21	(Very wide)	-0.68 to 2.73
V50	(Very wide)	(Very wide)	(Very wide)
Slope	(Very wide)	(Very wide)	(Very wide)
Goodness of Fit			

Degrees of Freedom	19	12	12
R square	0.98	0.99	0.95
Absolute Sum of Squares	0.03	0.02	0.05
Sy.x	0.04	0.04	0.06
Number of points analysed	23	16	16

Appendix 9.3.3 Analysis of actin co-sedimentation assay normalised data range 10-200 μM fitted to Boltzmann sigmoid model.

Analysis of Boltzmann sigmoid model fitted to the data range between 10-200 μM of FLNR10 protein, through GraphPad Prism software (version 6.00 for Windows, GraphPad Software).

9.4 Phosphorylation sites

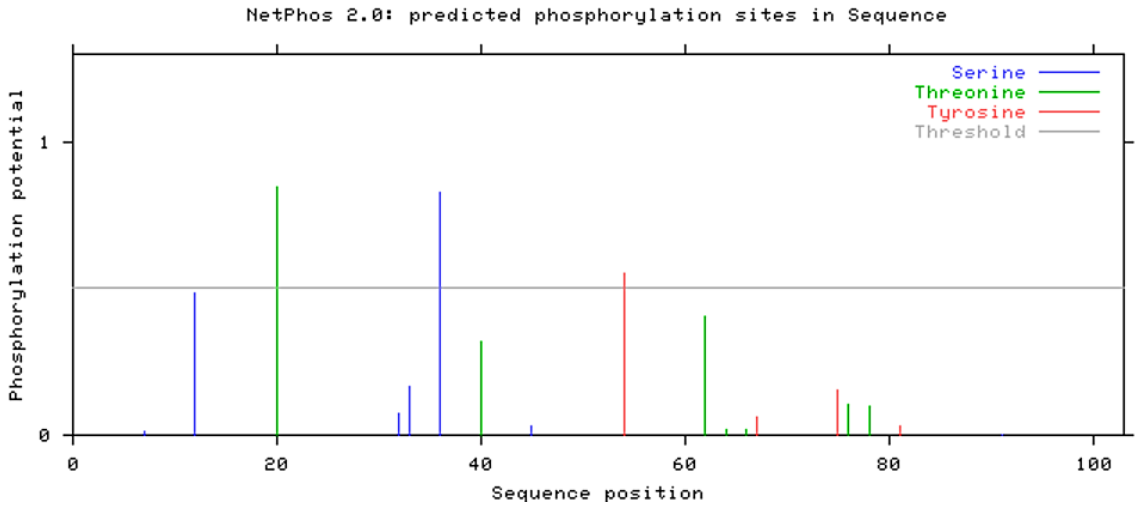


```
   98 Sequence
VPCFDASKVKCSGPGLERATAGEVGQFQVDCSSAGSAELTIEICSEAGLPAEVYIQDHGDGTHTITYIPLCPGAYTVTIK      80
YGGQPVPNFPSKLQVEPA                                                                  160
...................T................S.................Y.........................      80
..................                                                                  160

Phosphorylation sites predicted:        Ser: 1  Thr: 1  Tyr: 1
```

Appendix 9.4.1 Possible phosphorylation sites within FLNAR10.

Analysis of the possible phosphorylation sites within the FLNAR10 sequence using NetPhos 2.0 Server..